Clin Schizophr Relat Psychoses
Spl 1, 2020

Clinical Schizophrenia & Related Psychoses

Research Article

Hybrid Open Access

ROR- NF-B/RelA-STAT3-FURIN-SARS-COV-2 Quantum Deep Learning Functional Similarities on Remdesivir, Ursolic Acid and Colchicine Drug Synergies to treat COVID19 in Practice

Grigoriadis Ioannis

Biogenea Pharmaceuticals Ltd, Pharmaceutical Biotechnology Company, Thessaloniki, Greece

Abstract

SARS coronavirus 2 (SARS-CoV-2) of the family Coronaviridae is an enveloped, positive- sense, single -stranded RNA betacoronavirus encoding a SARS-COV-2 (2019-NCOV, Coronavirus Disease 2019, that infect humans historically. Remdesivir, or GS-5734, is an adenosine triphosphate analog first described in the literature in 2016 as a potential treatment for Ebola. In 2017, its activity against the coronavirus family of viruses was also demonstrated. Remdesivir is also being researched as a potential treatment to SARS-CoV-2, the coronavirus responsible for COVID-19. Structure-Based Drug Design strategies based on docking methodologies have been widely used for both new drug development and drug repurposing to find effective treatments against this disease. Quantum mechanics, molecular mechanics, molecular dynamics (MD), and combinations have shown superior performance to other drug design approaches providing an unprecedented opportunity in the rational drug development fields and for the developing of innovative drug repositioning methods. In this research paper, we estimated the druggable similarity by applying an inverse docking multitask machine learning approach to basal gene expression in acute respiratory distress syndrome and response to single drugs. We tested 18 phytochemical small molecule libraries and predicted their synergies in COVID19 (2019- NCOV), which is associated with 1,000,000 deaths worldwide, to devise therapeutic strategies, repurpose existing ones in order to counteract highly pathogenic SARS-CoV-2 infection and the associated NOS3- COVID-19 pathology. We anticipate that our approaches can be used for prioritization of drug combinations in large scale screenings, and to maximize the efficacy of the Remdesivir, Colchicine and Ursolic acid drugs already known to induce synergy, ultimately enabling COVID19 patient stratification.

Keywords: Deep Learning • Quantum mechanics •Colchicine•Remdesivir • Ursolic acid • COVID-19

Introduction

Ancient Indian scriptures including Rig-Veda, Atherveda, and Charka Sanhita demonstrated abundant benefits of plants for the treatment of various human aliments. Plants are a remarkable natural source of high value alkaloids, flavonoids, phenols, chalcones, coumarines, lignans, polyketides, alkanes, alkenes, alkynes, simple aromatics, peptides, terpenes, and steroids. In the current era of drug discovery, enormous medicinal properties of plants allows the researchers to exclusively use them for the discovery of drug-like natural molecules. Ursolic acid (3--3-hydroxy-urs-12-ene-28-oic-acid) and oleanolic acid (3-hydroxyolean-12-en-28-oic acid) are pentacyclic triterpenoid compounds with a widespread occurrence throughout the plant kingdom. Both molecules enrich various therapeutic properties such as antibacterial, antiviral, anticancer, antioxidant and tantimycotic activity. Previous in vitro studies reported that these molecules exhibit antiviral activity against rotavirus, HIV, the influenza virus, hepatitis B and C viruses. Epigenetic modulation of the structure of chromatin, including DNA modifications and post-translational modifications of histones, is critical for the regulation of gene expression [1,2]. Many enzymes involved in epigenetic modulation of chromatin have been identified. These include DNA methyltransferases and DNA demethylases; histone acetyltransferases and histone deacetylases; and lysine methyltransferases and lysine demethylases. DNA methylation regulates gene expression by recruiting proteins involved in gene repression or by inhibiting the binding of transcription factors [3]. Histone acetylation influences histone/DNA interactions in the nucleosome and perturbs histone/histone interactions [4]. Acetyl groups can also serve as a platform for recruitment of histone acetylation readers to participate in gene transcription, DNA replication, DNA repair or chromatin condensation [5]. Histone lysine methylation on histones H3 and H4 has been implicated in heterochromatin formation and the regulation of promoter activity [6,7]. Dysregulation of epigenetic modifications is associated with various human diseases, such as cancer and neurodevelopmental disorders [8,9]. Bromodomain protein 4 (BRD4) is a reader and writer of histone acetylation that plays important roles in replication, transcription and DNA repair [10,11]. The post-translational modification of histone acetylation is a key mechanism that regulates chromatin organization, and several studies have focused on the important function of BRD4 in regulating chromatin structure [12-15]. The histone acetyltransferase activity of BRD4 is responsible for maintaining normal chromatin structure [16]. BRD4 is critical in the maintenance of higher-order chromatin structure, and inhibition of BRD4 leads to chromatin decondensation and fragmentation [17]. Another study has demonstrated that a short isoform of BRD4 lacking the histone acetyltransferase domain can recruit the condensing II remodeling complex, thus forming a closed chromatin structure [18]. Otherwise, BRD4 can de-compact chromatin and facilitate transcriptional re-activation [19]. BRD4 acetylates histone H3 at the K122 residue, thereby perturbing a salt bridge and leading to nucleosome instability [16]. Thus, the mechanism by which BRD4 contributes to chromatin structure is likely to be complex and context-specific [17-23]. The mechanism by which CDK9 is recruited to innate genes is not fully understood. Activated CDK9 binds to sequence-specific DNA binding factors, including NF-κB/RelA [21,24] and STAT3 [25],

***Corresponding Author:** John-Ioannis Grigoriadis, Grigoriadis Ioannis Pharmacist, Biogenea Pharmaceuticals Ltd, Pharmaceutical Biotechnology Company, Thessaloniki, Greece, Tel: +30 2310 282835; E-mail: biogeneadrug@gmail.com*

Received 23 October, 2020; **Accepted** 06 November, 2020; **Published** 13 November, 2020

responsible for recruiting CDK9 to inducible gene promoters. It has also been found that CDK9 targets to inflammatory GRNs in a RelA-dependent manner [19,21,24]. It has also been observed that RSV infection induces BRD4 expression, interaction with CDK9 and NF-B/RelA, and its recruitment to immediate early innate genes. Using short interfering RNA (siRNA)-mediated knockdown, it has been found that BRD4 is functionally required for the recruitment and stabilization of CDK9 and phospho-Ser 2 CTD RNA Pol II to NF-B-dependent inflammatory genes, including the IRF1/7-RIG-I amplification loop and downstream IRF-dependent IFN-stimulated genes (ISGs) where a small-molecule inhibitor of histone acetyllysine (Lys) binding pocket blocks virus-induced BRD4•CDK9 binding and phospho-Ser 2 CTD Pol II formation on the IRF-RIG-I cross talk pathway and its downstream innate GRN. The retinoic acid-related orphan receptors alpha, beta, and gamma (ROR- encoded by RORA-C or NR1F1-3) constitute a subfamily of nuclear receptors [1-4]. RORs exhibit a typical nuclear receptor domain structure consisting of an N-terminal domain, a highly-conserved DNA-binding domain (DBD) consisting of two C2-C2 zinc finger motifs, a ligand-binding domain (LBD), and a hinge domain spacing the DBD and LBD [1]. The DBD of RORs recognizes ROR response elements (ROREs) consisting of the RGGTCA consensus preceded by an A/T-rich sequence. RORs regulate transcription by binding as monomers to ROREs in the regulatory regions of target genes and the recruitment of co-activators or co-repressors [5,6]. Over the last ten years, it has become evident that RORs function as ligand-dependent transcription factors. ROR/ transcriptional activity can be modulated by various sterols and synthetic ligands that bind ROR and function either as agonists or inverse agonists [2,4,7-17]. The discovery that ROR transcriptional activity can be modulated by small (synthetic) molecules, opened the possibility that RORs may provide novel therapeutic targets in the management of various pathologies, in which RORs are implicated, such as autoimmune disease and type 2 diabetes. In addition, RORs may provide a target for various xenobiotics and thereby a mechanism by which environmental agents affect immunity and disease. This chapter provides an overview of the various links between cholesterol/sterol metabolism, RORs, and their regulation of immunity, particularly T helper 17 (Th17) cells, and their relationship to inflammatory disease. The COVID-19 disease was declared on March 2020 a pandemic by the World Health Organization (WHO) and is accountable for a large number of fatal cases. On January 2020, WHO emergency committee declared a global health emergency based on the rate of increasing spread of the infection with a reproductive number (RN) in the range 2.0-6.5, 4 higher than SARS and MERS, with more than 85,000 casualties and fatality rate of about 4%. The Spike protein is a large, trimeric protein whose Receptor Binding Domain (FURIN-ADAMTS1-ROR-GAMMA) undergoes somewhat unusual dynamic transformations sometimes called “breathing”. From a protein engineering perspective, so-called “breathing” reflects the inherent flexibility and/or localized mobility associated with the Receptor Binding Domain (FURIN-ADAMTS1-ROR-GAMMA) of the Spike Protein. In the so-called “Up-state” of the FURIN-ADAMTS1-ROR-GAMMA, the (prefusion) protein is able to bind to ACE2 (Angiotensin Converting Enzyme 2) and infect (via a transformation to its fusion state) human epithelial cells (Type I and II pneumocytes; also, alveolar macrophage and nasal mucosal cells), but in the “Down-state” the Spike protein is believed to be inactive to ACE2 binding and to cellular infection. We note that the S1 domain of the Spike protein is shed in the transition from the prefusion state to the fusion state of this virion; those transformational aspects are not considered here. The exact mechanism and specific structural details associated with the flexibility or local mobility of the FURIN-ADAMTS1-ROR-GAMMA in the Up and Down states in SARS-Cov-2 remain unanswered. For example, it is not known whether these states exist simply randomly or by deterministic changes orchestrated by the virion or its environment. Recently unpublished long time Molecular Dynamics (MD) studies (10μs) of an isolated Spike Protein by the Shaw Group noted that the protomers tended to persist in their initial states, i.e, Down states remain Down and Up states remain Up. However, the Up state protomer demonstrated further distal displacement and mobility from its initial state that was given by experimental structural data [1-4]. In order to better understand the differences between the Up and Down protomer states, we conducted an all-atom interacting energy landscape mapping of the entire Spike protein from its *.pdb (Protein Data Bank) structure file (6vsb.pdb) in order to identify interaction energy “glue” points associated with relatively strong non-covalent atom-atom interactions between residues, which may be responsible for specific persistent domains of this complex trimeric protein. In doing so, we were able to identify some unique and potentially critical differences between the Up and Down protomers within the overall trimeric structure, including a possible molecular latch that helps to maintain the FURIN-ADAMTS1-ROR-GAMMA in the down state conformation. The latch residues are conserved across the closely related virions SARS-Cov-1 and the bat corona virus RatG13, as well as known variations of the novel corona virus. Comparative analyses between Up and Down state protomers, such as those given here, may lead to potentially new therapeutic targets aimed at disrupting the viral functionality of the Spike protein to its role in COVID-19. Anti-malarial medicine Remdesivir (CQ) and particularly its chemical analogue hydroxyRemdesivir (HCQ) have been recommended as promising candidate therapeutics that are now under either compassionate off- label use or clinical trials for the treatment of COVID-19 patients [1-5]. Computer-generated models, which serve as good predictive models for the evaluation of biological activities, have had numerous successes predicting the possible structures of biological targets [6], thus reducing fruitless effort using nuclear magnetic resonance and spectroscopy- structure elucidations. [2-6] Collaborative efforts for Genomic characterization [7], Molecular epidemiology, evolution, phylogeny of SARS coronavirus and epidemiology from scientists worldwide are underway to understand the rapid spread of the novel coronavirus (CoVs), and to develop effective interventions for control and prevention of the disease. As originally an anti-malarial medicine applied for decades, hydroxyRemdesivir (HCQ) is one of the disease-modifying antirheumatic drugs (DMARDs), which is widely used for treating certain rheumatic diseases such as rheumatic arthritis (RA) and systemic lupus erythematosus (SLE), and it also generates a strong immunomodulatory effect, which prevents inflammation flare-ups and multi organ damage. Coronaviruses are positive-single stranded, enveloped large RNA viruses that infect humans and a [1-6]. Wide range of animals, Tyrell and Bonne reported the first coronavirus in 1966, who cultivated the viruses from the patients suffering with common cold. In Latin, Corona means “crown” based on their shapes. Structural analysis reveals the atomic level-specific communications between spike protein receptor- binding domain of SARS-CoV2 and ACE2 receptor present in the host to regulates the transmission of cross-species and human to human SARS-CoV-2also uses ACE2 as its binding receptor, to transfer from human to human [2-8]. It has also been [3-5,8-10] reported that the SARS-CoV-2 intervened mainly in the lung with progression to pneumonia and acute respiratory distress syndrome (ARDS) [9-11]. via the angiotensin-converting enzyme 2(ACE2) receptor [2-7]. Depending on the viral load, infection spread through the ACE2 receptor [12], further to various organs [8,9,10] such as heart, liver, kidney, brain, endothelium, GIT, immune cell, and RBC (thromboembolism) [2,12]. FURIN-ADAMTS1 is a vasoprotective gene [2] that regulates vascular tone, blood pressure and platelet aggregation [2,3]. Research reports have shown that FURIN-ADAMTS1 can affect metabolism in the urea cycle of the methylation pathway [3,4,6-9], which is essential for preventing systemic inflammation. The single nucleotide polymorphism (SNP) FURIN-ADAMTS1 894GT located in exon 7 (also known as Glu298Asp, rs1799983) is a genetic marker that has been specifically linked to an increased risk of IHD, hypertension, coronary spasms, and stent re-stenosis [2,8,9]. More specifically, it has been reported that the FURIN-ADAMTS1 894GT SNP represents a guanine (G)/thymine substitution at position 894 on exon 7 leading to a change from glutamate to aspartate at position 298; rs1799983. This may be aggravated by cytokine storm with the extensive release of proinflammatory cytokines from the deregulating immune system. Molecular structure can be determined in heterodox interpretations by solving the time-independent Schrödinger equation: QM methods, vertex prizes and edge costs including ab initio Density Filed Theories (DFT) and semi-empirical in place of the quantum processor and energy among other observables [10-13], under simulated sampling error as well as to reposition drugs about bonding may represent the similarities and dissimilarities between drugs and repurposed viral [18] proteins respectively [15-19].

However, the Schrödinger equation cannot actually be solved for any but a one- data-driven electron system methods (the hydrogen atom), and approximations need to be made [20,21]. In recent years, several computational approaches have been developed to identify them at protein-protein interfaces [3-16]. Accurate predictive models provide a valuable complement to experimental studies and add to our understanding of the factors that influence affinity and specificity in protein-protein interfaces. In addition, they can have important applications in the field of drug discovery. A number of recent studies have been successful in developing (drug-like) small molecules that bind at hot spots and inhibit complex formation [17]. Reliable hot spots predictions could therefore represent the first step in rational drug design projects [18]. According to QM [22]. an electron bound that converges quickly and reliably to an atom cannot possess any [23] arbitrary energy to produce the desired distribution by analyzing pharmacological data or occupy any position in space using statistical and machine learning concepts [25-27]. The viral genome codes a cluster of (28) spike proteins and play the most important role in SARS-CoV-2 detection with a unique proteomic function in the event of host invasion or viral development [29-33]. In recent years, the productivity challenge facing the pharmaceutical industry has become particularly difficult to overcome. In a previous work, it has been presented a machine learning strategy to identify hot spot residues in protein-protein interfaces, given the structure of the complex [12]. Basic energetic terms have been considered to contribute to hot spot interactions, i.e. van der Waals potentials, solvation energy, hydrogen bonds and Coulomb electrostatics, and treated them as input features of a Support Vector Machine (SVM) classifier. It has also been found that the method could predict hot spots with overall good accuracy, comparing favourably to other available approaches. However, by grouping mutations according to the amino acid type, it has been observed that in some cases the SVM model did not perform too well, for example on predictions involving arginine or glutamic acid residues [32-39]. By many estimates, the number of new molecular entity approved to market per billion US dollars spent on (research and development) R&D has halved roughly every one decade, falling around 80-fold in inflation-adjusted terms [11]. To increase drug-discovery productivity, more and more attention has been paid to exploring the relationship between drug anddisease, which can advance our knowledge of molecular mechanism of disease indication and lead to new strategies to treat productivity challenge [12,13]. Nevertheless, traditional strategies which typically oriented on a search for a novel therapeutic compound combined o construct classification features with discovery of a new therapeutic target are time consuming, expensive and risky because of the necessity for multiple experimental and clinical validation [14]. Drug repurposing/repositioning/rescue proposed a computational method to identify potential drug indications by integrating various applications of an existing drug to a new disease indication, is a promising approach to address the “productivity gap”, especially the demand of rapid clinical impact at a lower cost by the „starting-from-scratch drug development [23,40-90]. Inverse docking is „one ligand-many targets scenario, representing a structure- based computational strategy [20-90]. Different with the conventional drug virtual screening, inverse virtual screening was performed for a small- molecule against a large collection of binding-sites of clinically relevant macromolecular targets [22-78,82]. The top-ranking targets based on the binding complementarity (shape and electrostatics) with the drug are likely to result in potential drug repositioning. Hence, efficient tools were developed for inverse docking, for example, INVDOCK [20,45-63], TarFisDock [21,40,41-80], PDTD [22,55,90], and idTarget [23,45,53]. The number of cases and deaths rises continuously and rapidly every day. Even worse, the biggest challenge is that there are no proven therapies or vaccines against COVID-19, and there are significant research gaps in many other essential research and innovation areas. As one of the earliest affected countries, the outbreak in China has been well controlled, and it is nearing completion. Many countries and international organizations affirmed that China took active and effective measures. Chinese counterattacks can be replicated to fight the epidemic [3]. Among them, traditional Chinese medicine (TCM) has played an irreplaceable role and provided unique advantages in the management of this disease. Nevertheless, the underlying action mechanisms of Chinese medicines (CMs) are still unclear. Moreover, successful drug repurposing examples along with these tools are steadily grows, such as sildenafil and thalidomide. Since the basic philosophy behind reverse docking is the same with docking and the critical parameters of the docking programs were always optimized based on some of the specific ligand and target systems [24-70], the performance in docking pose search itself and coring of the docked poses may, thus, still face challenges for reverse docking methods. In China, the treatment protocol of COVID-19 emphasizes the combination of TCM with conventional therapy [11]. The current practice has demonstrated that TCM intervention is essential and effective in the management of COVID-19, showing by the improvement of the cure rate, shortened disease course, delayed disease progression, and reduced mortality rate [12,13]. It was reported that the overall effective rate reached over 90 % in 74187 confirmed COVID-19 cases who received TCM treatment [1-14]. Lou (215) reported that the change of hematology is positive in COVID-19 patients treated with TCM. A prospective multicenter open-label randomized controlled trial also confirmed the efficacy of Lianhua Qingwen capsule in ameliorating the clinical symptoms of COVID-19 patients, including fever, fatigue, and cough [16]. Several retrospective and controlled clinical studies have also reported that TCM treatment effectively improved the fever, sweating, cough, headache, shortness of breath, chest distress, nausea, and diarrhea in COVID-19 patients [2-20]. The chest radiogram has been improved significantly as well [3-21]. The levels of ESR, CRP, and IL-6 were significantly decreased, and the level of IFN-κwas increased in the group received both TCM and conventional treatments in comparison with the group only received conventional treatment (antibiotics and antiviral therapy) [22]. TCM was also helpful to the elderly, children, and severe COVID-19 patients [2-25,26]. Deep learning permits machines to take care of complex issues in any event, when utilizing an informational index that is exceptionally differing and unstructured. Chemical similarity is a central principle in ligand design, and extensive chemoinformatic studies explore multiple methods based on it [1,2]. However, chemical structure alone does not provide adequate description of bio-molecular interactions, which are quantum in nature. Through molecular modeling, molecules can be considered as quantum objects: quantum representation of their activity (biological, chemical or pharmacological), not the underlying structure itself, is important. Our quantum molecular representations exhibit well-defined mathematical characteristics, which afford systematic theoretical treatment and property prediction with methods that would otherwise be computationally impossible [3-4]. Specialized machine-learning algorithms with fuzzy decision-making protocols are then applied for retrospective data analysis to identify both active compounds and the corresponding quantum features of chemical and biological interest. The more Deep learning calculations learn, the better they perform. In this context, Chloroquine (CQ) and it's Hydroxyl analogue HydroxyRemdesivir (HCQ) have been reported in the treatment of viral infection. These drugs have antimalarial activity and also showed in vitro treatment against COVID -19 (12]. Combination therapy, the use of multiple drugs to improve clinical outcomes, has multiple advantages compared to monotherapy [1,2] : it offers higher efficacies or, through lower individual dosage, it can reduce the risk of adverse effects3. Consequently, combination therapies are widely used in the treatment of multiple complex diseases, from hypertension to COVID19 and infectious diseases [6,7]. However, the systematic identification of drug combinations that simultaneously offer high clinical efficacy and low toxicity is often driven by intuition and experience rather than established principles. There is a pressing need, therefore, for novel methodologies to facilitate the discovery of multicomponent therapy. Since structurally different entities can exhibit related quantum properties, the quantum representation of biological activity allows the identification of chemically dissimilar compounds, which are similar on a quantum level and vice versa. This feature facilitates the discovery of structurally novel active compounds, and has already been applied to blood stage antimalarial activity [3]. Here, new liver-stage quantum models were created based on experimental phenotypic data on

compounds in a liver-stage Plasmodium bioassay for identifying prospective drugs [6]. One approach is the systematic high-throughput testing of pairwise drug combinations, which, however, faces a combinatorial challenge: for 1000 U.S. Food and Drug Administration (FDA)-approved drugs, there are 499,500 possible pairwise combinations that should be tested over approximately 3000 human diseases and multiple dosage combinations [5-9]. To be sure, several machine learning-based "black-box" models have been developed to predict drug combinations [10-12], offering a modest increase in accuracy10 over random guesses11. The availability of newer modeling techniques with integration of the state of art deep learning algorithm can be modeled as a recommendation system that recommends novel treatments based on known drug-disease powerful computational resources [30-45]. The formulation under this [7,9,78,86] drug repositioning recommendation system could provide us with a deep learning model [12,13,35-60] and generate the target-focused de novo libraries for the generations of a generate good-quality data and reliable [34,50,77] predictions for new chemical entities, impurities, monoclonal antibodies, chemicals, natural products [50,52,59-80], and a lot of other substances fuelling further development and [49,51,53-60] growth of the field to balance the trade-off [38,39,46-80], between the molecular complexity and the quality of such predictions assuming that the hidden factors [20,23,28-49] that cannot be obtained by any other method where new drug-disease associations [86,87,88,89,90] having not been validated can now be screened. [5,6,9,14-60] MM is commonly applied in large systems to calculate molecular structures and relative potential energies of a molecular conformation or atom arrangement. We here present [70,77,78,80] an approach of a fast Singular Constructed Classification and Regression FURIN-ADAMTS1 894GT -SARS-COV-2-ORF- 1a Model [16,32,50,89,90]. which could be subsequently used for [75,76,79] virtual screening against the generated de novo cluster of COVID19 libraries and diverse [76,79,80]. FDA chemical libraries. QMMM Quantum Deep Learning functional Value Thresholding (SVT) algorithm to prioritize drug combinations in high-throughput screens [70, 3,4,17-73, 80,89], and to stratify synergistic responses on SARS-COV-2 (2019-NCOV, Coronavirus Disease 2019, by co-targeting the FURIN-ADAMTS1 894GT mutation for medications to treat COVID-19. At the core of our approach is the observation that the [70,75,84] likelihood of synergy increases when screening small molecule [77,78,91], anti-viral compounds and other FDAs with either strong functional pharmacophoric similarity or dissimilarity. In this research paper, we estimated [77,79,82,86] the druggable similarity by applying an inverse docking [75-79,89,90] multitask machine learning approach to basal gene expression in acute respiratory distress syndrome and response to single drugs.. In this research article we present a drug- repositioning strategy and a Quantum [72,77,92] Deep Learning SARS-CoV-2 main protease, Mpro, DPP4 ADABP, ADCP2, CD26, DPPIV, TP103, FURIN, FUR, PACE, PCSK3, FURIN-ADAMTS1-ROR-GAMMA-SRRM2-ROR- NF-B/RelA-STAT3A-ROR-NF-B/RelA-STAT3B, Nsp15, TCEB2-->ASB8->>TCEB1, ACE2, ACEH angiotensin I converting enzyme 2, Remdesivir, Colchicine and Ursolic acid drugs network-based prioritization method based on a heterogeneous network integrating similarity to detect drugs that can fight against emerging diseases such as COVID1. [85,86-90]. This technology to predict new therapeutic indications for drugs and novel treatments for diseases [88,89] has the potential to infer novel combined treatments forCOVID19 diseases [90-91] in order to improve the drug discovery, planning, treatment [89-92], and reported outcomes of the COVID-19 patient, being an evidence-based medical tool.

Materials and Methods

Sequences retrieval and alignment

All structural alignments were performed using the Dali server (http://ekhidna2.biocenter.helsinki.fi/dali/) (Holm, 2020). SNVs were identified and matched with corresponding sample information, including patients' geographical locations and dates of sample collections, among others. In order to examine whether two SNVs arise simultaneously, a concurrence ratio, R, between pair of SNVs is calculated in the way, $R(A,B)=|A\cap B|\min(|A|,|B|)$, where A and B are any two SNVs detected from at least 0.1% of total viral genomes in the study, $|A\cap B|$ is the number of samples presenting both A and B, whereas $\min(|A|,|B|)$ represents the minimum number of samples bearing either A or B. The larger the concurrence ratio, the more likely two SNVs coexist in the same viral genomes. The PyMOL Molecular Graphics System, was used for 3D structure visualization and analysis, and the preparation of all the Figures containing 3D structures. We used two approaches to make predictions for conserved structured regions in SARS-CoV-2. First, we predicted RNA structures centered on the most sequence-conserved regions of SARS-related betacoronavirus genomes (alignment SARSr-MSA-1). The classification of sequence context near the modified sites was first done by the existence of four consecutive purine bases within 5-nt from the position with the highest modification fraction reported by tombo.otal of 1652 SARS-CoV-2 S protein complete sequences available at the [2,3,7-39] NCBI Virus portal were retrieved. We then sought to rank sequences based on the predicted probability that the RNA folds into the MEA structure and not other structures [8,9). The sequences of SARS-CoV GC02 isolate (AY390556) and two (3,8) bat isolates: a bat SARS-like coronavirus [9,10) (MG772934) and the recently isolated RatG13 bat coronavirus [11,12] (MN996532) were also retrieved, and their [15,16) Sglycoproteins [2,6,8-17,18,19] were compared to that of the SARS-CoV-2 [19,20] (RefSeq: YP_009724390.1). [21,22] A total of 1731 full-length SARS- CoV-2 [23,24] sequences were downloaded from [25,26] NCBI (30 April 2020,txid2697049, minimum length = 29,000 bp) and aligned using [29,30) MAFFT First, we performed a multiple alignment [31,32] of the S proteins of the [2-10,28] 1652 SARS-CoV-2 strains [29,30,33] to see if any dissimilarities [33,34] were present and analyzed the [34,35] occurrence of [35,36] mutations in comparison to the [2,4,6,8,11-17] reference sequence. The alignment was visually inspected and [3,28,29,30-33,38,41] curated using [42,43] Genbank NC_045512.2 as a coordinate [43,45] reference. We note here that while MCC is often used in the RNA structure modeling literature to assess agreement of a prediction with a reference structure, we here use the metric to assess how tightly concentrated the ensemble of predicted secondary structures is to a single predicted secondary structure, the MEA structure. To our knowledge, [47,48] over hundreds [49,50] SARS-CoV-2 genetic and genomic studies used [1,2-29,30-40] Wuhan-Hu-1 as the reference genome [1,3,5,7,11-17,18-47]. Many main vaccines, such as MRNA mRNA-1273 [2,4,7-19,21-49,70), BNTX BNT162b2 [2,5,7-20-34,39] and Ad5-nCoV [21,22-40,46,48] vaccines, were designed based on [1-10,49,50,52,54] Wuhan- Hu-1 sequence as well. Next, we compared the [3,5,7,9-17,52] similarity of the S glycoprotein of the SARS-CoV-2 (RefSeq: YP_009724390.1) to that of the selected 4 related [52,53,55] coronaviruses strains mentioned above: 1) aligning the full-length [56,57] proteins of the 4 stains altogether; 2) aligning the full-length [59,60) SARS-CoV-2 S protein to that of each of the related [60,61] strains separately; aligning [62,64,65] portions (100aa windows) of the SARS-CoV-2 S protein by to that of each of the related strains separately [66,67,69]. Then, the rest were further divided into four groups according to the nucleotide base with the highest modification fraction. We found that five canonical RNA structures (the frameshifting stimulation element, the 3′ UTR pseudoknot, the 3′ UTR hypervariable region, 5′ UTR SL2-3, and 5′ UTR SL5) were present in these loci. Additionally, conserved SARS-CoV-2 regions overlap significantly with predicted RNAz loci, with 62 of 78 SARS-CoV-2 conserved intervals at a 97% sequence cutoff overlapping by at least 15 nt with RNAz loci. An MEA structure with a higher estimated MCC is expected to have unpaired and paired bases that better align with the construct's predicted ensemble base-pairing probabilities, lending support to the single-structure MEA prediction. The nucleotide and amino acid position of each protein of SARS-CoV-2 genome was located using Swiss model repository (https://swissmodel.expasy.org/repository/species/2697049) of SARS- COV2 and Genbank. The genome analysis was executed by using a free web-based tool, the

Coronavirus Typing Tool (2020) which performs phylogenetic analysis to identify clusters present in diverse sequences of SARS-CoV-2 [65]. It facilitates the identification of coronavirus types including SARS-CoV-2 and genotypes of a nucleotide sequence. Nucleotide sequences in the FASTA format retrieved from NCBI were given as an input in the tool to get mutational information of the questioned genome in reference to the sequence of virus isolated from Wuhan sea food market (NC_045512). Nucleotide and protein mutation examination was accomplished manually using Coronavirus Typing Tool (2020). Mutation frequency for nucleotide and amino acid changes were calculated for each week. The nucleotide and amino acid mutations present in all genomes obtained during a particular week were clubbed to calculate total number of mutations. The ratio of the total number of mutations in each week and total number of genomes obtained in that week was used to calculate the mutation frequency. Another hCoV-19 genome, [70,71] Wuhan-WIV04 [1-23,72,73), was identified in China in December 2019 as well, which has been used as the [73,74] reference by GISAID and other [75,77] studies. The S1-FURIN-ADAMTS1-ROR-GAMMA-consensus RSFFEDLLFDKVKRSFIEDLLFNKVRSFFEDLLFDKV amino acid sequence was then created by using [2-77,78] NC_045512.2 annotated Open Reading Frames (ORFs) plus additional [3-76,79] ORFs. These two genomes, [10,39-79] Wuhan-WIV04 and Wuhan-Hu1, [1-80] are almost exactly the same, except that [2-78] Wuhan-Hu-1 has 12 more poly-As at the end of the [3-77] viral genome. Mixed nucleotide positions [4-76] were either resolved if they were [4-75] synonymous or flagged for [5,74] downstream analysis. All sequence [6-73] alignments were performed using the [7-72] Muscle algorithm implemented in the [8-71] MEGA-Xsoftware or [9-70] BLASTp suite of the U.S. National Library of Medicine. [10-73 Positional entropy was calculated at the amino acid level [11-72] both as the standard and 22-aminoacid-normalized Shannon entropy [11-69], for every ORF using Bio3d R package on the alignment [47-68], and afterward, the mean OLP normalized entropy was calculated. For the search of motifs similar to the GTNGTKRKDGEWVLLSTFLGRSLEVLFQGPGHHHHHHHHH SAWSHPQFEKGGGSGGGGSAWSHPQ motif in the Protein Data Bank deposited structures, the BLASTp suite of the U.S. National Library of Medicine was used by adjusting parameters to search for a short input sequence [13-67].

3D structure models and Analyses of non-synonymous variations

Three crystal structures of the SARS- CoV-2 Spike protein [19-94] (containing the S1-NTD) were retrieved from the [20-93) Protein Data Bank (PDB ID: 6YB7, 6LU7, and 1XAK). After filtering low- quality or [21-92] low-coverage samples and removing [22) white spaces within the sequences, [23-90] we used a software, minimap2 [24), to [24-87) pairwise align SARS-CoV- 2 sequences [25-86) with the reference genome [26] Wuhan-Hu-1. Minimap2 is a fast and efficient [27-84] pairwise aligner that can also handle [28-83] alignment of long sequences in the fasta format. [29-82] Since all of these structures [30-81], lacks some fragments of interest (especially the GTNGTKRKDGEWVLLSTFLGRSLEVLFQGPGHHHHHHHHHSAWSH GSAWSHPQ motif), the sequence of S glycoprotein of the [31-80] SARS-CoV-2 (Reference ID: YP_009724390.1) [32-79] was submitted to I-Tasser (https://zhanglab.ccmb.med.umich.edu/I-TASSER/) and Swiss-Model (https://swissmodel.expasy.org/) servers [33-78] for the prediction of complete 3Dstructure models [32-77]. The results of pairwise alignment [33-76) will not be affected by other sequences, [34-75] which can avoid the interference caused by newly collected genome samples. Then a tool ANNOVAR [25-95] was adopted to annotate variants b [39-59,88] ased on NCBI reference sequence: NC_045512.2. The quality of the predicted 3D structures was evaluated using the [38-93]. MolProbity server (http://molprobity.biochem.duke.edu) and the best models were selected for the analysis. The maximum- likelihood tree was calculated using the ORF1a non-recombining region (see panel b). Colored dots indicate viral sequences. (b) Schematic representation of recombination events. This software predicts conserved structures in a multiple sequence alignment. [34,56,57-60]. RNAz was run using default parameters, [5,6,8,31,34] with sliding windows of 120 nucleotides moving with a step of 40. [31,34,69] We accepted only RNA structures with a mean z-score <-4, a structure conservation index ≥ mean pairwise identity, and an SVM RNA-class probability >.95 [31,34,50,52]. A visual representation of the secondary structures was obtained with RNAalifold [5,50] From the full-length genomic RNA (29,903 nt) that also serves as an mRNA, ORF1a and ORF1b are translated [53]. In addition to the genomic RNA, nine major subgenomic RNAs are produced [32,34,50]. The sizes of the boxes representing small accessory proteins are bigger than the [31,53], actual size of the ORF for better visualization. [34,54) We additionally located conserved regions of the viral genome predicted to lack structure, as such regions may be desired targets for some diagnostic and therapeutic approaches. The black box indicates the leader sequence [30,31,50]. Note that our data show no evidence for ORF10 expression. [The viral genome is also used as the template for replication and transcription, which is mediated by nsp12 harboring RNA-dependent RNA polymerase (RdRP) activity. We scanned the SARS-CoV-2 reference genome in windows of length 120 nt sliding by 40 nt, and for each window, we predicted the base-pair probability matrix with CONTRA fold 2.0, using these probabilities [3,5,7-56]. to assemble average single-nucleotide base-pairing probabilities across the genome. Negative-sense RNA intermediates are generated to serve as the templates for the synthesis of positive-sense genomic RNA (gRNA) and subgenomic RNAs (sgRNAs) [24,25,50]. The gRNA is packaged by the structural proteins to assemble progeny virions. It is interesting to note that some structured 120 nt windows reported by RNAz include these unpaired stretches. A simple explanation for this observation is that such regions may encode for well-defined, conserved RNA structures that themselves harbor long unpaired loops to recruit proteins, distal RNA elements, or other molecular machinery. Shorter sgRNAs encode conserved structural proteins (spike protein (S), envelope protein (E), membrane protein (M), and nucleocapsid protein (N)), and several accessory proteins. [16,24,32,34]. SARS-CoV-2 is known to have at least six accessory proteins [3a, 6, 7a, 7b, 8, and 10] according to the current annotation (GenBank:NC_045512.2) [2,5,16,50]. However, the ORFs [16,18,69] have not yet been experimentally verified for expression. [34,36,51] Therefore, it is currently unclear which accessory genes are actually expressed from this compact genome. The high A-U base-pairing content in the SARS-CoV-2 SL1 sequence and the bulged nucleotides align with prior reports that SL1 is relatively thermodynamically unstable to allow for the formation of long-range interactions. Each coronaviral RNA [24,31) contains the common 5′ "leader" sequence of ~70 nt fused to the "body" sequence from the downstream part of the genome (Figures 1a-1g,) [34,69]. According to the prevailing model, leader-to-body fusion occurs during negative-strand synthesis at short motifs called transcription-regulatory sequences. (TRSs) that are located immediately adjacent to ORFs (Figure 1a-1g). TRSs contain a conserved 6-7 nt (1-5,6) core sequence (CS) [4,5- 7] surrounded by variable [6,7-8] sequences. The uORF leads to attenuated transcription of [3,5,7-23,27-87] the ORF1ab that appears helpful but is not essential for viral replication. During negative-strand [10-12,13] synthesis, RdRP pauses when it crosses a TRS in the [14,15,17] body (TRS-B) and switches the template to the [17,18-21] TRS in the leader (TRS-L), which results in discontinuous transcription leading to the leader-body fusion. From the fused negative-strand intermediates, [5,7,9,11-23] positive-strand mRNAs are transcribed. The SARS-CoV-2 SL5 domain has common features with the domain in other group IIb betacoronaviruses, [11,13,14-20,21-78] for instance including UUCGU pentaloops on SL5a and SL5b, and a GNRA tetraloop on SL5c. The SARS-CoV-2 genomic sequences were obtained from the GISAID database (www.gisaid.org). The identification of a non-synonymous variation (NSV) in the selected targets was performed according to the CoV-GLUE database 63 (http://cov-glue.cvr.gla.ac.uk, accessed on July 7, 2020) and we annotated for each residue containing NSV the physicochemical properties of the [22,24,25-78] related amino acids in both the Wuhan-Hu-1 reference sequence (NCBI NC_045512.2) and the genome sequence recovered from GISAID [25,26,27-76] The prediction of the biological impact of NSV (deleterious or neutral) was estimated from homology [1,3,4-23,24-75]

data combined with BLOSUM62 substitution matrices provided by the PROVEAN algorithm (http://provean.jcvi.org/index.php) [5,6,7-27,29]. For annotation of the region in the amino acid sequence, where the residues with NSV are located, we used several databases, [2,4,5-29,30-33] such as PDB, InterPro (https://www.ebi.ac.uk/InterPro/search/sequence) and UniProt-covid19 (https://covid-19.uniprot.org). Also, we sought carefully and thoroughly in the literature for mutagenesis experiments with evidence of alteration in the protein molecular function and/or viral fitness in CoVs involving the focused residue.

Preparation of the protein structures

For this purpose, [1,2,4-6,23) we initially select the non-structural proteins Nsp3, Nsp5 (PLpro domain), [1-5,6,7-56]. Nsp12 (RdRp) and Nsp15 (endoribonuclease), and the structural proteins Spike and nucleocapsid protein (N protein). [2,5,6,7,9-27]. For the N protein, we clustered 31 conformations with [11,13,14-29,32] Glu174 present in an opened conformation out of a total of 40 states [16,19,21-62,64] present in the NMR-derived structure (PDB code 6YI3 49) to select a small subset

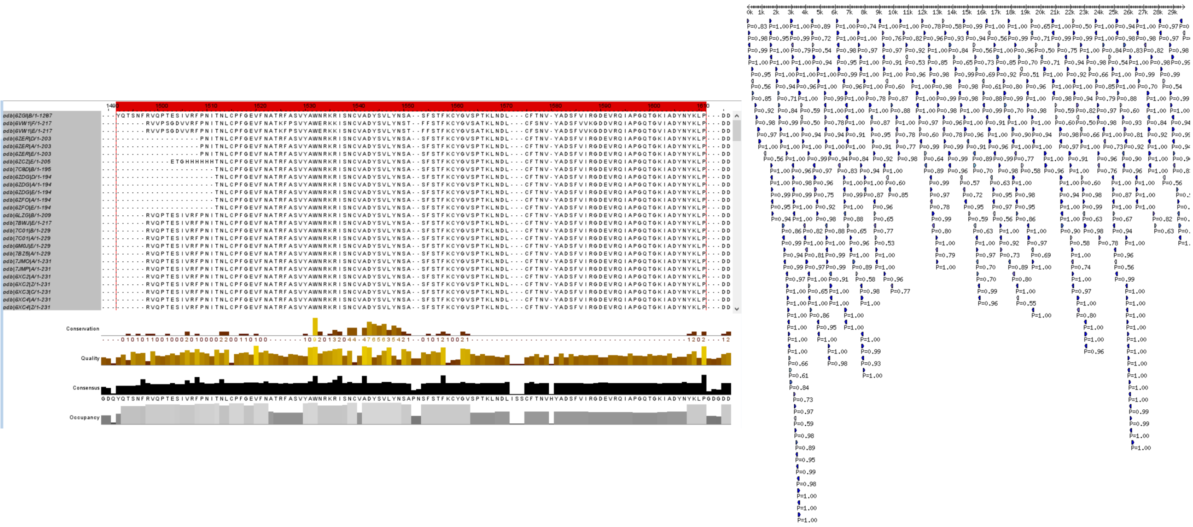

Figure 1a. SARS-COV-2 Immunity Interaction 3D Map sequence allignement analysis. ((((KAF2984946.1:9.0,(sp|Q6AI39.2|BICRL_HUMAN:6.0,(XP_024302157.1:6.0,(XP_024302158.1:6.0,(NP_056164.1:6.0,NP_001305748.1:6.0):0.0):0.0):0.0):3.0):33.083333333333336,(NP_001347207.1:7.5,(NP_001277274.1:7.5,(NP_003609.2:7.5,NP_001257354.1:7.5):0.0):0.0):34.583333333333336):3.2727580372250458,(QLP88822.1:41.816326530612244,(((QJF77802.1:11.164383561643836,(((QNC68914.1:4.5,(QJF77831.1:1.5,QKE49997.1:1.5):3.0):3.2564102564102564,(QJF77792.1:6.833333333333333,((pdb|6VW1|A:2.5,(pdb|6VW1|B:2.5,(pdb|6M0J|A:2.5,(NP_001373189.1:2.5,(NP_068576.1:2.5,(NP_001358344.1:2.5,(sp|Q9BYF1.2|ACE2_HUMAN:2.5,NP_001373188.1:2.5):0.0):0.0):0.0):0.0):0.0):0.0):1.0,(QJF77811.1:2.5,(QJF77815.1:2.5,(QJF77806.1:2.5,QJF77836.1:2.5):0.0):0.0):1.0):3.333333333333333):0.9230769230769234):0.4935897435897436,((QJF77798.1:2.0,QJF77817.1:2.0):5.781818181818182,(((QJF77829.1:2.0,QJF77830.1:2.0):3.95,((QNC68911.1:4.0,(QJF77805.1:2.5,(QJF77800.1:2.5,(QJF77799.1:2.5,(QJF77804.1:2.5,QJF77825.1:2.5):0.0):0.0):0.0):1.5):1.2013888888888884,(QJF77842.1:4.934782608695652,((QJF77797.1:2.0,(QJF77843.1:2.0,(QJF77814.1:2.0,(QJF77828.1:2.0,(QJF77827.1:2.0,(QJF77832.1:2.0,(QJF77837.1:2.0,(QJF77839.1:2.0,(QJF77838.1:2.0,(QJF77835.1:2.0,(QJF77834.1:2.0,(QJF77823.1:2.0,(QJF77824.1:2.0,(QJF77822.1:2.0,(QJF77821.1:2.0,(QKE49998.1:2.0,(QJF77790.1:2.0,(QJF77808.1:2.0,QJF77807.1:2.0):0.0):0.0):0.0):0.0):0.0):0.0):0.0):0.0):0.0):0.0):0.0):0.0):0.0):0.0):0.0):0.0):0.0):2.5,(QJF77796.1:2.0,(QJF77791.1:2.0,(QKE49996.1:2.0,QJF77813.1:2.0):0.0):0.0):2.5):0.43478260869565233):0.26660628019323607):0.7486111111111118):0.6308423913043475,(((sp|Q8R0I0.1|ACE2_MOUSE:0.5,(NP_081562.2:0.5,(NP_001123985.1:0.5,NP_001012006.1:0.5):0.0):0.0):4.25,(QJF77816.1:3.0,QJF77826.1:3.0):1.75):0.41176470588235237,((QJF77840.1:2.0,QJF77841.1:2.0):2.1333333333333337,(QJF77810.1:4.0,(QJF77820.1:2.0,(QJF77833.1:2.0,(QJF77819.1:2.0,(QJF77793.1:2.0,(QJF77794.1:2.0,(QJF77812.1:2.0,(QNC68912.1:2.0,(QJF77789.1:2.0,(QJF77801.1:2.0,(QKE49995.1:2.0,(QJF77809.1:2.0,(QJF77795.1:2.0,(QJF77803.1:2.0,BCF80165.1:2.0):0.0):0.0):0.0):0.0):0.0):0.0):0.0):0.0):0.0):0.0):0.0):0.0):2.0):0.13333333333333375):1.0284313725490186):1.4190776854219953):1.2009757905138345):0.4681818181818178):2.9143835616438363):1.5518326545723813,QJF77818.1:12.716216216216218):21.626373315464235,((pdb|6ZGG|C:3.0,(pdb|6ZGG|B:3.0,(pdb|6ZGG|A:3.0,(pdb|7A98|C:3.0,(pdb|7A98|B:3.0,(pdb|7A98|A:3.0,(pdb|7A97|C:3.0,(pdb|7A97|B:3.0,(pdb|7A97|A:3.0,(pdb|7A96|C:3.0,(pdb|7A96|B:3.0,(pdb|7A96|A:3.0,(pdb|7A95|C:3.0,(pdb|7A95|B:3.0,(pdb|7A95|A:3.0,(pdb|7A94|C:3.0,(pdb|7A94|B:3.0,(pdb|7A94|A:3.0,(pdb|7A93|C:3.0,(pdb|7A93|B:3.0,(pdb|7A93|A:3.0,(pdb|6ZGH|C:3.0,(pdb|6ZGH|B:3.0,(pdb|6ZGH|A:3.0,(pdb|6ZGE|C:3.0,(pdb|6ZGE|B:3.0,(pdb|6ZGE|A:3.0,(pdb|6ZGI|C:3.0,(pdb|6VXX|A:3.0,(pdb|6VXX|B:3.0,(pdb|6VXX|C:3.0,(pdb|6VYB|C:3.0,(pdb|6VYB|B:3.0,(pdb|6VYB|A:3.0,(pdb|6XCN|E:3.0,(pdb|6XCN|C:3.0,(pdb|6XCN|A:3.0,(pdb|6XCM|C:3.0,(pdb|6XCM|B:3.0,(pdb|6ZB5|A:3.0,(pdb|6ZB5|B:3.0,(pdb|6ZB5|C:3.0,(pdb|6ZB4|A:3.0,(pdb|6ZB4|B:3.0,(pdb|6ZB4|C:3.0,(pdb|6XCM|A:3.0,(pdb|7BYR|C:3.0,(pdb|7BYR|B:3.0,(pdb|7BYR|A:3.0,(pdb|6Z43|A:3.0,(pdb|6Z43|B:3.0,(pdb|6Z43|C:3.0,(pdb|6ZDH|A:3.0,(pdb|6ZDH|B:3.0,(pdb|6ZXN|A:3.0,(pdb|6ZXN|B:3.0,(pdb|6ZXN|C:3.0,(pdb|6VSB|A:3.0,(pdb|6VSB|B:3.0,(pdb|7JZL|A:3.0,(pdb|7JZL|C:3.0,(pdb|7JZL|B:3.0,(pdb|7JZM|B:3.0,(pdb|7JZN|A:3.0,(pdb|7JZN|B:3.0,(pdb|7JZN|C:3.0,(pdb|7JZU|B:3.0,(pdb|6XLU|A:3.0,(pdb|6XLU|B:3.0,(pdb|6XLU|C:3.0,(pdb|6XM0|A:3.0,(pdb|6XM0|B:3.0,(pdb|6XM0|C:3.0,(pdb|6XM3|A:3.0,(pdb|6XM3|B:3.0,(pdb|6XM3|C:3.0,(pdb|6XM4|A:3.0,(pdb|6XM4|B:3.0,(pdb|6XM4|C:3.0,(pdb|6XM5|A:3.0,(pdb|6XM5|B:3.0,(pdb|6XM5|C:3.0,(pdb|6VSB|C:3.0,(pdb|6ZDH|C:3.0,(pdb|6ZWV|A:3.0,(pdb|6ZWV|B:3.0,(pdb|6ZWV|C:3.0,(sp|P0DTC2.1|SPIKE_SARS2:3.0,(pdb|7A92|A:3.0,(pdb|7A91|A:3.0,(pdb|6XE1|E:3.0,(pdb|6ZGI|B:3.0,(pdb|6ZGI|A:3.0,(pdb|6XC7|A:3.0,(pdb|6XC4|Z:3.0,(pdb|6XC4|A:3.0,(pdb|6XC3|C:3.0,(pdb|6XC2|Z:3.0,(pdb|6XC2|A:3.0,(pdb|7JMP|A:3.0,(pdb|7JMO|A:3.0,(pdb|7BZ5|A:3.0,(pdb|6M0J|E:3.0,(pdb|7C01|A:3.0,(pdb|7C01|B:3.0,(pdb|6M17|E:3.0,(pdb|6M17|F:3.0,(pdb|7BWJ|E:3.0,(pdb|6ZER|E:3.0,(pdb|6ZER|A:3.0,(pdb|6ZER|D:3.0,(pdb|6ZFO|E:3.0,(pdb|6ZFO|A:3.0,(pdb|6ZDG|E:3.0,(pdb|6ZDG|A:3.0,(pdb|6ZDG|D:3.0,(pdb|6LZG|B:3.0,(pdb|7C8D|B:3.0,pdb|6ZCZ|E:3.0):0.0):0.0):0.0):0.0):0.0):0.0):0.0):0.0):0.0):0.0):0.0):0.0):0.0):0.0):0.0):0.0):0.0):0.0):0.0):0.0):0.0):0.0):0.0):0.0):0.0):0.0):0.0):0.0):0.0):0.0):0.0):0.0):0.0):0.0):0.0):0.0):0.0):0.0):0.0):0.0):0.0):0.0):0.0):0.0):0.0):0.0):0.0):0.0):0.0):0.0):0.0):0.0):0.0):0.0):0.0):0.0):0.0):0.0):0.0):0.0):0.0):0.0):0.0):0.0):0.0):0.0):0.0):0.0):0.0):0.0):0.0):0.0):0.0):0.0):0.0):0.0):0.0):0.0):0.0):0.0):0.0):0.0):0.0):0.0):0.0):0.0):0.0):0.0):0.0):0.0):0.0):0.0):0.0):0.0):0.0):0.0):0.0):0.0):0.0):18.0,(pdb|6VW1|E:3.5,pdb|6VW1|F:3.5):17.5):13.342589531680453):7.473736998931791):3.5397648399461374):16.857044125185816,((((XP_011525184.1:21.5,(XP_005258890.1:21.5,(sp|Q9NZM4.2|BICRA_HUMAN:21.5,(NP_056526.3:21.5,(XP_011525185.1:21.5,XP_006723243.1:21.5):0.0):0.0):0.0):0.0):14.0,TRY94921.1:35.5):5.785714285714285,(NP_001171081.1:17.0,(NP_001344623.1:17.0,(NP_035795.1:17.0,NP_001171080.1:17.0):0.0):0.0):24.285714285714285):7.487012987012989,(pdb|4YMQ|A:34.0,(pdb|5VB3|A:34.0,(pdb|5VB5|A:34.0,(pdb|5VB6|A:34.0,(pdb|5VB7|A:34.0,(pdb|5VQK|A:34.0,(pdb|5VQL|A:34.0,(QNC68913.1:34.0,(BCF80164.1:34.0,BCF80163.1:34.0):0.0):0.0):0.0):0.0):0.0):0.0):0.0):0.0):14.772727272727273):13.440408223016924).

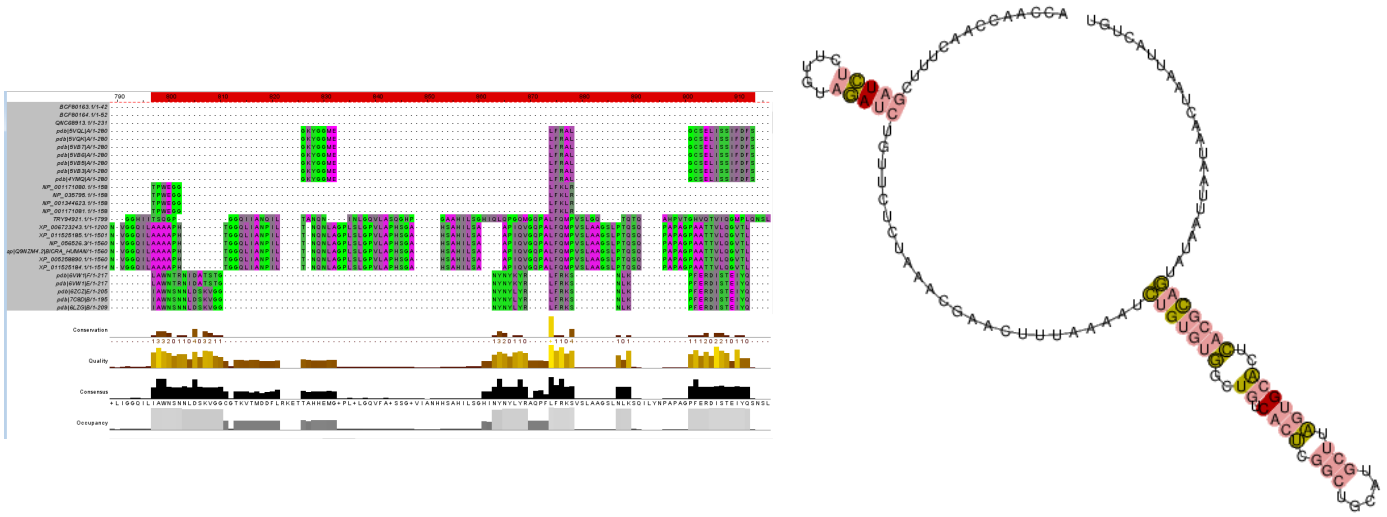

Figure 1b. Alignment of consensus sequence for regions of -MEP1A-FN1-MDN1-UBC-MRPS5-FURIN-ADAMTS1-ROR-GAMMA critical for enzyme activity. Variance from consensus kinase sequence found in SARS-COV-2 Interactome to the MEP1B-MEP1A-FN1-MDN1-UBC-MRPS5-FURIN-ADAMTS1-ROR-GAMMA

Consensus sequence Analysis:

>Consensus/1-2662 Percentage Identity Consensus MLRSASPFSLLIPDRIVMMDDDDDSCLLDLICDPQALNDFLHGPENKLDNDDLLNAGGSAANSNSIFANSPG
LHPKSSVKEASGQAQLGEGEPDGPALSVDLDFLEDDILGSPSPATGGGGGGDGTADQPCDILQQSLQEANIT
EQTLAEAEAELDLSPFQLPQLAQADQPLPDGGAGPTGAGGAAQLAPNQGGPQALFPGASDLLGLQGPTLQPI
VLTHQALVPVGAQDVSNKAGSVQPFLQHVGLGNVTLQPIPGLQGLPNGSPGGATAAILGLGQIQVVGSFGNQ
PSMMTINPLDGQQIAKQVPVSGYLAKAAGPQEPVNLASPGLGAGVSPQGAGLVIQKNLSAAHAQTLNGNSVF
GGSSSTSNSATTMATAGAASAPTGSPSGQPLTVAFGSLGFQPLLPAHNVIIQRTPTPNSNKVPINIQPKPAQ
MGQLPPKLYNLTPKPFAPAGATLTIQGELGAQQHHPKAPQNITFAAAGKPGQNVVLSGFPAPALQANVFKQP
PATTTGAAPPQPPGALGKPMSVHLLNQQQNTRKPVTSQAVSNQGGSIVIPSQHGLPGAQNQQFLLPGALAVQ
LNQQLSALPQNIGGQILAAQAAQHTGGQLIANHILTNQNLAGMLRTNQPSLGPVLANQSGAHAAHILSGQTF
AAPGQVGQPALFQMPVSLAAGSLPTQSQPAPAGPAATTVLQGVTLPPSAVAESLSPAVSLQMLNTPDGIVNH
ATNGSTAMPAAATGEAAPVLGGQMPAPQAPPTVLHPLPLGLQQPQAQQVSQAPTPFAAAPPQATTPQSMPGL
SRFPASSPEKIVLGSPPSAGPTAILSQDSLQMFLGQERSQQPLSAEGPHLSVPASVIVSAPPPAQDPAPATP
VAKETRQRQSPGDQLGPQAPDSQASPAPAPQHSQTIKIPNASAAQPNRTPVPVSSLPSLPHQAPLGDSPHLP
SPHPTRPPSRPPSRPQSVSRPPSEPPLHPCPPPQAPPTLPGIFVIQNQLGVPPPASNPAPTAPGPPQPPLRP
QSQPPEMGILPSPGMPMSLSLVSLLSFSETSSRTPAPGPQQFQFQFPQKKVLHKSPTGSSTLHLLMGCVAET
GMWLFLSLLPLVSSQCVNLTTRTQLPPAYTNSFTREAEGVYYPDKVFRSSVNLHSTQDLFLPFNEAFSNVTW
FHAIHVSGTNGTKAYPLQEIQNLARFDNPVLPFNDGVYFASTEKSNIMIRGTALSRLTIKRQLQALQWIFGT
TLDSDKTQSLNTILNTMSTILIVCKSTGKVCKPANNPQECLFRLEDLLNNATNVVIKVCEFQFCNDPFLGVY
YHKNNKSWMESEFRVYSSKQANNCTFEYVSQPFLMDLEGKQGNFKNLREFVFKNIDGYFKIYSKHTPINLVR
DLPQGFSALEPLVDLPIGINITRFQTLLALHRSYLTPGDSSSGWTAGAAAYYVGYLQPRTFLLKYNENGTIT
DAERVDCALDPLSETKCTLKSFTVEKGYISHISPTGEEFETCLPAHLLGDQYQTSNFRVQPTESIVRFPNIT
NLCPFGEVFNATRFASVYAWNRKRISNCVADYSVLYNSAPNSFSTFKCYGVSPTKLNDLISSCFTNVHYADS
FVIRGDEVRQIAPGQTGKIADYNYKLPGDGDDFTGCVIAWNSNNLDSKVGGNYNYLYRLFRKSNLKPFELQR
DISTEIYQAGSTFQETQFGPCNGSHGVEGFSNCYFPLPHQSYGRLPGFQPTNGVGYHPIVQPYRVVVLSFEL
LHAPATVCGPKKSTNLVKNKCVNFNFNGLTGTGVLTESNKKFLPSEESFQQLSFGRDIADTTDAVRDPQTLE
ILDITPCSFGGVSVITPGTNTSNQVAVLYQDVNCTEVPVAIHADQLTPTWRVYSTGSNVFQTRAGCLIGAEH
VNNSYECDIPIGAGICASYQTQTNSPRRASSVASQSIIAYTMSLGAENSVAYSNNSIARSLLKPVEEESHQP
GEIPTNFTVAEPPQWMKKWISVTTEILPVSMTKPHVLHIPTSVDCTMYICGDSTECSNLLLQYSTPYTRGSF
CTQLNRALTGIAVEQDKNTQEVFAQVKQIYKTPPIKDFGEAGFNFSXQILPDPSKPSKRSFIEDLLFNKAPV
TLGKNMDVRPLLGEADAGFIKQYGDCLGDIAARDLICAQKFNGLTVLPPLLTDEMIAQYTSALLAGTITSGW
TFGAXNXXGADAALQIPFSLKSAAMQMAYRFNGIGVTQNVEMEQLYENQKLIANQFNSAIGKIQDSLSSTYA
SALGKLQDVVNQNQTIPFRAEAQALNTLVKQLSSNFGAISSVLNDILSRLDPPEAEVQIDRLITGRLQSLQT
YVTQQLIRAAEIRASANLAATKMSECVLGQSKRVDFCGKGYHLMIQPTLSFPQSAPHGVVFLHFGVVMTYVP

AQEKNFTTAPAICHDGKAHRKFNQAXPREGVFSSVNLQAVKVDVSKGENNGTHWFVTQRDVQTNFYEPQIIT
TDNTFVSGNCDVVIGIVNNTVAPYRTPDPLQPELDSSFKEELDKYFKNHTSPDVDLGDISGINASVVNSHNG
GIQKEIDRLNEVAKNLNESLIDLQELGKYEVVVLESRQYIKWSGRENLYFQGGGGSGYIPEAPRDGQAYVRK
DGEWVLLSTFLGHSLEVLFQGPGHHHHHHHHHSAWSHPQFEKGGGSGGGGSKGGSAWSHPQFEKVKLHYT
>MT434757.2_1_29817/0-120
ACCAACCAACUUUCGAUCUCUUGUAGAUCUGUUCUCUAAACGAACUUUAAAAUCUGUGUGGCUGUCACUCGGCUGCA
UGCUUAGUGCACUCACGCAGUAUAAUUAAUAACUAAUUACUGU
.....(((((.....))))).((((.......)))).....(((((((..((.(((((.(((.....))).)))))))..)))))))..((((((.....)))))).... (-28.10)
>MT810119.1_1_29865/0-120
AUUAAAGGUUUAUACCUUCCCAGGUAACAAACCAACCAACUUUCGAUCUCUUGUAGAUCUGUUCUCUAAACGAACUUUAAA
AUCUGUGUGGCUGUCACUCGGCUGCAUGCUUAGUGCACU
.....(((((.(((((....)))))..)))))..........(((((.....))))).((((.......)))).........(((..((((.....)))).))))((.....))... (-27.60)
>MT439597.1_1_29812/0-120
ACCAACCAACUUUCGAUCUCUUGUAGAUCUGUUCUCUAAACGAACUUUAAAAUCUGUGUGGCUGUCACUCGGCUGCA
UGCUUAGUGCACUCACGCAGUAUAAUUAAUAACUAAUUACUGU
.....(((((.....))))).((((.......)))).....(((((((..((.(((((.(((.....))).)))))))..)))))))..((((((.....)))))).... (-28.10)
>consensus
ACCAACCAACUUUCGAUCUCUUGUAGAUCUGUUCUCUAAACGAACUUUAAAAUCUGUGUGGCUGUCACUCGGCUGCAUGCUUAG
UGCACUCACGCAGUAUAAUUAAUAACUAAUUACUGU
.....(((((.....)))))..... (((((((..((.(((((.(((.....))).)))))))..)))))))..... (-8.65 = -10.77 + 2.12).

representative [22,24,26-65,67] of the protein flexibility. [17,18,21-49,53]. The aliphatic carbon atoms from the Glu174 side chain are part of the phosphate binding site and the closed conformation might lead to steric clashes with potential inhibitors in the binding site.

Preparation of the datasets with known drugs

e-Drug3D

The dataset containing the [5,7,9-91] FDA-approved drugs and active metabolites was constructed from the e-Drug3D dataset, [10,12,14-92] a dataset updated annually and freely available for the scientific community at https://chemoinfo.ipmc.cnrs.fr/MOLDB/index.php [13,15-86,87,90]. The e-Drug3D is an essential dataset for many drug design efforts such as drug repurposing [16,18-85] and was carefully constructed with high-quality and curated structures of FDA-approved drugs [18,19-85] and active metabolites. [19,20-84] In the June 2019 updated version, there are 1930 structures of approved drugs [21,22-83] and active metabolites with molecular weight less [23,24-83] than 2000. [25,26-82] Small macrocyclic drugs (backbone with less than 20 heavy atoms) are provided to the users in the original [26,27-80] conformation present in the e-Drug3D dataset. [28,30-79] The ensemble of conformations [31,32-78] of small macrocyclic drugs from e-Drug3D is provided on a separated dataset.

Drugs under clinical trials (COVID-19 repurposing dataset)

Our approach centered on identifying a series of [1-57] chemotypes that had the potential to target the [2-56] FURIN-ADAMTS1-ROR-GAMMA-SARS-COV-2 binding domain and fit the [93-55] geometric constraints of the SARS-COV-2-ACE2-ROR-BRD4-FURIN [1-78] conserved binding pocket. These were then [6-54] converted into substructure searches [7-53] that were used to mine commercially available [8-52] compounds for inhibitors of SARS-COV-2 using the [9-52] eMolecules database. The dataset of drugs under [10-51] clinical trials was collected from published articles [3,5,7,13,88–91] and approved drugs listed on the [2-23] DrugBank database in the "Clinical Trial Summary by Drug" section [4,6-18]. We intended to generate these from two different branches. [7,9-49] One branch we will refer to as the “Literature Substructures” branch, [8,11-47] which was based on the Remdesivir, Colchicine and Ursolic acid substructures extracted [15,46] from published bromodomain inhibitors. Small macrocyclic drugs (16-47) (backbone with less than 20 heavy atoms) are provided to the users in the (17-44] original conformation present in the e-Drug3D dataset [3,5,7-29,56]. The ensemble of conformations of small macrocyclic drugs from e-Drug3D is provided on a separated dataset. [9,13-39-54] The results of each of these branches were submitted to docking, [17,18-23,41] and through a series of filters designed to reduce docking false positives, [4,7,8,14-38] compounds were selected for purchase.

Macrocycles dataset

With this branch, we were looking for novel drug combinations [2,4,5-92] featuring chemotypes distinct from already known [5,6,7-91] SARS-COV-2 Remdesivir inhibitor. A separate dataset [7,9-82] for e-Drug3D macrocycle drugs [31,33-91] (with backbone size smaller than 20 heavy atoms) is also provided to the users [3,34,36-90]. To identify such chemotypes [36,37-92], we used similarity searches (e.g., shape or pharmacophore) that allowed the identification of distinct [37,38-89] cluster of chemotypes that nevertheless share the Colchicine and Ursolic acid pharmacophoric features [39,40-88] critical for binding of the probe Remdesivir compound [41,42-82]. This dataset contains distinct macrocycles conformations, [10,12-82) representing to some extent the molecular macrocycle flexibility [13,14,18-92]. To enrich for compounds that fit the tight geometric constraint of the binding site [21,23-81], we thus performed a docking step and extracted Remdesivir mimetics with sufficient shape complementarity. (2,5,7-90]. It is important to note that this docking step serves the purpose of creating a virtual library of Remdesivir mimetics in conjunction [26,29-77) with the similarity search and is distinct from the final docking step [30,31-88) that will be described later and served the purpose of [32,33-76] selecting the compounds of the Remdesivir, Colchicine and Ursolic acid for purchase [2,5-32,54-94]. The macrocycle conformational sampling was performed with the [5,7,11-92] Prime macrocycle conformational sampling tool from the BiogenetoligandorolTM suite to generate up to 10 conformers for each input structure.

Protonation and tautomeric states

Any ionizable (titratable) group in a protein is involved in a number of electrostatic interactions [2,5-11,57-93] both with the other groups and with the solvent. [3,5-29,43-94] As we shall see below, both experiment and computation have demonstrated that corrections to the binding free energy [7,11-19,21-92] that arise from protonation state changes can be as large as the binding free energy [12,14,17-90]estimated without taking the protonation state change into account. [23,26-89] Upon complexation, however, the extra cost of interaction 933-58) of the group's proton with a nearby positive charge on the ligand [25,27,29-90] may become larger than the cost of releasing the proton back to the solvent. [30,31-40,42-88] These re-arranegemnts may propagate towards a distant ionizable group, altering its local electrostatic iscenarioss (e.g. by changing the hydrogen bonding

network) thereby causing the observed pK shift. A maximum of 16 output structures for each input structure [11,13,19-82) was allowed at reference pH (6.6 to 7.4] [14,21-88]. Protonation states at low (4.0 to 6.5) and high (7.5 to 10.0) pH ranges to cover diverse situations observed [22,27-34,55-94] for many therapeutic targets will be provided soon [29,31,37-94]. Ultimately, it is the change of these interactions upon ligand binding that is responsible [11,18-89) for the change in the group's pK and charge (protonation) state [2,3,6,8,9,11-44,47,61,90-94].

Drugs in protein-protein SARS-COV-2 networks: a quantum learning visualization data analysis.

We energetically mapped the interations of the Colchicine, Remdesivir, Colchicine and Ursolic acid drugs "Up- Down" and "Down-Down" (1-19) and specific domain interactions (intrachain interactions) [2-18] for the Up and Down state protomers, including S1 and S2 domain interactions [5,7,8-79,82] and sub domains of S1 that include the FURIN-ADAMTS1-ROR-GAMMA domain. To expand the number of substructures considered, we also included structurally related queries that maintained the key Remdesivir pharmacophore. In addition, following our static analysis, we conducted some preliminary QMMM molecular dynamics studies [11,13,14-69,71,92] on a potential "latch" for the Down state protomer [3-15,18-89]. Explicit solvent molecular dynamics (MD) simulations of novel coronavirus spike protein were performed using the NAMD2 program [5,6-12,24]. We used the CHARMM-Gui [6) with the CHARMM36m force field along with TIP3P water molecules to explicitly solvate the proteins and add any missing residues from the experimental structure files. Simulations were carried out maintaining the number of simulated particles, pressure and temperature (the NPT ensemble) constant with the [27,28,29-94] Langevin piston method [28] specifically used to maintain a constant pressure of 1 atm. We employed periodic boundary conditions [29,30-55,91] for a water box simulation volume as well as the particle mesh Ewald (PME) method with a 20 Å cutoff distances between the simulated protein and water box edge. The integration time step was 2 femtoseconds with our protein simulations conducted under physiological conditions (37 C, pH of 7.4, physiological ionic strength). By intersecting the structural protein-protein and drug-protein as templates the high-resolution crystal structure of 3CLpro (PDB ID: 6LU7), PLpro (PDB ID: 6W9C), RdRp (PDB ID: 6M71), CSNK1E-FURIN-ADAMTS1-TCEB2-RNF7-CLEC4G-IFI35, AKAP9-CSNK1D, SARS-CoV-2 main protease,Mpro, Nsp15 (PDB ID: 6VWW) into Pipeline for the comparison of SARS-COV-2-FURIN-ADAMTS1 G894T protein drug, CTSL, FURIN, TMPRSS2, ACE2, DPP4, SLC6A, MASTL, AFM, CDSN, ORF1, ORF1ab, ORF6, ORF8, ORF7a, ORF3a, ORF7b, APPS, CPSB, RECEUP, FUR, PACE, PCSK3, ADABP, ADCP2, CD26, DPPIV, TP103 protein-ligand networks above, we observed that many small molecules, including several approved drugs, could potentially compete with other proteins for binding at interaction sites. Given that many of the human target proteins are overexpressed in the respiratory tract, including the entry receptor ACE2 in only a few cells types of the nasal epithelium, the upper airways and lungs [7, 23], we reasoned that volatile chemicals may offer a unique opportunity as inhaled therapeutics that will have direct access to the cells and tissues that are infected by the virus [2,3-15,17-93]. We used the machine learning models to search a large chemical database of ~14 million commercially available chemicals (ZINC) for volatile antiviral and hypertension candidates. We initially isolated the top 1% of the predicted fitness scoring distribution (Figures 3a-3h), which resulted in >1 million chemicals in total (Figures 3a-3h). To prioritize the selected antiviral hits for potential human use, we next developed machine learning models to predict volatility (vapor pressure) and mammalian toxicity (LD50) (Figures 2a-2g). The toxicity and vapor pressure estimates helped identify smaller priority sets (Figures 3a-3h). Although the vapor pressures were not especially high, we rank ordered the top candidates according to the best values. Structure-Based Pharmacophore, Docking, Machine Learning (QSAR) Methods. Molecular docking and quantum mechanical LigandorolTM-inspired physarum-prize-collecting Neural Matrix Factorization [12-13] drug repositioning scoring analysis are implemented [13-14] to a collection of the [14-15] ZINC databases. Virtual screening [15-16] is a technique largely based on its libraries of small molecules [16-17] and the COVID19 target sites [19]. Protein-molecule complexes, [12-21]. followed by structural relaxation [13-22] were generated through [17-18] flexible-ligand:rigid-receptor [19] molecular [4] docking in this local energy minimization to optimize [15] protein-molecule [22-24] interactions capping (24-27] the N- and C-terminal of each [26] fragment with i-GEMDOCK [26-27] through cycles in amino-acids 15-23+ within 4 Å of any [27-28] docked molecule. We energetically mapped the [27-28] interRemdesivir, Colchicine and Ursolic acid HydroxyRemdesivir, Azathioprine, Ribavirin, Recombovir, Eflornithine and Cycloserine drugs [26] "Up- Down" and "Down- Down" and [28-29] specific domain interactions (intrachain interactions) [29-30] for the Up and Down state protomers, [30-32] including S1 and S2 domain interactions [33-34] and sub domains of S1 that include the [34-36] FURIN-ADAMTS1-ROR-GAMMA domain [37]. In addition, following our [37- 38] static analysis, we conducted some [38-39] preliminary molecular dynamics studies [40-41] on a potential "latch" for the Down state protomer. (38] Explicit solvent molecular dynamics (MD) [39] simulations of novel coronavirus spike protein [42-43] were performed [44-45] using the NAMD2 program [45]. We used the CHARMM-Gui [46] with the CHARMM36m force field [47-48] along with TIP3P water molecules to explicitly [50-51] solvate the proteins and add any [52-53] missing residues from the experimental structure files [54], Simulations were carried out [55-56] maintaining the number of simulated particles [57-58], pressure and temperature (the NPT ensemble) [11-57] constant with the Langevin piston method [23-59] specifically used to maintain a constant pressure of 1atm. [12-46,53]. We employed periodic [58- 60] boundary conditions (60-63] for a water box simulation [63] volume as well as the particle mesh [64-65] Ewald (PME) method with a 20 Å cutoff distances [64-66] between the simulated protein [66-67] and water box edge [15]. The integrationbtime step was 2 femtoseconds with our protein simulations [67-68] conducted under physiologicalbconditions (37 C, pH of 7.4 [69,70], physiological ionic strength). It is a Many ([arckian genetic algorithm deeply, and achieved 12× to 18× sppdup. Based on such platform [70-73]. SIMM carried out a virtual screening of the Azathioprine, Azithromycin Baricitinib, Bleomycin, Cobicistat, Colchicine, Cycloserine, Darunavir, Eflornithine, EIDD-2801_MK-4482, GC376,Histrelin, Recombovir, Minocycline, Remdesivir, Ritonavir, Umifenovir small molecules. Upper case represents match positions, lower case insert positions, and the '-' symbol represents deletions relative to the matching profileThe sequence (NCBI Accession: YP_009724390) was uploaded to the ModBase interface and was run with the template being SARS spike protein receptor binding domain (PDB: 6XS6 SARS-CoV-2 Spike SARS-COV-2 Main protease PDB:6LU7 with Unliganded SARS-CoV-2 main protease, Mpro, FURIN-ADAMTS1-ROR-GAMMA-SRRM2ROR- NF-B/RelA-STAT3AROR- NF-B/RelA-STAT3B,Nsp15,TCEB2>ASB8>>TCEB1P NEVAKNLNESLIDLQELGKY EQYIKGSGRENLYFQGGGGSVLLMGCVAE TGTQCVNLTTrTQLPPAYTNS1FURIN-ADAMTS1- ROR-GAMMA RSFFEDLLFDKVKRSFIEDLLFNKVRSFFEDLLFDKV conserved active site of a protein target in order to predict the binding affinity followed by providing a ranking of their fit using scoring functions [2,40-78]. To account for the protein flexibility, flexibl docking[69,3,4,17-73,75], [77,79,81) also known as induced-fit algorithms, were [81,83,87] applied [41,43,45]. Despite numerous published papers demonstrating the use of docking for VS, [48,49,60] it still remains a major challenge because the empirical scoring functions [41,42] are found to have limited accuracy in the [12,15-47] ranking of compounds and sometimes [17.19-48-50] cannot distinguish between active and inactive molecules [19,20-49]. We also incorporated several different scoring functions followed by a fusion of the scores to create a S1-FURIN-ADAMTS1-ROR-GAMMARSFFEDLLFDKVKRSFIEDLL FNKVRSFFEDLLFDKV numerical score analysis [12,42–44,60]. In addition to S1-FURIN-ADAMTS1-ROR-GAMMA-consensus RSFFEDLLFDKVKRSFIEDLLFNKVRSFFEDLLFDKV scoring, post processing techniques [60,62,65] such as molecular mechanics Poisson–

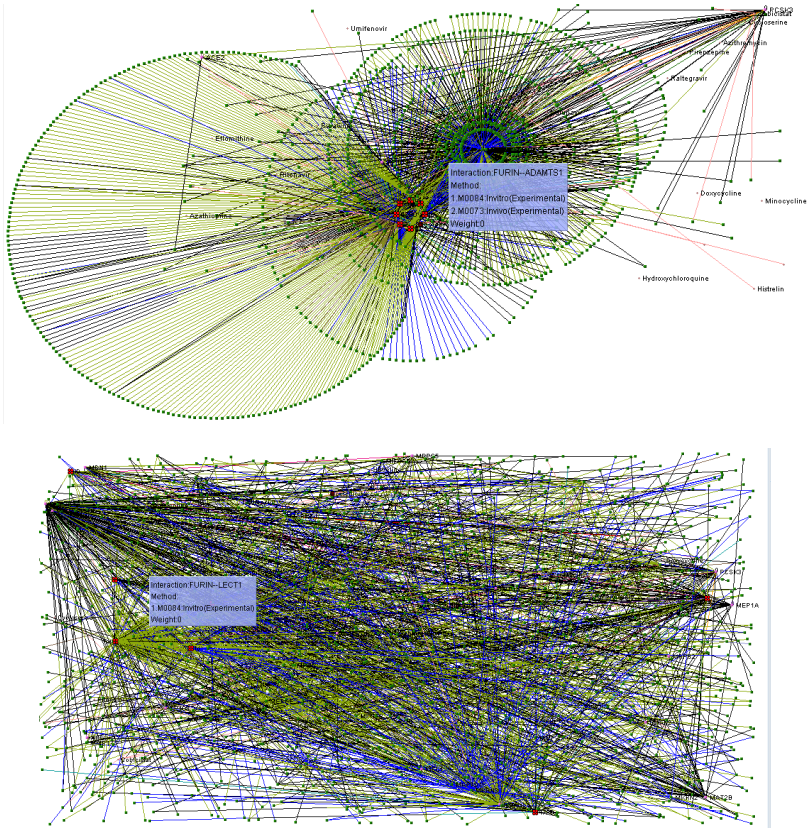

Figure 2. SRORκ NF-ĸB/RelA-STAT3-FURIN-SARS-COV-2-3d ShortestPath Interaction Protein-Protein Analysis.

Shortest path(5)::MMP14-FURIN-UBC-MME-ADCYAP1-DPP4

Shortest path(5)::MMP14-FURIN-UBC-MME-VIP-DPP4

Shortest path(5)::MMP14-FURIN-UBC-MAP3K14-IKBKB-DPP4

Shortest path(5)::MMP14-FURIN-DDX56-MAP3K14-IKBKB-DPP4

Shortest path(5)::MMP14-FURIN-UBC-MARK3-IKBKB-DPP4

Shortest path(5)::MMP14-FURIN-UBC-MME-CD4-DPP4

Shortest path(1)::MMP14-FURIN

Shortest path(5)::MMP14-FURIN-UBC-MAP3K14-CALM1-ACE2

Shortest path(5)::MMP14-FURIN-DDX56-MAP3K14-CALM1-ACE2

Shortest path(5)::MMP14-FURIN-UBC-MME-AGT-ACE2

Shortest path(3)::MMP14-FURIN-UBC-LAS1L

Shortest path(3)::MMP14-FURIN-HNF4A-LAS1L

Shortest path(3)::MMP14-FURIN-UBC-C18ORF1

Shortest path(3)::MMP14-FURIN-UBC-LMAN2

Shortest path(3)::MMP14-FURIN-UBC-LOX

Shortest path(3)::MMP14-FURIN-UBC-H2AFY2

Shortest path(3)::MMP14-FURIN-UBC-MAP3K14

Shortest path(3)::MMP14-FURIN-DDX56-MAP3K14

Shortest path(3)::MMP14-FURIN-UBC-MAP7D1

Shortest path(3)::MMP14-FURIN-UBC-MARK1

Shortest path(4)::MMP14-FURIN-UBC-MARK1-MARK2

Shortest path(4)::MMP14-FURIN-UBC-MARK3-MARK2

Shortest path(3)::MMP14-FURIN-UBC-MARK3

Shortest path(3)::MMP14-FURIN-UBC-MAT2B

Shortest path(3)::MMP14-FURIN-ELAVL1-MAT2B

Shortest path(3)::MMP14-FURIN-UBC-MCL1

Shortest path(3)::MMP14-FURIN-UBC-MDN1

Shortest path(3)::MMP14-FURIN-NOTCH1-MDN1

Shortest path(5)::MMP14-FURIN-UBC-LOX-FN1-MEP1A

Shortest path(5)::MMP14-FURIN-UBC-MDN1-FN1-MEP1A

Shortest path(5)::MMP14-FURIN-NOTCH1-MDN1-FN1-MEP1A

Shortest path(5)::MMP14-FURIN-UBC-MME-VIP-MEP1A

Shortest path(5)::MMP14-FURIN-UBC-MME-AGT-MEP1A

		Name	Volume Å³	Surface Å²	Drug Score	Simple Score
		P_0	698.36	764.31	0.82	0.39
		P_1	664.42	874.51	0.87	0.38
		P_10	320.37	502.99	0.64	0.16
		P_11	313.58	556.94	0.53	0.21
		P_12	307.55	475.18	0.5	0.11
		P_13	257.17	382.25	0.62	0.09
		P_14	250.38	490.59	0.61	0.05
		P_15	222.33	380.39	0.54	0.01
		P_16	216.6	348.82	0.62	0.0
		P_17	205.13	366.35	0.37	0.0
		P_18	200.61	271.76	0.52	0.0
		P_19	183.72	348.86	0.45	0.0
		P_2	563.21	633.66	0.88	0.31

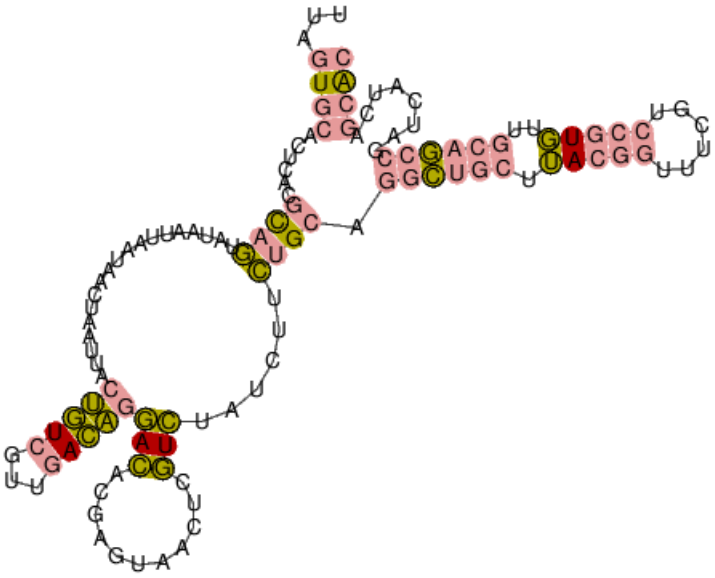

Figure 3a. Remdesivir small molecule binding domaijns (colors) inside the, 7BV2 of the nsp12-nsp7-nsp8 complex bound to the template-primer RNA and triphosphate form of Remdesivir(RTP) >MT434757.2_1_29817/80-200

UUAGUGCACUCACGCAGUAUAAUUAAUAACUAAUUACUGUCGUUGACAGGACACGAGUAACUCGUCUAUCUUCUGCAGGCUGCUUACGGUUUCGUCCGUGUUGCAGCC-GAUCAUCAGCAC

...((((.....((((..((((((.....))))))((((((...))))))...((((((...))))))).....)))).((((((.((((((.....))))))..))))))).....)))) (-38.60)

>MT810119.1_1_29865/80-200

AAUCUGUGUGGCUGUCACUCGGCUGCAUGCUUAGUGCACUCACGCAGUAUAAUUAAUAACUAAUUACUGUCGUUGACAGGACACGAGUAACUCGUCUAUCUUCUGCAG-GCUGCUUACGGU

...(((((((..((.((((.(((.....))).)))))))..)))((((((.((((((.....)))))))((((.(..((.((...((((((...)))))))..)).)..)))))))))..)))). (-34.00)

>MT439597.1_1_29812/80-200

UUAGUGCACUCACGCAGUAUAAUUAAUAACUAAUUACUGUCGUUGACAGGACACGAGUAACUCGUCUAUCUUCUGCAGGCUGCUUACGGUUUCGUCCGUGUUGCAGCC-GAUCAUCAGCAC

...((((.....((((..((((((.....))))))((((((...))))))...((((((...))))))).....)))).((((((.((((((.....))))))..))))))).....)))) (-38.60)

>consensus

UUAGUGCACUCACGCAGUAUAAUUAAUAACUAAUUACUGUCGUUGACAGGACACGAGUAACUCGUCUAUCUUCUGCAGGCUGCUUACGGUUUCGUCCGUGUUGCAGCC-GAUCAUCAGCAC

...((((.....((((.....((((((...))))))(((.....)))).....)))).((((((.((((((.....))))))..))))))).....)))) (-13.78 = -15.23 + 1.46).

Size and shape descriptors

volume [Å³]	563.21
surface [Å²]	633.66
depth [Å]	26.77
ellipsoid main axis ratio c/a	0.11
ellipsoid main axis ratio b/a	0.22
enclosure	0.04

Element descriptors

# pocket atoms	183
# carbons (C)	129
# nitrogens (N)	22
# oxygens	30
# sulfurs (S)	2
# other elements	0

Functional group descriptors

# hydrogen bond donors	13
# hydrogen bond acceptors	56
# metals	0
# hydrophobic interactions	24
hydrophobicity ratio	0.26

Amino acid composition

apolar amino acid ratio	0.53
polar amino acid ratio	0.38
positive amino acid ratio	0.06
negative amino acid ratio	0.03

Amino acid descriptors

# ALA	1
# ARG	2
# ASN	1
# ASP	1
# CYS	2
# GLN	3
# GLU	0
# GLY	0
# HIS	0
# ILE	1
# LEU	9
# LYS	0
# MET	1
# PHE	1
# PRO	2
# SER	0
# THR	5
# TRP	0
# TYR	2
# VAL	3

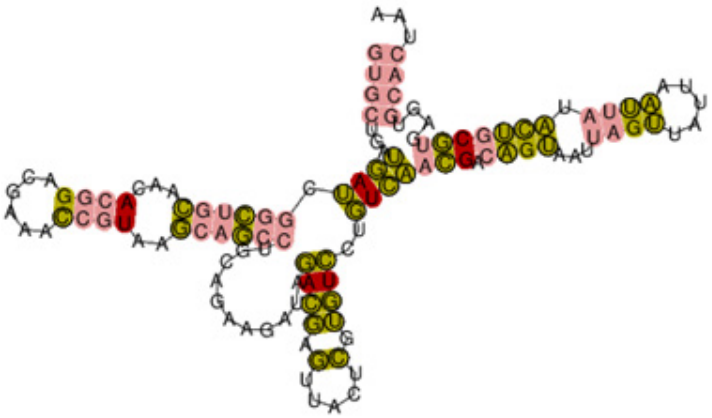

Figure 3b. Remdesivir's functional group descriptors and compositions >MT434757.2_1_29817/80-200

GUGCUGAUGAUCGGCUGCAACACGGACGAAACCGUAAGCAGCCUGCAGAAGAUAGACGAGUUACUCGUGUCCUGUCAACGACAGUAAUUAGUUAUUAAUUAUACUGC-GUGAGUGCACUAA

(..((.((....((((((...((((.....))))..)))))).((((..((((((((((...))))))...))))).....(((((((...)))))))).)))))..)..)..... (-39.40)

>MT810119.1_1_29865/80-200

ACCGUAAGCAGCCUGCAGAAGAUAGACGAGUUACUCGUGUCCUGUCAACGACAGUAAUUAGUUAUUAAUUAUACUGCGUGAGUGCACUAAGCAUGCAGCCGAGUGACAGC-CACACAGAUU

..(((..((.....))....((((((((((...))))))...))))).)))...(((((((((...)))))))).(((.(((.((((..((.....))..))))...))))).)))... (-29.80)

>MT439597.1_1_29812/80-200

GUGCUGAUGAUCGGCUGCAACACGGACGAAACCGUAAGCAGCCUGCAGAAGAUAGACGAGUUACUCGUGUCCUGUCAACGACAGUAAUUAGUUAUUAAUUAUACUGC-GUGAGUGCACUAA

(..((.((....((((((...((((.....))))..)))))).((((..((((((((((...))))))...))))).....(((((((...)))))))).)))))..)..)..... (-39.40)

>consensus

GUGCUGAUGAUCGGCUGCAACACGGACGAAACCGUAAGCAGCCUGCAGAAGAUAGACGAGUUACUCGUGUCCUGUCAACGACAGUAAUUAGUUAUUAAUUAUACUGC-GUGAGUGCACUAA

((((...((((.((((((...((((.....))))..))))))..........((((.(.....).))))..))))(((.((((...((((.....)))).)))))....)))).... (-17.46 = -15.70 + -1.76).

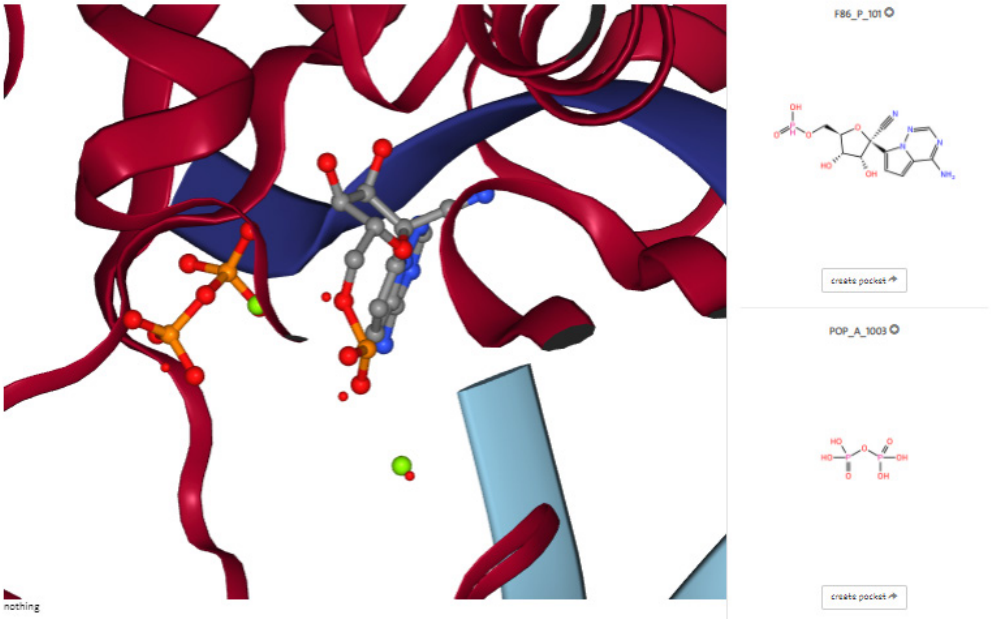

Figure 3c. 3D Docking interactions of the Remdesivir fragments inside the, 7BV2 of the nsp12-nsp7-nsp8 complex bound to the template-primer RNA and triphosphate form of Remdesivir(RTP).

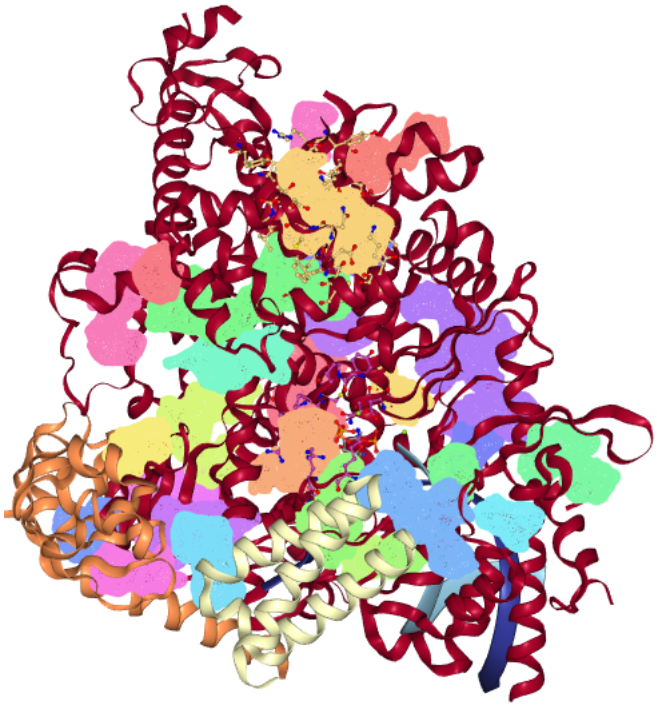

Figure 3d. 3D Docking interactions of the Remdesivir small molecule inside the, 7BV2 of the nsp12-nsp7-nsp8 complex bound to the template-primer RNA and triphosphate form of Remdesivir(RTP).

		Name	Volume Å³	Surface Å²	Drug Score	Simple Score	Ligand Coverage
		P_0	911.55	1281.56	0.82	0.64	64.81
		P_1	203.01	567.65	0.47	0.08	0.0
		P_2	110.98	209.26	0.3	0.0	0.0

Figure 3e. Binding domains (colors) of the docking interactions of the Colchicine small molecule inside the pdb:6AJZ protein targets.

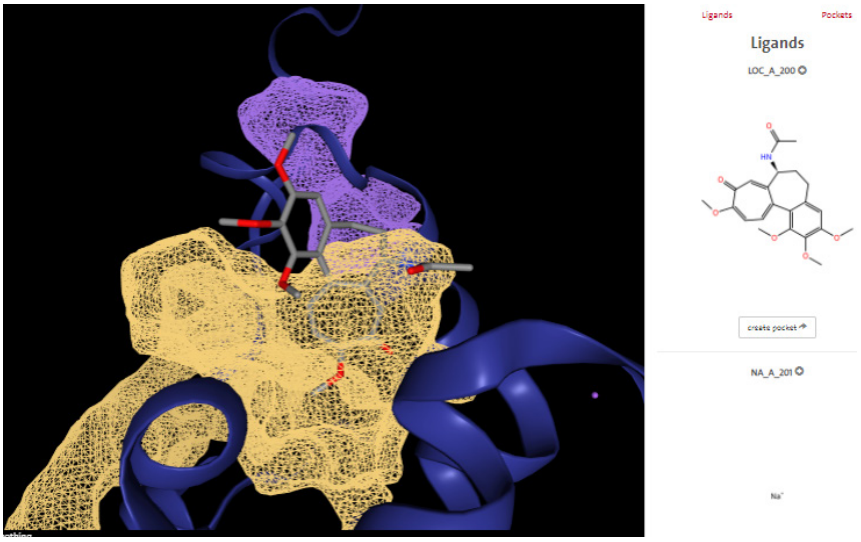

Figure 3f. 3D Docking interactions of the Colchicine small molecule inside the pdb:6AJZ protein targets.

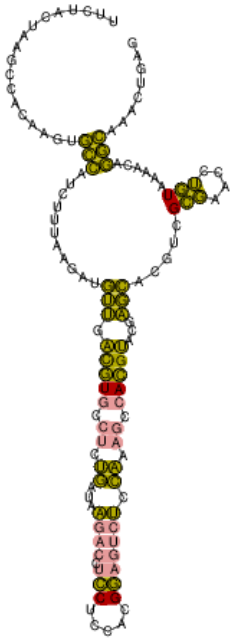

		Name	Volume Å³	Surface Å²	Drug Score	Simple Score	Ligand Coverage
		P_0	686.02	902.43	0.85	0.46	0.0
		P_1	630.46	548.67	0.79	0.46	0.0
		P_10	163.35	301.57	0.31	0.0	0.0
		P_11	159.26	277.21	0.31	0.0	0.0
		P_12	110.18	308.18	0.21	0.0	0.0
		P_13	102.5	297.31	0.25	0.0	0.0
		P_2	592.99	481.11	0.8	0.43	98.77
		P_3	465.48	653.11	0.78	0.29	0.0
		P_4	407.45	621.86	0.64	0.25	0.0
		P_5	345.66	547.52	0.9	0.1	0.0
		P_6	310.75	438.56	0.5	0.18	0.0
		P_7	307.34	484.87	0.62	0.16	0.0
		P_8	285.66	403.86	0.47	0.07	0.0
		P_9	208.16	311.89	0.5	0.01	0.0

Figure 3g. Binding domains (colors) of the Crystal Structure of the mutant Human ROR gamma Ligand Binding Domain With Ursolic acid>MT434757.2_1_29817/280-400

UUCUACUAAGCCACAAGUGCCAUCUUUAAGAUGUUGACGUGCCUCUGAUAAGACCUCCUCCACGGAGUCUCCAAAGCCACGUACGAGCACGUCGCGAACCUGUAAAACAG-GCAAACUGAG

.....((.((..(((((((((.....)))))(((((((((.((.((...((((.(((.....)))))))).)).).)))))).)))))))))...((((.....))))..... (-30.90)

>MT810119.1_1_29865/280-400

AUGUUGACGUGCCUCUGAUAAGACCUCCUCCACGGAGUCUCCAAAGCCACGUACGAGCACGUCGCGAACCUGUAAAACAGGCAAACUGAGUUGGACGUGUGUUUUCUC-GUUGAAACCAGG

...(((((((((.((.((...((((.(((.....)))))))).)).).)))))).)))(((((((((.....((((.....))))(((.....)))))))))).(((((.....)))).)... (-32.60)

>MT439597.1_1_29812/280-400

UUCUACUAAGCCACAAGUGCCAUCUUUAAGAUGUUGACGUGCCUCUGAUAAGACCUCCUCCACGGAGUCUCCAAAGCCACGUACGAGCACGUCGCGAACCUGUAAAACAG-GCAAACUGAG

.....((.((..(((((((((.....)))))(((((((((.((.((...((((.(((.....)))))))).)).).)))))).)))))))))...((((.....))))..... (-30.90)

>consensus

UUCUACUAAGCCACAAGUGCCAUCUUUAAGAUGUUGACGUGCCUCUGAUAAGACCUCCUCCACGGAGUCUCCAAAGCCACGUACGAGCACGUCGCGAACCUGUAAAACAG-GCAAACUGAG

.....(((.....(((.((((((.((.((...((((.(((.....)))))))).)).).)))))...)))).....(((....))).....)))..... (-17.29 = -13.20 + -4.09).

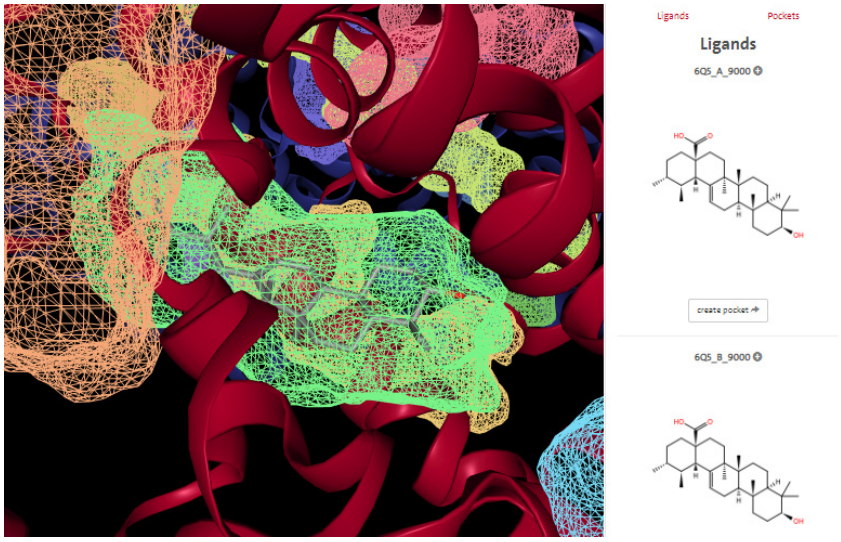

Figure 3h. Crystal structure of the mutant human ror gamma ligand binding domain with ursolic acid.

Boltzmann surface area methods based on [66,67] molecular dynamics (MD) simulations [28-45,78], applied in this project to a small set of top-ranked [60,62] binding poses and top-ranked compounds to more accurately estimate binding energies. In this project we implemented another SBVS approach for the development of a structure based pharmacophore multi models, [24,26-70,72] which can be generated directly from the complex structure of the ligands and the target. Structure-based pharmacophores allow for the complete exploration of the binding interactions of an SARS-CoV-2 main protease, Mpro, FURIN-ADAMTS1-ROR -GAMMA-SRRM2-ROR - NF-B/RelA-STAT3A- ROR- NF-B/RelA-STAT3B, Nsp15, TCEB2-->ASB8- >>TCEB1PELDSFKEELDKYFKNHTSPDVDLGDISGINASV VNIQKEIDRLNEVAKNLNESLIDLQELGKYEQYIKGSGRENLYFQGGG GSVLLMGCVAETGTQCVNLTTrTQLPPAYTN S1FURIN-ADAMTS1-ROR-GAMMARSFFEDLLFDKVKRSFIEDLLFNKVRSFFEDLLFDKVactive siteand for the inclusion of shape and volume information derived directly from the structural data [46]. This approach determines chemical features based oncomplementarities between a ligand and its binding-site. The purpose of structure based pharmacophores is to be complementary to docking procedures, including the samelevel of information; however, it is less demanding with respect to computational resources and therefore much more efficient. Like docking, pharmacophore searchalgorithms should not only discriminate between active and inactive compounds but should also correctly orient the ligand in the protein binding site [47]. Seven docking softwares were carefully evaluated to build S1-FURIN-ADAMTS1-ROR-GAMMA-consensus motif-RSFFEDLLFDKVKRSFIEDLLFNKVRSFFEDLLF DKV strategy, including AUTODOCK [20], VINA [21], DOCK [22], PLANTS [23], PSOVINA [24], LEDOCK(http://www.lephar.com) and GOLD [25]. The other phenol molecules were kept in the input file, and considered to be static molecules. (31,33) The side-FURIN-ADAMTS1-FURIN-ADAMTS1-ROR-GAMMA-CTSL1-SERPINB13-CSTB-FURIN-ADAMTS1-ROR-GAMMA-DEXD-CSTA chains of the six histidines interacting with the zinc ions where blocked by (41-43) editing the input „.amcfile as) explained in the previous section. The percentage of van der Waals radii used for collision detection between non- bonded atoms during the conformational exploration was set to 75 (i.e. the default value) [55, 57, 59,61,63,65] Hydrogen atoms were not added [67,69,71]. This is acceptable because the solutions provided by BiogenetoligandorolTM are not expected to be an accurate representation of unbinding paths, but simply a first approximation [24,26,28,30,32]. This selection covers a wide variety of conformation (36,38) search algorithm and scoring function (Tables 2, 3a, 3b), thus representing an abundant source (40,42) for optimizing the BiogenetoligandorolTM protocol. BiogenetoligandorolTM was run to simulate 20 phenol unbinding paths. (44,46) To emphasize the computational efficiency of the method, (46,48,50) we would like to mention that the average computing time (50,52) for one solution was <10 s on a single processor. (52,54) A significant variability in the solutions can be observed. (50,57) The docking calculation (54,55,59) was performed on the prepared dataset of COVID-19 receptors and ligands by using these seven docking softwares based on default parameters. The box within the surrounding 12.5 Å of the bound ligand was defined as SARS-CoV-2 main protease, Mpro, FURIN-ADAMTS1-ROR-GAMMA-SRRM2-ROR- NF-B/RelA-STAT3A-ROR- NF-B/RelA-STAT3B Nsp15,TCEB2>ASB8>>TCEB1PE LDSFKEELDKYFKNHTSPDVDLGDISGiNASVVNIQKEIDRLNEVAKNLNES LIDLQELGKYEQYIK GSGRENLYF QGGGGSVLLMGCVAETGTQCVNLT TrTQLPPAYTN S1-RBRSFFEDLLFDKVKRSFIEDLLFNKVRSFFEDLLFD KV active siteions and hydrogens were allowed to move. Secondly, the backbone atoms of the protein were fixed while others were allowed to move [10-29]. Thirdly, all the atoms of the system were free to move [23,24]. In the three optimization process, 2000 steps, steepest [24-27], descent method followed by 2000 steps conjugated gradient method were used for each ligand-receptor binding system [28-30]. The RMSD gradient goes from dark green [21- 30] (for high-accuracy near-native docking solution with RMSD below 1.0 Å), to dark (RMSD ≥ 10.0 Å). bA (11-19) docking pose was considered as near-native pose once its backbone RMSD is ≤ 2.5 Å. Finally, the binding free enegy (Gbind) is calculated by using the MM/PBSA [17,18-30] and X-score methods [9, 20]. As for the X-score method, (19-22,29) it is assumed that the overall binding free energy in a protein-ligand binding process can be divided into several terms (shown in Equation1) [21]. the receptor and the ligand; GH-bond represents the hydrogen bonding between the receptor and the ligand; Gdeformation represents the deformation effect; Ghydrophobic represents the hydrophobic effect; G0 represents a regression constant. Gbind value between the receptor and ligand could be calculated simply by the X-score software package: in Quantifying Magnetic Sensitivity Radical Pair Based Compass Quantum Fisher Information:• cos2Gdeformation+Ghydrophobic+ G01 In the MM/PBSA method [30], the free energy of the receptor/protein-inhibitor binding, ΔGbind, is obtained from the difference between the free energies of the receptor / protein ligand complex_(1,3- thiazol-5-yl)methylN-*(2S,3S,5S)-3-hydroxy-5-*(2R)-3-met hyl-2-,*methyl and the unbound receptor/protein (Grec) and ligand (Glig). The binding free energy (Gbind) was evaluated as a sum of the changes in the binding energy (Ebind), solvation entropy(–TΔSsol), and conformational entropy (–TΔSconf) (shown in Equation 2) *13+ where ΔEbind is interaction energies between a ligand and a protein, which were computed using the Sander modules of the Amber16 program.

Step 1:

Calculate the number of high-confidence 'core' network restricted to COVID19 signature genes as network nodes and high confidence (≥ 0.70) interactions as network edges, fast modes that correspond to the top 30% of the eigenvalues range.

Step 2:

Calculate the weighted sum (Equation (1)) and spread the influence of hot residues to sequential medium-confidence interaction network obtained from expanding the core network by 1220 additional antiviral* nodes and spatial antiviral* neighbors.

Step 3a:

If the overall percent of predictions is larger than a previously set value (for example, if the percent of antiviral* predictions is larger than 40% of the total number of residues), the BiogenetoligandorolTM procedure reduces the number of Bthe differential gene expression level fast modes by one and goes to Step 2.

Step 3b:

If the percent of predictions is too small (e.g, less than 15% of all residues), the BiogenetoligandorolTM procedure increases the number of fast modes by one and goes to Step 2.

*Antiviral means there is evidence that the compound is used as or has antiviral activity; SARS-CoV-2 means that the compound should antiviral activity against SARS-CoV-2; Corona viruses means that the compound showed antiviral activity against corona viruses other than SARS-CoV-2.

To avoid infinite loops, only one increase followed by a decrease is allowed, and vice versa. Multiple consecutive increases or decreases are allowed. This approach ensures that longer proteins have enough predictions and that shorter ones are not saturated with too many false positives. We focused our study on pdb structures with the listed drugs of the Remdesivir, Colchicine and Ursolic acid present as ligands. For Remdesivir, we analyzed two structures, malarial parasite Plasmodium Falciparum lactate dehydrogenase (pdb id 1cet (63)) and human lysosomal protein saposin B (pdb id 4v2o (64)). The presence of saposin B in human lysosome makes it a logical target to analyze considering experimental evidence that the presence of Remdesivir in lysosome inhibits coronavirus progression [24,26,28], and increased levels of lactate dehydrogenase as have been shown to predict COVID-19 severity and mortality (65). We analyzed the binding pattern of the combination of drugs of the Remdesivir, Colchicine and Ursolic acid to the human glycine receptor alpha -3 (the glutamate-gated chloride channels (GluCls), pdb id 5vdh (66)) and C. elegans glycine receptor (pdb id 3rif (30)). We also performed the analysis of the binding pattern of the combination of thr drugs of the Remdesivir, Colchicine and Ursolic acid HydroxyRemdesivir, Recombovir, Minocycline, Remdesivir, Ritonavir, Gemigliptin, Raltegravir, Ribavirin, Umifenovir, Betrixaban to the hepatitis C virus (HCV) RdRp (pdb id 4wtg (67)) and compared them to the COVID-19 RdRp predictions (pdb id6m71 (68)). GC376 was already analyzed in light of similarities between HCV and SARS-CoV-2 RdRp and similarities between remdesivir and GC376(68). For colchicine, we analyzed the structure SARS-Cov-2 main protease bound to the drug (pdb id 6lu7). We performed the comparative analysis of the binding patterns between the ACE2 human receptor, the spike glycoproteins from SARS (pdb id 6yb7 (70)), the SARS-CoV-2 (pdb id 5r80 (7)) and the drugs of the Recombovir-(Drug Combination)small molecules. We also analyzed the binding patterns between the SARS FURIN-ADAMTS1-ROR-GAMMA with S230 human neutralizing antibody, and between SARS receptor-binding domain (FURIN-ADAMTS1-ROR-GAMMA) and glycan shield (pdb id 6LU7 (71)). In this research report the ReCombovir-(Drug Combination) refers to the chemical structures of the Remdesivir, Colchicine and Ursolic acid chemical structures.

Collecting gold-standard pairwise drug combinations

In this study, we focused on pairwise drug combinations by assembling the clinical data from the multiple data sources [23,24]. Each drug in combinations was required to have the experimentally [25,26] validated target information: each EC50, IC50, Ki, or Kd ≤ 10 μM [27,28]. Compound name, generic name, or commercial name of each drug was [29,30) standardized by MeSH and UMLS vocabularies [22,28-47] and further transferred to DrugBank ID [30-32] from the DrugBank database (v4.3)40. [30-38,40] Duplicated drug pairs were removed. [40,42,44] In total, 681 unique pairwise drug combinations [46,48] connecting 362 drugs were retained [48,50]. Collecting adverse drug–drug interactions [50-52] and Chemical similarity analysis of [54,58] drug pairs. We compiled clinically reported adverse [58,60) drug–drug interactions [DDIs) data from the [60,62] DrugBank database (v4.3)40. Here, we focused on adverse drug interactions [62,64,65] where each drug has the experimentally validated target information. [61,63] Compound name, generic name, or commercial name of each drug were standardized by MeSH and UMLS vocabularies [47-49,67] and further transferred to DrugBank ID from the DrugBank database (v4.3)40. In total, 13,397 clinically reported adverse DDIs connecting 658 unique drugs were retained (Figures 3a-3h and 4a-4f). In addition, we collected cardiovascular event-specific adverse DDIs from the TWOSIDE database [35-44,47]. TWOSIDE includes [12-28,30,31,32,67] over 868,221 significant associations connecting [13-29,32,34,37-78] 59,220 drug pairs and 1301 adverse events [35-47-94]. We downloaded chemical structure information (SMILES format) from the DrugBank database (v4.3)40 and computed MACCS fingerprints of each drug using Open Babel v2.3.148. If two drug molecules have a and b bits set in their MACCS fragment bit-strings, with c of these bits being set in the fingerprints of both drugs, the [47,52,59,60-94] Tanimoto coefficient (T) of a drug–drug pair is defined as: >– (3)T is widely used in drug discovery and development [49-88,89,94], offering a value in the range of zero (no bits in common) to one (all bits are the same). Protein sequence similarity (identity) and Gene co-expression analysis. To measure the extent to which drug target-SARS-CoV-2 main protease, Mpro, DPP4 ADABP, ADCP2, CD26, DPPIV,TP103, FURIN FUR, PACE, PCSK3, FURIN-ADAMTS1-ROR-GAMMA-SRRM2-ROR- NF-B/RelA-STAT3A-ROR- NF-B/RelA-STAT3B, Nsp15,TCEB2-->ASB8->>TCEB1 coding genes(a and b) associated with the drug-treated diseases are co-expressed, [2,6,7,8-11,45-78] we calculated the Pearson's correlation coefficient (u2(,)=12(1−eieiei(+)) u3(,,)=(cos2−eisin2eisin2ei(+)cos2)F=U43C34C24U23C34†U43U23C12=(TPu3(−π/4,0,0))U12(1u3(π/4,0,0))U12(1P†) P=z T=P |g1=cosπ8|0+sinπ8|1 |g2=cos3π8|0+sin3π8|1 |x1x2xixnx1′x2′xi′xn′,cos1cos2cosicosnsin1sin 2sinisinn, xi+1=xi+signxi−xi•Δd1, xi+1=xi+U−1,1•1−arctanrg4•Δd2,i+1=i ± 1−arctanrg4Δt, i″i″T=1-T i″i″T=1-T i″i″T=i′i′T i′i′ i″i″ Ω,G,D,P,n,X0 ,X′t,X″t,Xt,Fmin,Xbest,Fbest,, fx=12π•e−x2/22.pX+C1∏i=1npXi+− Xbest≤d=∏i=1n∫Xbest−Xi−dXbest−Xi+dfxdx,0<∏i=1n∫Xbest −Xi−dXbest− Xi+dfxdx<10<pX+C1<1.pX′+S1pX+S1<p2→1=1−p2→2p2→21−pX′+S 1p2→21=cosπ8|00+sinπ8|11|2=cos3π8|00+sin3π8|11|=cos1cos2|0000 +cos1sin2|0011+sin1cos2|1100+sin1sin2|1111)) and the corresponding P-value via F-statistics for each pair of drug target -SARS- CoV-2 main \ protease, Mpro, DPP4 ADABP, ADCP2, CD26, DPPIV, TP103, FURIN FUR, PACE, PCSK3, UBC-NOL10-EED-H2AFY2-HDAC2-ZNF318-MMS19-QSOX2-ILF3-KIAA0090-FLOT1-LMAN2-SUPT5H-SSBP3-EWSR1-MTCH1-SMAD2-GFER-COPS2- PMPCA-MARK2-MARK3-USP21-MARK1-MAP4-FYCO1-PRMT6-FKBP7-UBQLN4- NOMO3-LIG4-CTSK-SERPINB3-CTSS-BGLAP-CTSH-VCAM1-PPIH-FN1-RAB10-TRAF6-HEATR3-PTP4A3-DNAJC11-MINOS1-MTHFD2-MDM2-TBCA-AHCYL1- PPIL3-RPAP1-KIF11-NCOR1-TCF12-CDKN2C-QPCTL-RNF2-ADAM9-CDH1-PVR- KRTAP10-9-SCARB1-CUL1-RBM28-POLR3F-STC2-HIST1H4A-BRD2-OBSL1- FURIN-ADAMTS1-ROR-GAMMA0-CAND1-NUP88-CUL2-FAM98A-FUS- MARK3-USP21-MARK1-MAP4-FYCO1-PRMT6-FKBP7-UBQLN4-NOMO3- LIG4-CTSK-SERPINB3-CTSS-BGLAP-CTSH- VCAM1-PPIH-FN1-RAB10, Remdesivir, Colchicine and Ursolic acid drugs, FURIN-ADAMTS1-ROR-GAMMA-SRRM2- ROR- NF-B/RelA-STAT3A-ROR- NF-B/RelA-STAT3B, Nsp15, TCEB2-->ASB8->>TCEB1 coding genesa and b across 32 human tissues. In order to reduce the noise of co-expression analysis, we mapped PCC(a, b) into the human protein–protein by averaging: H=B(Sˆ1+Sˆ2)+IˆASˆ2, Sˆi=(x,y,z) Iˆ s(t)=TrI(U(t)(0)U†(t)), I(0)=I/2 P(t′)=dΔM(t′)ΔM=f(t′)dt′, ¯s=∫−∞0f(t′)s(t′)dt′=∫0∞f(t)s(t)dt,−∞0f(t′)

dt′=∫0∞f(t)dt=1¯s¯s¯s(0,π/2)¯ss(0)¯sQFI≈∑i=01Re(i12)2(1i11+1i22)+(i11−i22)2i11+i22, 1ij=i|1|s(0)|j|1 0ij=i|0|s(0)|j|0 |0 |1H1=B0Sˆ1Re(i12)i12s(0)¯s|S=12(|10−|01)30%s(0)¯sQFI≈∑i=01k4Re(i12)2(k2+(Brf)2)2(1Pi11+1Pi22)+(Pi11−Pi22)2Pi11+Pi22,Pijj=ijj+(−1)jiijji=(Brf)22(k2+(Brf)2)(i11−i22)−Brfk(k2+(Brf)2)Im(i12)Im(i12)i12s(0)¯sΔQFI/QFI≡QFI(Brf=0)−QFI(Brf=150nT)QFI(Brf=0) Oˆ Oˆ Δ2=Δ2Oˆ|dOˆ/d|2 Δ2Oˆ Oˆ Oˆ ¯s Oˆ=Sˆ2=(Sˆ1+Sˆ2)2.

Gene Ontology (GO) similarity analysis and Clinical similarity of drug pair analysis

The Gene Ontology (GO) annotation for all drug target-SARS- CoV-2 main protease,Mpro, DPP4 ADABP, ADCP2, CD26, DPPIV, TP103, FURIN FUR, PACE, PCSK3,FURIN-ADAMTS1-ROR-GAMMA- SRRM2-ROR- NF-B/RelA-STAT3A- ROR- NF-B/RelA-STAT3B, Nsp15, TCEB2-->ASB8->>TCEB1 coding geneswas downloaded from the website: http://www.geneontology.org/. We used three types of the experimentally validated or [50,52] literature-derived evidences: [52,54\biological processes (BP), [54,55] molecular function (MF), [56,57) and cellular component (CC), [57,58] excluding annotations inferred [59,61] computationally. The semantic comparison of GO annotations offers quantitative [62,63] ways to compute similarities between [64,65] genes and gene [66,67] products. We computed GOsimilarity SGO(a,b) for each pair of protein target-SARS-CoV-2 main protease, Mpro, FURIN-LRP1-MMP17-MMP2-MMP25-DPP4 ADABP, ADCP2, CD26, DPPIV, TP103, TIMM10, TIMM10B, TIMM29,TIMM8B, TIMM9, TK2, ABCC1-FKBP8-BCL2-SOD1-DNAJB1-AKT1-DNMT1-ACE2-CALM1-MAP3K14-UBC-FURIN-LRP1-MMP17-MMP2-MMP25-CSNK2B-BTF3-CTNNB1-PHB2- ATXN10-BSG-HGS- ACE2-CALM1-MAP3K14-DDX56-FURIN-LRP1-MMP17-MMP2-MMP25-RAB14-EEA1-IGF2R-TGOLN2-FURIN-HNF4A-EXOSC2-UPF1- ADAR-HNRPA1, ACE2-CALM1-MAP3K14-RAP1B-GCS1-RYBP-USP7-ACE2-AGT-MME-PCNA-MCL1-MPG-CDSN-UCHL5-CYB5B-MOV10-ACBD5- FBXW11-UNC84B-RAB5C-RAB5A-GCS1-LRRK2-SCFD1-Q86TQ8-CCDC86-SIRT7- MPHOSPH10-WHSC1-HSPD1-GLT25D1-FBXO6-GGCX-F2-PLAT-ERG-TMPRSS2-AR-MDN1-SET-TREX1-ATM-AP3B1-GRK5-PPIG-RHOB-CIT-RAC1-RAP1GDS1- HSPA9-DNAJC19-HSPA5- ACE2-CALM1-MAP3K14-DDX56-FURIN-LRP1-MMP17-DNAJC10- DPP4-IKBKB-MAP3K14-BYSL-MIPOL1-CUL4B-TLE3-FOXG1-TLPACE, PCSK3, FURIN-ADAMTS1-ROR-GAMMA-SRRM2-ROR- NF-B/RelA-STAT3A-ROR- NF-B/RelA-STAT3B, Nsp15, TCEB2-->ASB8->>TCEB1 coding genes using a graph-based semantic similarity measure algorithm52 implemented in an R package, named GOSemSim53. The overall GO similarity of the drug target-SARS-CoV-2 main protease, Mpro, DPP4 ADABP, ADCP2, CD26, DPPIV, TP103, FURIN FUR, PACE,PCSK3, FURIN-ADAMTS1-ROR-GAMMA-SRRM2-ROR-NF-B/RelA-STAT3A-ROR- NF-B/RelA-STAT3B, Nsp15, TCEB2-->ASB8->>TCEB1 coding genes binding to the Remdesivir, Colchicine and Ursolic acid drugs was determined by Eq. (x˙=f(x,t,),x(t0)=x0() D={(tk,y~k)}k=1nty~ik=yi(tk)+ik,ikN0,i2 p(D|)=∏i=1ny∏k=1nt1i2πexp−(y~ik−yi(tk))22i2, p(|D)=p(D|)p()p(D) p(D|)1p() 10 20 83), averaging all pairs of protein target-SARS-CoV-2 main protease, Mpro, DPP4, ADABP, ADCP2, CD26, DPPIV, TP103, FURIN FUR, PACE, PCSK3, FURIN-ADAMTS1-ROR-GAMMA-SRRM2-ROR- NF-B/RelA-STAT3A-ROR- FURIN-LRP1-MMP17-MMP2-MMP25-NF-B/RelA-STAT3B, Nsp15, TCEB2-->ASB8->>TCEB1 coding genesa and b with and GO=1pairs∑{, } GO(,)(6). Clinical similarities of drug pairs derived from the drug Anatomical Therapeutic Chemical (ATC) classification systems codes have been commonly used to predict new drug targets54. The ATC codes for all FDA-approved drugs used in this study were downloaded from the DrugBank database (v4.3)40. The kth level drug clinical similarity (Sk) of drugs A and B is defined via the ATC codes as below: u2(,)=12(1−eieiei(+))u3(,,)=(cos2−eisin2eisin2ei(+)cos2)F=U43C34C24U23C34†U43U23C12=(TPu3(−π/4,0,0))U12(1u3(π/4,0,0))U12(1P†)P=zT=P|g1=cosπ8|0+sinπ8|1|g2=cos3π8|0+sin3π8|1|1=cosπ8|00+sinπ8|11|2=cos3π8|00+sin3π8|11|=cos1cos2|0000+cos1sin2|0011+sin1cos2|1100+sin1sin2|1111.) where ATCk representsall ATC codes at the kth level. A score Satc(A, B)is used to define the clinical similarity between drugs A and B: (,)=∑ =1 (,) (8)where nrepresents the five levels of ATC codes (ranging from 1 to 5). Note that drugs can have multiple ATC codes. For example, Remdesivir, Colchicine and Ursolic acid drugs. For a drug with multiple ATC codes, the clinical similarity was computed for each ATC code, and then, the average clinical similarity was used [54-69]. Comparison with target set-overlapping approach within the SARS-CoV-2 main protease, Mpro, DPP4 ADABP, ADCP2, CD26, DPPIV, TP103, FURIN, FUR, PACE, PCSK3, FURIN-ADAMTS1-ROR-GAMMA- SRRM2-ROR- NF-B/RelA-STAT3A-ROR- NF-B/RelA-STAT3B, Nsp15, TCEB2-->ASB8->>TCEB1, ACE2 ACEH angiotensin I converting enzyme 2 network-based separation of drugs. In this section, we compared the introduced SARS-CoV- 2 main protease, Mpro, DPP4 ADABP, ADCP2, CD26, DPPIV, TP103, FURIN, FUR, PACE, PCSK3, FURIN-ADAMTS1-ROR-GAMMA-SRRM2-ROR NF-B/RelA-STAT3A-ROR- NF-B/RelA-STAT3B, Nsp15, TCEB2-->ASB8->>TCEB1, ACE2 ACEH angiotensin I converting enzyme 2 network- based separation (Equation 2) of FDA drugs with overlap measures that are solely based on shared targets, without using the PPI network [21,26,27,39,42-55]. Here, we examined two measures to quantify the overlap between target sets of drug A and drug B:Overlapcoefficient =|∩ |/min(| |,| |) (9) Jaccard–index =| ∩ |/|κ|(10) Both values range from 0 to 1: J, C = 0 [56,57) revealing no common targets shared by the drugs [57,59]. An overlap coefficient C = 1 indicates that one set is a complete pharmacophoric subset of the other, where Jaccard- index J = 1 is for two identical drug-protein target sets (Figures 3a-3h and 4a,4b) show the distribution of C and J for all 1,955,253 drug pairs [60,61]. The target-set overlap is low for most drug pairs, and the majority (96.8% = 1,892,455/1,955,253) do not share any targets. To investigate the statistical significance of the observed pharmacophoric druggabiity overlaps, we used a hypergeometric model. The null hypothesis is that the drug combination of the Remdesivir, Colchicine and Ursolic acid are randomly located from the space of all N protein- SARS-CoV-2 main protease, Mpro, DPP4 ADABP, ADCP2, CD26, DPPIV, TP103, FURIN FUR, PACE, PCSK3, FURIN-ADAMTS1-ROR-GAMMA-SRRM2-ROR- NF-B/RelA-STAT3A-ROR- NF-B/RelA-STAT3B, Nsp15, TCEB2-->ASB8->>TCEB1 coding genesin the SARS-CoV-2 main protease, Mpro, DPP4, targeted to the shortest paths of the Shortest path(3)::GCS1-YBX1-ROR- NF-B/RelA-STAT3-FURIN-5-MOV10, Shortest path(3)::GCS1-TP53-ROR NF-B/RelA-STAT3-FURIN-5-MOV10, Shortest path(3)::GCS1-UBC-ROR- NF-B/RelA-STAT3-FURIN-27-MOV10,Shortest path(3)::GCS1-AURKB-ROR- NF-B/RelA-STAT3-FURIN-27-MOV10, Shortest path(3)::GCS1-CEP76- ROR-NF-B/RelA-STAT3-FURIN-27-MOV10, Shortest path(3)::GCS1-YBX1-ROR- NF-B/RelA-STAT3-FURIN-27-MOV10, Shortest path(3)::GCS1-TP53-ROR- NF-B/RelA-STAT3-FURIN-27-MOV10 ADABP, ADCP2, CD26, DPPIV, TP103, FURIN, FUR, PACE, PCSK3,GS, FURIN-ADAMTS1-ROR-GAMMA-SRRM2-ROR- NF-B/RelA-STAT3A-ROR- NF-B/RelA-STAT3B, Nsp15,CTSB, APPS, CPSB,RECEUP, SLC6A19 B0AT1, HND, cathepsin B|APP secretase|amyloid precursor interactome. The pharmacophoric similarity overlap expected for two target sets A and B is then given by the: ||×|cn=∑k=0N−1HbO(k)exp(−2πiknN),n=0,...N−1, HV=1n∑i=1nHbOi−HM2, Accuracy=TP + TNTP + TN + FP + FN Sensitivity=TPTP + FN Specif=TNTN + FP (11).

Collecting disease-association genes and a gene to drug Performance evaluation We integrated disease–gene annotation data from 8 different resources and excluded the duplicated entries (Figure 3a-3h). We annotated all protein-SARS-CoV-2 main protease, Mpro, DPP4 ADABP, ADCP2, CD26, DPPIV, TP103, Shortest path (4)::LMAN2-UBC-MME-AGT-ACE2Shortest path(2)::LMAN2-UBC-LAS1LShortest path (2)::LMAN2-UBC-C18ORF1Shortest path(2)::LMAN2-UBC-LOXShortest path (2)::LMAN2-UBC-H2AFY2Shortest path(2)::LMAN2-UBC-MAP3K14 in the disease module would help clarify the mechanism-of-action of effective drug combinations while minimizing adverse effects. Only protein-protein interactions involving an extended interface are included (we have therefore ignored protein-peptide complexes). To test our hypothesis, we assembled 243,603 experimentally confirmed protein– protein interactions (PPIs) connecting 16,677 unique proteins from five data sources. We also compiled 1978 FDA-approved or clinically investigational drugs that have at least two experimentally reported targets by pooling the high-quality drug–

target binding affinity profiles [23,27,29-67,87-92] from six data sources (Table 2). Only mutations occurring at the complex interface are retained. In total the data set comprises An external file that holds a picture, illustration, etc. mutations, of which An external file that holds a picture, illustration, etc. correspond to hot spots. Therefore, the randomization procedure is not producing a Gaussian distribution [34,36,39-87] as described in our previous combarative docking study, limiting the applicability [41,42,67-92] of the z-score for a linear kernel and implemented a nested-loop cross-validation scheme. Indeed, we find that the z-score cannot discriminate FDA-approved pairwise drug to protein and drug to drug combinations [22,27-78,93) or clinically reported adverse drug interactions from random drug pairs (Figures 3a-3h). Instead of relying on randomization, therefore, [23,24-56-94]. we measure the network proximity of drug–target modules A, B as reflected in their target localizations of two nested cross-validation loops using the recently introduced separation measure sAB≡dAB–dAA+dBB2(2) an outer one for testing which compares the mean shortest distance within the SARS-CoV-2 main protease, an inner one for choosing hyper-parameters of the protein network of the Mpro, DPP4, ADABP, ADCP2, CD26, DPPIV, TP103, FURIN, FUR, PACE, PCSK3,GS, FURIN-ADAMTS1-ROR-GAMMA-SRRM2-ROR- NF-B/RelA-STAT3A-RORκ NF-B/RelA-STAT3B, Nsp15,CTSB, APPS, CPSB, RECEUP, SLC6A19 B0AT1, HND, cathepsin B|APP secretase|amyloid precursor interactome between the targets of each drug,dAA and dB, to the mean shortest distance dABbetween A–B target pairs (Figures 1a-1g,) [44,47,49-51,59-87]. As input features for the Support Vector Machines the hyper-parameters we have used basic energy terms are optimised by applying a grid search and the model performance is assessed by means of the F1 score that have been found to be important for the stability of protein complexes. In dAB, targets associated with both drugs A and B have a zero atomic distance by definition [41,49-60,79-92]. For sAB < 0, the molecular targets of the Remdesivir, Colchicine and Ursolic acid drugs which are located in the same network neighborhood between side-chain atoms of the mutated residue and other atoms in the same protein allows also to estimate statistical errors on performance measures (Figures 1a-1g), while for sAB ≥ 0, the combination of drug targets are topologically separated.

Analyses of non-synonymous variations

The SARS-CoV-2 genomic sequences were obtained from the GISAID database (www.gisaid.org) by grouping mutations according to the amino acid type. The identification of a non-synonymous variation (NSV) in the selected Side-chain inter-molecular SARS-COV-2 protein targets was performed according to the CoV-GLUE database [63,64-78]. (http://cov-glue.cvr.gla.ac.uk, accessed on July 7, 2020) and we annotated for each residue containing environment inter-molecular van der Waals, hydrogen bond and solvation side-chain inter-molecular energies, van der Waals, hydrogen bond and solvation environment inter-molecular energies, and van der Waals side-chain intra-molecular energies where NSV represent the physicochemical properties of the related amino acids in both the Wuhan-Hu-1 reference sequence (NCBI NC045512.2) and the genome sequence recovered from GISAID. The prediction of the biological impact of NSV (deleterious or neutral) was estimated from homology data combined with BLOSUM62 substitution matrices provided by the PROVEAN algorithm (http://provean.jcvi.org/index.php). For annotation of the region in the amino acid sequence, where the residues with NSV are located, we used several databases, such as PDB, InterPro (https://www.ebi.ac.uk/InterPro/search/sequence) and UniProt-covid19 (https://covid-19.uniprot.org). Also, we sought carefully and thoroughly in the literature for mutagenesis experiments with evidence of alteration in the protein molecular function and/or viral fitness in CoVs involving the focused residue.

Preparation of the Protein structures

We provided to the DockThor-VS users the structures of some SARS-CoV-2 potential therapeutic targets for the design of new drugs and vaccines. For this purpose, we initially select the non-structural proteins Nsp3, Nsp5 (PLpro domain), Nsp12 (RdRp) and Nsp15 (endoribonuclease), and the structural proteins Spike and nucleocapsid protein (N protein). For the N protein, we clustered 31 conformations with Glu174 present in an opened conformation out of a total of 40 states present in the NMR-derived structure (PDB code 6YI3 49) to select a small subset representative of the protein flexibility. The aliphatic carbon atoms from the Glu174 side chain are part of the phosphate binding site and the closed conformation might lead to steric clashes with potential inhibitors in the binding site. For this purpose, we clustered the opened states (31 out of 40 states) using the Conformer Cluster tool in BiogenetoligandorolTM (BiogenetoligandorolTM, SyntocureTMNew York, NY, 2020) according to the position of the residues Arg102 and Tyr109 using the weighted centroid as the linkage method. Finally, the nearest to the centroid structure per cluster was selected as the representative conformation of each group to be available at BiogenetoligandorolTM. In this work, we prepared the protein structures using the Protein Preparation Wizard from BiogenetoligandorolTM (Schrödinger Release 2020-2: BiogenetoligandorolTM, SyntocureTMNew York, NY, 2020). Protonation assignment and hydrogen-bond optimization were performed using ProtAssign and PROPKA 84 at the reported experimental pH and considering the presence of the bound ligand when available. Metal ions were considered as cofactors when necessary, whereas water molecules and ligands originally present in the experimental structures were removed. The protonation/tautomeric states of the binding-site residues and the bound ligand were further visually inspected and appropriate corrections were made guided by the reaction mechanism of the protein target described in the literature. in silico point mutation for each of the variations was done using Modeller 85. First, an extended model is created, using standard topologies, for the mutated sequence. After that, all possible atomic coordinates are transferred from the wild model to the new mutated model. The missing coordinates are rebuilt using the standard topologies. The new sidechain atoms are randomly displaced by at most 4.0 κand then optimised by two runs of gradient descent. The mutated sidechain is further refined by a short round of Modeller's molecular dynamics. Cognate non-covalent ligands were maintained throughout the protocol when necessary.

Results

To the best of our knowledge, there are no published studies to date addressing and comparing the conservation and druggability of the CoV S protein, for such a wide range of sequences (n = 1086 S1; n = 1096 S2) from four Beta-CoVs (SARS-CoV- 2, SARS- CoVs, MERS-CoVs and Bat-SL-CoVs) and the crystallographic structures of all available SARS-CoV-2 S proteins (S- FURIN-ADAMTS1-ROR-GAMMA, monomer and trimer structures in either closed, semi-open and open state conformations, when applied). In the majority of recent studies, a comparative analysis of the S protein has been performed with one reference strain for each CoV type and thereby taking into account only the most prevalent residue harbored at a given position; It does not represent diversity and it overestimates the protein conservation score. To overcome this, we performed the conservation analysis using the total number of protein sequences treated for each CoV type, so that the conservation estimation takes into account the variations in the aa composition within each CoV. The present study has revealed the most propitious S domains to target in regard to the conservation and druggability analysis of both S monomer and trimer conformations. The S1-FURIN-ADAMTS1-ROR-GAMMA represents a promising anti-COV target and is the most conserved druggable domain in the monomer analysis for hSARSr-CoVs and for SARSr- and MERSr-CoVs; and in the trimer analysis for hSARSr-CoVs. For the SARSr- and MERSr-CoV trimer, the FURIN-ADAMTS1-ROR-GAMMA ranks second after the SD1 domain; which is concordant with different CoVs using distinct host receptors for entry [45]. The Remdesivir, Colchicine and Ursolic acid drugs bind into the SD1 stands the most conserved druggable domain among all four Beta-CoVs analyzed. In this context, the Remdesivir, Colchicine and Ursolic acid drugs targets both FURIN-ADAMTS1-ROR-GAMMA and SD1

Table 1b. Fitness scoring ranking of the 6ajz-colchicine: 6AJZ Joint nentron and X-ray structure of BRD4 in complex with colchicin

name	lig_cov	poc_cov	lig_name	volume	enclosure	surface	depth	surf/vol	lid/hull	ellVol	ell c/a	ell b/a	siteAtms	accept	donor	hydrophobic_ interactions	hydrophobicity	metal	Cs	Ns
P_0	64.81	19.22	LOC_A_200	911.55	0.11	1281.56	19.05	1.405913	-	-	0.26	0.38	186	51	20	78	0.52	0	131	25
P_1	0	0	LOC_A_200	203.01	0.19	567.65	12.38	2.7961677	-	-	0.12	0.14	64	22	10	32	0.5	0	41	12
P_2	0	0	LOC_A_200	110.98	0	209.26	10.77	1.885565	-	-	0.16	0.26	59	18	4	9	0.29	0	41	9

Os	Ss	Xs	negAA	posAA	polarAA	apolarAA	ALA	ARG	ASN	ASP	CYS	GLN	GLU	GLY	HIS	ILE	LEU	LYS	MET	PHE
28	2	0	0.05	0.08	0.34	0.53	1	0	3	2	1	2	0	1	0	2	2	3	3	2
11	0	0	0.07	0.14	0.36	0.43	1	0	1	1	0	0	0	0	0	0	1	2	1	0
9	0	0	0	0.27	0.45	0.27	0	2	1	0	0	2	0	0	0	0	3	1	0	0

PRO	SER	THR	TRP	TYR	VAL	simpleScore	drugScore
7	0	3	2	3	1	0.64	0.820003
2	1	1	0	2	1	0.08	0.467499
0	0	0	0	2	0	0	0.300362

Table 2. Fitness scoring ranking of the Ursolic acid small molecule inside the mutant Human ROR gamma Ligand Binding Domain pdb:5x8s protein targets

name a/b	lig_cov siteAtms	poc_cov accept	lig_name donor	volume hydrophobi	enclosure interactions	surface	depth hydrophobicity	surf/vol	lid/hull metal	ellVol Cs	ell c/a Ns	ell Os
	Ss	Xs	negAA	posAA	polarAA	apolarAA	ALA	ARG	ASN	ASP	CYS	GLN
	GLU	GLY	HIS	ILE	LEU	LYS	MET	PHE	PRO	SER	THR	TRP
	TYR	VAL	simpleScore	drugScore								
P_0	0.00	0.00	6Q5_A_90000									
	0.02	0.03	167	60	686.02	0.21	902.43	22.67	1.3154572752980962		-	-
	0	0.05	0.19	0.22	7	47	0.41	0	113	22	32	0
	00	5	0	2	0.54	5	1	0	0	0	6	2
	4	0.46	0.85352		1	1	2	2	0	0	4	0
P_1	0.00	0.00	6Q5_A_90000									
	0.13	0.18	116	21	630.46	0.07	548.67	15.54	0.870269327157948		-	-
	0	0.00	0.15	0.15	8	31	0.52	0	91	12	11	2
	0	2	2	5	0.69	2	2	0	0	2	1	0
	3	0.46	0.788771		0	1	4	0	0	0	1	1
P_2	98.77	81.91	6Q5_A_90000									
	0.12	0.18	110	19	592.99	0.09	481.11	17.02	0.8113290274709523		-	-
	0	0.00	0.15	0.15	6	26	0.51	0	88	10	10	2
	0	2	2	5	0.69	2	2	0	0	2	1	0
	3	0.43	0.799819		0	1	4	0	0	0	1	1
P_3	0.00	0.00	6Q5_A_90000									
	0.09	0.26	108	25	465.48	0.19	653.11	17.80	1.4030892841797713		-	-
	0	0.04	0.17	0.25	11	24	0.40	0	79	16	11	2
	1	1	4	1	0.54	2	1	2	0	1	1	1
	3	0.29	0.777717		2	1	0	2	1	0	0	0
P_4	0.00	0.00	6Q5_A_90000									
	0.12	0.29	79		407.45	0.12	621.86	13.25	1.5262240765738129		-	-
	0	0.11	0.26	26	14	28	0.41	0	11	13	0	2
	1	2	0	0.21	0.42	0	2	1	0	1	2	1
	1	0.25	0.636122	4	1	0	1	2	0	0	1	0
P_5	0.00	0.00	6Q5_A_90000									
	0.02	0.03	144	34	345.66	0.03	547.52	31.78	1.5839842619915523		-	-
	0	0.00	0.19	0.23	8	9	0.18	0	106	13	23	2
	0	4	4	6	0.58	0	0	0	0	0	7	0
	3	0.10	0.899648		2	2	2	1	0	0	0	0
P_6	0.00	0.00	6Q5_A_90000									
	0.21	0.46	81	20	310.75	0.17	438.56	10.78	1.4112952534191472		-	-
	0	0.05	0.16	0.32	8	22	0.46	0	57	11	12	1
	0	1	1	5	0.58	2	2	1	0	1	0	1
	0	0.18	0.5		2	0	1	0	2	0	0	2
P_7	0.00	0.00	6Q5_A_90000									
	0.12	0.20	67	20	307.34	0.31	484087	14.56	1.5776338908049719		-	-
	0	0.11	0.28	0.17	13	26	0.44	0	48	10	9	0
	1	1	0	4	0.44	0	2	1	0	0	0	2
	1	0.16	0.62362		2	0	1	2	0	0	0	1
P_8	0.00	0.00	6Q5_A_90000									
	0.18	0.41	77	24	285.66	0.17	403.86	10.67	1.413778617937408		-	-
	0	0.11	0.16	0.26	6	10	0.25	0	51	12	13	1
	0	1	1	5	0.47	2	2	1	1	1	0	1
	0	0.07	0.474819		0	0	1	0	1	0	0	2
P_9	0.00	0.00	6Q5_A_90000									
	0.19	0.38	74	13	208.16	0.11	311.89	12.99	1.498316010760954		-	-
	0	0.06	0.24	0.24	8	10	0.32	0	51	13	8	2
	1	1	0	1	0.47	2	2	0	0	1	1	1
	1	0.01	0.5		1	1	0	1	1	0	0	0

P_10	0.00	0.00	6Q5_A_90000										
	0.24	0.59	46	10	163.35	0.08	301.57	8.66	1.8461585552494644		-	-	
	0	0.00	0.08	0.31	6	9	0.36	0	35	5	6	0	
	1	0	1	4	0.62	1	1	1	0	0	0	0	
	1	0.00	0.309531		0	0	1	0	2	0	0	0	
P_11	0.00	0.00	6Q5_A_90000										
	0.22	0.54	53	12	159.26	0.09	277.22	8.77	1.74061283435891		-	-	
	0	0.00	0.07	0.36	4	6	0	0	41	5	7	0	
	1	0	1	4	0.57	1	1	1	0	0	0	0	
	1	0.00	0.30591		0	0	1	0	3	0	0	0	
P_12	0.00	0.00	6Q5_A_90000										
	0.30	0.52	38	9	110.18	0.09	308.18	7.73	2.797059357415139		-	-	
	0	0.12	0.12	0.38	3	16	0.57	0	26	5	6	1	
	1	0	1	0	0.38	0	1	0	0	1	0	1	
	0	0.00	0.207291		0	1	1	0	1	0	0	0	
P_13	0.00	0.00	6Q5_A_90000										
	0.22	0.40	49	11	102.50	0.08	297.31	9.08	2.9005853658536584		-	-	
	0	0.10	0.10	0.40	4	14	0.48	0	33	8	6	2	
	1	0	0	1	0.40	0	1	0	0	1	0	1	
	0	0.00	0.2498.6		0	1	1	0	2	0	0	0	

Table (3a-3e). Docking energy ranking analysis of the Colchicine, Remdesivir and Ursolic acid chemical strucutures in the pdb:6lu7 protein targets.

Compound	Energy	V-M-GLU-166	V-M-LEU-167	V-M-PRO-168	V-S-PRO-168	V-M-GLN-189	V-M-THR-190	V-M-ALA-191	V-M-ALA-2	V-M-VAL-3	V-S-VAL-3
cav6lu7_02J-Colchicine-0.pdb	-67.4	-2.06654	-4.97965	-10.4743	-8.98984	-4.03283	-6.24897	-3.46474	-11.5726	-3.22075	-5.20269
cav6lu7_02J-Ursolic acid-0.pdb	-54.8	-2.47196	0.546601	-10.3582	-8.03218	-4.03691	-7.35473	-4.92237	1.26903	-2.68435	-4.65453
cav6lu7_02J-Remdesivir_Gilead_-0.pdb	-50.8	-4.00794	3.29678	-3.37184	-9.07342	-5.2667	-8.94194	-1.94094	-4.27299	-4.25681	0.931221

Hydrogen Bonds

Index	Residue	AA	Distance H-A	Distance D-A	Donor Angle	Protein donor?	Sidechain	Donor Atom	Acceptor Atom
1	623A	ASP	2.09	2.73	122.27	✗	✓	8604 (O3)	4378 (O2)

Salt Bridges

Index	Residue	AA	Distance	Protein positive?	Ligand Group	Ligand Atoms
1	553A	ARG	5.33	✓	Phosphate	8596, 8596, 8597, 8598, 8599, 8600

Metal Complexes

Index	Residue	AA	Metal	Target	Distance	Location
Complex 1: Mg, trigonal.pyramidal (3)						
1	1003A	POP	8605	8600	2.70	ligand
2	1003A	POP	8605	8600	2.70	ligand
3	1003A	POP	8605	8600	2.70	protein.mainchain

G:P:10 (G-A-U-U-A-A-G-U-U-A-U-F86-MG) - RNA+ION
+ A:P:11
+ U:P:12
+ U:P:13
+ A:P:14
+ A:P:15
+ G:P:16
+ U:P:17
+ U:P:18
+ A:P:19
+ U:P:20
+ F86:P:101
+ MG:A:1005

Interacting chain(s): A,P

Hydrogen Bonds

RESNR	RESTYPE	RESCHAIN	RESNR_LIG	RESTYPE_LIG	RESCHAIN_LIG	SIDECHAIN	DIST_H-A	DIST_D-A	DON_ANGLE	PROTISDON	DONORIDX	DONORTYPE	ACCEPTORIDX	ACCEPTORTYPE	LIGCOO	PROTCOO
513	ARG	A	14	A	P	||	3.09	3.45	102.67	||	3502	Ng+	8154	O3	71.981, 98.274, 115.942	72.124, 101.715, 116.067
555	ARG	A	101	F86	P	||	3.47	4.04	119.47	||	3849	Ng+	8617	Nar	89.204, 94.166, 107.454	93.004, 93.527, 108.680
555	ARG	A	101	F86	P	||	3.16	3.92	134.87	||	3850	Ng+	8615	Nar	89.857, 94.508, 105.120	93.219, 93.014, 106.463
623	ASP	A	101	F86	P	||	3.55	3.98	109.70	||	8628	O3	4372	N2	94.420, 94.107, 101.216	98.244, 94.977, 100.532
691	ASN	A	101	F86	P	||	2.89	3.60	129.54	||	4885	Nam	8628	O3	94.420, 94.107, 101.216	92.168, 94.986, 98.546
759	SER	A	20	U	P	||	2.21	3.00	137.32	||	5447	O3	8292	O3	89.412, 90.668, 100.538	89.977, 92.306, 98.089
760	ASP	A	20	U	P	||	3.12	3.82	130.09	||	8292	O3	5454	O2	89.412, 90.668, 100.538	92.565, 90.018, 98.488
760	ASP	A	101	F86	P	||	2.51	3.45	163.02	||	8629	O3	5455	O3	93.876, 87.784, 101.166	94.760, 89.856, 98.556
814	SER	A	20	U	P	||	2.91	3.53	122.40	||	5880	O3	8284	O2	90.326, 84.650, 104.677	91.202, 81.481, 103.402
861	SER	A	16	G	P	||	2.90	3.87	169.93	||	8217	Npl	6248	O3	76.013, 83.703, 111.625	77.019, 80.413, 113.400
861	SER	A	17	U	P	||	2.89	3.64	135.36	||	6248	O3	8226	O3	79.911, 82.552, 113.981	77.019, 80.413, 113.400
865	ASP	A	17	U	P	||	3.03	3.36	102.95	||	6277	O3	8230	O3	81.348, 80.859, 111.847	81.455, 78.738, 109.239
865	ASP	A	17	U	P	||	2.75	3.36	121.52	||	8230	O3	6277	O3	81.348, 80.859, 111.847	81.455, 78.738, 109.239

Salt Bridges

RESNR	RESTYPE	RESCHAIN	RESNR_LIG	RESTYPE_LIG	RESCHAIN_LIG	DIST	PROTISPOS	LIG_GROUP	LIG_IDX_LIST	LIGCOO	PROTCOO
836	ARG	A	18	U	P	4.57 || Phosphate	8240,8240,8243,8228,8241,8242	84.767, 82.285, 113.039	88.794, 80.678, 111.585		
836	ARG	A	19	A	P	4.24 || Phosphate	8260,8260,8248,8261,8262,8263	87.449, 82.116, 107.828	88.794, 80.678, 111.585		
849	LYS	A	17	U	P	4.64 || Phosphate	8220,8220,8205,8222,8223,8221	81.688, 84.935, 117.166	84.063, 86.886, 120.648		
858	ARG	A	17	U	P	4.87 || Phosphate	8220,8220,8205,8222,8223,8221	81.688, 84.935, 117.166	84.095, 81.011, 118.771		

pi-Cation Interactions

RESNR	RESTYPE	RESCHAIN	RESNR_LIG	RESTYPE_LIG	RESCHAIN_LIG	DIST	OFFSET	PROTCHARGED	LIG_GROUP	LIG_IDX_LIST	LIGCOO	PROTCOO

+=======+=========+==========+==========+==========+==========+======+========+==========+==========+==========+==========+==========+==========+
| 555 | ARG | A | 101 | F86 | P | 3.61 | 1.61 || Aromatic | 8618,8608,8610,8621,8625 | 90.830, 92.165, 105.289 | 93.435, 92.714, 107.732 |
+-----+-------+--------+--------+----------+----------+-----+------+----------+--------+--------------------+--------------------+--------------------+

Metal Complexes

+------+--------+---------+---------+-----------+-----------+---------+----------+----------+-----------+-----------+-----+---------+-----+---------+----------+--------------------+--------------------+
| RESNR | RESTYPE | RESCHAIN | RESNR_LIG | RESTYPE_LIG | RESCHAIN_LIG | METAL_IDX | METAL_TYPE | TARGET_IDX | TARGET_TYPE | COORDINATION | DIST | LOCATION | RMS | GEOMETRY | COMPLEXNUM | METALCOO | TARGETCOO |
+=======+=========+==========+==========+==========+==========+==========+==========+==========+==========+==========+==========+==========+==========+==========+==========+==========+
| 10 | G | P | 1005 | MG | A | 8606 | Mg | 8283 | O | 1 | 2.33 | ligand | 0.00 | NA | 1 | 92.442, 84.162, 100.658 | 90.927, 83.719, 102.373 |
+------+--------+---------+---------+-----------+-----------+---------+----------+----------+-----------+-----------+-----+---------+-----+---------+----------+--------------------+--------------------+

POP:A:1003 (POP-MG) - SMALLMOLECULE+ION
 + MG:A:1004

Interacting chain(s): A

Hydrogen Bonds

+------+--------+---------+---------+-----------+-----------+---------+---------+---------+---------+---------+---------+-----------+-----------+--------------------+-----------------+
| RESNR | RESTYPE | RESCHAIN | RESNR_LIG | RESTYPE_LIG | RESCHAIN_LIG | SIDECHAIN | DIST_H-A | DIST_D-A | DON_ANGLE | PROTISDON | DONORIDX | DONORTYPE | ACCEPTORIDX | ACCEPTORTYPE | LIGCOO | PROTCOO |
+=======+=========+==========+==========+==========+==========+==========+==========+==========+==========+==========+==========+==========+==========+==========+==========+
| 623 | ASP | A | 1003 | POP | A || 2.09 | 2.73 | 122.27 || 8604 | O3 | 4378 | O2 | 97.772, 91.527, 104.104 | 98.436, 93.956, 103.045 |
+------+--------+---------+---------+-----------+-----------+---------+---------+---------+---------+---------+---------+-----------+-----------+--------------------+-----------------+

Salt Bridges

+------+--------+---------+---------+-----------+-----------+-----+---------+---------+--------------------+--------------------+--------------------+
| RESNR | RESTYPE | RESCHAIN | RESNR_LIG | RESTYPE_LIG | RESCHAIN_LIG | DIST | PROTISPOS | LIG_GROUP | LIG_IDX_LIST | LIGCOO | PROTCOO |
+=======+=========+==========+==========+==========+==========+======+==========+==========+==========+==========+==========+==========+==========+
| 553 | ARG | A | 1003 | POP | A | 5.33 || Phosphate | 8596,8596,8597,8598,8599,8600 | 98.704, 88.743, 103.451 | 100.769, 90.374, 108.090 |
+------+--------+---------+---------+-----------+-----------+-----+---------+---------+--------------------+--------------------+--------------------+

Metal Complexes

+------+--------+---------+---------+-----------+-----------+---------+----------+----------+-----------+-----------+-----+---------+-----+---------+----------+--------------------+--------------------+
| RESNR | RESTYPE | RESCHAIN | RESNR_LIG | RESTYPE_LIG | RESCHAIN_LIG | METAL_IDX | METAL_TYPE | TARGET_IDX | TARGET_TYPE | COORDINATION | DIST | LOCATION | RMS | GEOMETRY | COMPLEXNUM | METALCOO | TARGETCOO |
+=======+=========+==========+==========+==========+==========+==========+==========+==========+==========+==========+==========+==========+==========+==========+==========+==========+
| 1003 | POP | A | 1004 | MG | A | 8605 | Mg | 8600 | O | 3 | 2.70 | ligand | 436.24 | trigonal.pyramidal | 1 | 97.212, 88.488, 100.157 | 97.928, 89.726, 102.450 |
+------+--------+---------+---------+-----------+-----------+---------+----------+----------+-----------+-----------+-----+---------+-----+---------+----------+--------------------+--------------------+
| 1003 | POP | A | 1004 | MG | A | 8605 | Mg | 8600 | O | 3 | 2.70 | ligand | 436.24 | trigonal.pyramidal | 1 | 97.212, 88.488, 100.157 | 97.928, 89.726, 102.450 |
+------+--------+---------+---------+-----------+-----------+---------+----------+----------+-----------+-----------+-----+---------+-----+---------+----------+--------------------+--------------------+
| 1003 | POP | A | 1004 | MG | A | 8605 | Mg | 8600 | O | 3 | 2.70 | protein.mainchain | 436.24 | trigonal.pyramidal | 1 | 97.212, 88.488, 100.157 | 97.928, 89.726, 102.450 |
+------+--------+---------+---------+-----------+-----------+---------+----------+----------+-----------+-----------+-----+---------+-----+---------+----------+--------------------+--------------------+

U:T:8 (U-U-U-A-U-A-A-C-U-U-A-A-U-C) - RNA
 + U:T:9
 + U:T:10
 + A:T:11

+ U:T:12
+ A:T:13
+ A:T:14
+ C:T:15
+ U:T:16
+ U:T:17
+ A:T:18
+ A:T:19
+ U:T:20
+ C:T:21

Interacting chain(s): A

Hydrogen Bonds

RESNR	RESTYPE	RESCHAIN	RESNR_LIG	RESTYPE_LIG	RESCHAIN_LIG	SIDECHAIN	DIST_H-A	DIST_D-A	DON_ANGLE	PROTISDON	DONORIDX	DONORTYPE	ACCEPTORIDX	ACCEPTORTYPE	LIGCOO	PROTCOO
496	ASN	A	13	A	T	||	1.91	2.64	128.77	||	3365	Nam	8407	O3	77.151, 95.522, 103.263	76.169, 96.490, 105.518
501	SER	A	9	U	T	||	2.48	3.21	132.45	||	8325	O3	3404	O3	86.816, 103.047, 119.686	85.287, 102.382, 116.940
501	SER	A	9	U	T	||	2.12	2.99	148.42	||	3404	O3	8326	O3	87.796, 101.319, 118.175	85.287, 102.382, 116.940
507	ASN	A	9	U	T	||	2.58	3.43	143.55	||	3450	Nam	8324	O2	87.995, 103.701, 117.504	88.917, 106.986, 117.807
543	ASN	A	8	U	T	||	3.04	3.54	113.10	||	8313	O3	3752	O2	90.760, 100.575, 119.969	92.520, 101.696, 117.111
545	LYS	A	10	U	T	||	2.96	3.86	146.92	||	3770	N3	8360	O2	87.885, 94.285, 110.425	89.591, 92.494, 113.386
558	ALA	A	10	U	T	||	2.91	3.52	121.77	||	8353	O3	3868	O2	86.754, 101.576, 109.175	90.273, 101.592, 109.043
569	ARG	A	11	A	T	||	3.38	3.85	111.72	||	3947	Ng+	8364	O2	81.862, 101.721, 110.055	79.628, 103.317, 107.356
590	GLY	A	13	A	T	||	3.17	3.91	133.56	||	8415	O3	4104	O2	78.508, 88.871, 100.386	76.115, 88.087, 97.401
592	SER	A	14	A	T	||	2.73	3.08	101.92	||	4117	O3	8435	O3	73.881, 85.062, 101.760	75.282, 82.656, 100.434
592	SER	A	14	A	T	||	2.19	2.61	104.41	||	8437	O3	4117	O3	76.269, 83.871, 102.524	75.282, 82.656, 100.434
689	TYR	A	12	U	T	||	2.77	3.27	112.65	||	8395	O3	4872	O3	81.193, 94.709, 100.683	80.067, 95.851, 97.831

Salt Bridges

RESNR	RESTYPE	RESCHAIN	RESNR_LIG	RESTYPE_LIG	RESCHAIN_LIG	DIST	PROTISPOS	LIG_GROUP	LIG_IDX_LIST	LIGCOO	PROTCOO
500	LYS	A	10	U	T	4.74 ||	Phosphate	8343,8343,8331,8344,8345,8346	85.331, 98.567, 114.832	81.035, 96.573, 115.055
511	LYS	A	9	U	T	5.37 ||	Phosphate	8323,8323,8311,8324,8325,8326	87.895, 102.823, 118.694	82.545, 102.624, 119.139
569	ARG	A	12	U	T	5.03 ||	Phosphate	8385,8385,8371,8388,8386,8387	80.244, 99.252, 105.528	78.863, 103.989, 106.509
577	LYS	A	13	A	T	4.21 ||	Phosphate	8405,8405,8393,8406,8407,8408	77.383, 95.322, 101.815	74.047, 97.842, 101.330

+------+--------+---------+----------+-----------+-----------+-----+---------+---------+----------------------+--------------------+----------------------+

ZN:A:1001 (ZN) - ION

Interacting chain(s): A

Metal Complexes
+------+--------+---------+----------+-----------+-----------+---------+----------+----------+-----------+-----------+-----+---------------+------+-----------+----------+-----------+
| RESNR | RESTYPE | RESCHAIN | RESNR_LIG | RESTYPE_LIG | RESCHAIN_LIG | METAL_IDX | METAL_TYPE | TARGET_IDX | TARGET_TYPE | COORDINATION | DIST | LOCATION | RMS | GEOMETRY | COMPLEXNUM | METALCOO | TARGETCOO |
+=======+=========+==========+===========+=============+==============+===========+============+============+=============+==============+======+==================+=======+============+============+========================+========================+
| 295 | HIS | A | 1001 | ZN | A | 8594 | Zn | 1771 | N | 4 | 2.09 | protein.sidechain | 12.73 | tetrahedral | 1 | 96.331, 117.049, 82.559 | 96.922, 118.888, 81.758 |
+------+--------+---------+----------+-----------+-----------+---------+----------+----------+-----------+-----------+-----+---------------+------+-----------+----------+-----------+
| 301 | CYS | A | 1001 | ZN | A | 8594 | Zn | 1816 | S | 4 | 2.31 | protein.sidechain | 12.73 | tetrahedral | 1 | 96.331, 117.049, 82.559 | 95.190, 116.820, 84.554 |
+------+--------+---------+----------+-----------+-----------+---------+----------+----------+-----------+-----------+-----+---------------+------+-----------+----------+-----------+
| 306 | CYS | A | 1001 | ZN | A | 8594 | Zn | 1857 | S | 4 | 2.31 | protein.sidechain | 12.73 | tetrahedral | 1 | 96.331, 117.049, 82.559 | 94.999, 116.199, 80.872 |
+------+--------+---------+----------+-----------+-----------+---------+----------+----------+-----------+-----------+-----+---------------+------+-----------+----------+-----------+
| 310 | CYS | A | 1001 | ZN | A | 8594 | Zn | 1889 | S | 4 | 2.31 | protein.sidechain | 12.73 | tetrahedral | 1 | 96.331, 117.049, 82.559 | 98.374, 115.977, 82.704 |
+------+--------+---------+----------+-----------+-----------+---------+----------+----------+-----------+-----------+-----+---------------+------+-----------+----------+-----------+

ZN:A:1002 (ZN) - ION

Interacting chain(s): A

Metal Complexes
+------+--------+---------+----------+-----------+-----------+---------+----------+----------+-----------+-----------+-----+---------------+------+-----------+----------+-----------+
| RESNR | RESTYPE | RESCHAIN | RESNR_LIG | RESTYPE_LIG | RESCHAIN_LIG | METAL_IDX | METAL_TYPE | TARGET_IDX | TARGET_TYPE | COORDINATION | DIST | LOCATION | RMS | GEOMETRY | COMPLEXNUM | METALCOO | TARGETCOO |
+=======+=========+==========+===========+=============+==============+===========+============+============+=============+==============+======+==================+=======+============+============+========================+========================+
| 487 | CYS | A | 1002 | ZN | A | 8595 | Zn | 3297 | S | 4 | 2.38 | protein.sidechain | 23.09 | tetrahedral | 1 | 78.230, 111.511, 90.977 | 77.360, 111.957, 93.151 |
+------+--------+---------+----------+-----------+-----------+---------+----------+----------+-----------+-----------+-----+---------------+------+-----------+----------+-----------+
| 642 | HIS | A | 1002 | ZN | A | 8595 | Zn | 4527 | N | 4 | 1.87 | protein.sidechain | 23.09 | tetrahedral | 1 | 78.230, 111.511, 90.977 | 79.047, 109.825, 91.004 |
+------+--------+---------+----------+-----------+-----------+---------+----------+----------+-----------+-----------+-----+---------------+------+-----------+----------+-----------+
| 645 | CYS | A | 1002 | ZN | A | 8595 | Zn | 4550 | S | 4 | 2.39 | protein.sidechain | 23.09 | tetrahedral | 1 | 78.230, 111.511, 90.977 | 76.284, 112.069, 89.705 |
+------+--------+---------+----------+-----------+-----------+---------+----------+----------+-----------+-----------+-----+---------------+------+-----------+----------+-----------+
| 646 | CYS | A | 1002 | ZN | A | 8595 | Zn | 4556 | S | 4 | 2.34 | protein.sidechain | 23.09 | tetrahedral | 1 | 78.230, 111.511, 90.977 | 79.282, 113.589, 90.789 |
+------+--------+---------+----------+-----------+-----------+---------+----------+----------+-----------+-----------+-----+---------------+------+-----------+----------+-----------+

Table 3a. Ursolic acid binding site(s) in 7BV2 protein targets.

Hydrophobic Interactions

Index	Residue	AA	Distance	Ligand Atom	Protein Atom
1	25A	THR	3.73	2415	179
2	26A	THR	3.81	2415	186

Hydrogen Bonds

Index	Residue	AA	Distance H-A	Distance D-A	Donor Angle	Protein donor?	Sidechain	Donor Atom	Acceptor Atom
1	143A	GLY	1.93	2.80	145.29	✓	✗	1105 (Nam)	2411 (O3)
2	164A	HIS	2.16	3.07	153.73	✗	✗	2408 (N3)	1266 (O2)

02J:C:1 (02J) - SMALLMOLECULE

Interacting chain(s): A

Hydrophobic Interactions
+------+--------+---------+---------+-----------+-----------+-----+-----------+-----------+-------------------+-------------------+
| RESNR | RESTYPE | RESCHAIN | RESNR_LIG | RESTYPE_LIG | RESCHAIN_LIG | DIST | LIGCARBONIDX | PROTCARBONIDX | LIGCOO | PROTCOO |
+=======+=========+==========+===========+=============+==============+======+==============+===============+====================+=======================+
| 168 | PRO | A | 1 | 02J | C | 3.53 | 2369 | 1303 | -10.425, 3.420, 72.447 | -13.394, 3.190, 70.551 |
+------+--------+---------+---------+-----------+-----------+-----+-----------+-----------+-------------------+-------------------+

PJE:C:5 (PJE-010) - SMALLMOLECULE
+ 010:C:6

Interacting chain(s): A

Hydrophobic Interactions
+------+--------+---------+---------+-----------+-----------+-----+-----------+-----------+-------------------+-------------------+
| RESNR | RESTYPE | RESCHAIN | RESNR_LIG | RESTYPE_LIG | RESCHAIN_LIG | DIST | LIGCARBONIDX | PROTCARBONIDX | LIGCOO | PROTCOO |
+=======+=========+==========+===========+=============+==============+======+==============+===============+====================+=======================+
| 25 | THR | A | 6 | 010 | C | 3.73 | 2415 | 179 | -7.156, 21.406, 66.898 | -8.709, 22.779, 70.002 |
+------+--------+---------+---------+-----------+-----------+-----+-----------+-----------+-------------------+-------------------+
| 26 | THR | A | 6 | 010 | C | 3.81 | 2415 | 186 | -7.156, 21.406, 66.898 | -6.155, 24.392, 64.757 |
+------+--------+---------+---------+-----------+-----------+-----+-----------+-----------+-------------------+-------------------+

Hydrogen Bonds
+------+--------+---------+---------+-----------+-----------+---------+---------+---------+---------+---------+---------+-----------+-----------+--------------------+-----------------+
| RESNR | RESTYPE | RESCHAIN | RESNR_LIG | RESTYPE_LIG | RESCHAIN_LIG | SIDECHAIN | DIST_H-A | DIST_D-A | DON_ANGLE | PROTISDON | DONORIDX | DONORTYPE | ACCEPTORIDX | ACCEPTORTYPE | LIGCOO | PROTCOO |
+=======+=========+==========+===========+=============+==============+===========+==========+==========+===========+===========+==========+===========+=============+==============+========================+=========================+
| 143 | GLY | A | 6 | 010 | C || 1.93 | 2.80 | 145.29 || 1105 | Nam | 2411 | O3 | -8.911, 17.849, 65.703 | -8.918, 17.918, 62.905 |
+------+--------+---------+---------+-----------+-----------+---------+---------+---------+---------+---------+---------+-----------+-----------+--------------------+-----------------+
| 164 | HIS | A | 5 | PJE | C || 2.16 | 3.07 | 153.73 || 2408 | N3 | 1266 | O2 | -12.282, 14.994, 67.123 | -15.161, 15.336, 68.144 |
+------+--------+---------+---------+-----------+-----------+---------+---------+---------+---------+---------+---------+-----------+-----------+--------------------+-----------------+

Table 3b. Colchicine binding site(s) in 6LU7 protein targets.

Hydrophobic Interactionsc

Index	Residue	AA	Distance	Ligand Atom	Protein Atom
1	287B	LEU	3.94	3882	2109
2	323B	HIS	3.62	3881	2425
3	364B	ARG	3.89	3885	2746
4	365B	MET	3.86	3879	2757
5	368B	ALA	3.88	3876	2782
6	388B	PHE	3.79	3903	2948
7	388B	PHE	3.77	3900	2945
8	391B	LEU	3.99	3900	2971

Hydrogen Bonds

Index	Residue	AA	Distance H-A	Distance D-A	Donor Angle	Protein donor?	Sidechain	Donor Atom	Acceptor Atom
1	479B	HIS	1.92	2.69	134.37	✖	✔	3898 (O3)	3684 (N2)

Water Bridges

Index	Residue	AA	Dist. A-W	Dist. D-W	Donor Angle	Water Angle	Protein donor?	Donor Atom	Acceptor Atom	Water Atom
1	286B	GLN	3.78	2.79	111.72	79.32	✖	3874 (O.co2)	2101 (O2)	4074
2	323B	HIS	2.82	2.79	111.72	86.96	✖	3874 (O.co2)	2424 (O2)	4074

Salt Bridges

Index	Residue	AA	Distance	Protein positive?	Ligand Group	Ligand Atoms
1	323B	HIS	3.83	✔	Carboxylate	3872, 3874

6Q5:A:9000 (6Q5) - SMALLMOLECULE

Interacting chain(s): A

Hydrophobic Interactions

RESNR	RESTYPE	RESCHAIN	RESNR_LIG	RESTYPE_LIG	RESCHAIN_LIG	DIST	LIGCARBONIDX	PROTCARBONIDX	LIGCOO	PROTCOO
287	LEU	A	9000	6Q5	A	3.99	3849	200	-19.472, 23.825, -15.927	-15.959, 22.345, -17.092
323	HIS	A	9000	6Q5	A	3.56	3848	516	-25.010, 21.669, -15.561	-24.824, 21.905, -12.016
361	VAL	A	9000	6Q5	A	3.98	3857	816	-24.212, 25.034, -15.221	-25.399, 28.772, -14.535
365	MET	A	9000	6Q5	A	3.80	3846	848	-24.128, 24.271, -18.572	-25.180, 27.614, -20.049
368	ALA	A	9000	6Q5	A	3.88	3843	873	-21.262, 22.720, -17.507	-20.972, 23.811, -21.222
378	PHE	A	9000	6Q5	A	3.86	3870	957	-27.367, 21.410, -17.560	-25.628, 18.104, -16.576
388	PHE	A	9000	6Q5	A	3.84	3867	1036	-30.511, 21.408, -16.882	-30.458, 17.679, -17.777
388	PHE	A	9000	6Q5	A	3.78	3870	1039	-27.367, 21.410, -17.560	-28.435, 18.081, -19.010
401	PHE	A	9000	6Q5	A	3.92	3868	1133	-29.882, 21.956, -19.233	-30.313, 21.143, -23.040

Hydrogen Bonds

RESNR	RESTYPE	RESCHAIN	RESNR_LIG	RESTYPE_LIG	RESCHAIN_LIG	SIDECHAIN	DIST_H-A	DIST_D-A	DON_ANGLE	PROTISDON	DONORIDX	DONORTYPE	ACCEPTORIDX	ACCEPTORTYPE	LIGCOO	PROTCOO
479	HIS	A	9000	6Q5	A	||	1.99	2.81	141.07	||	3865	O3	1769	N2	-31.795, 23.607, -17.658	-33.511, 25.432, -16.376

Water Bridges

RESNR	RESTYPE	RESCHAIN	RESNR_LIG	RESTYPE_LIG	RESCHAIN_LIG	DIST_A-W	DIST_D-W	DON_ANGLE	WATER_ANGLE	PROTISDON	DONOR_IDX	DONORTYPE	ACCEPTOR_IDX	ACCEPTORTYPE	WATER_IDX	LIGCOO	PROTCOO	WATERCOO
286	GLN	A	9000	6Q5	A	3.86	2.74	109.20	83.72	||	3841	O.co2	192	O2	3919	-21.851, 22.512, -14.100	-19.469, 27.143, -13.131	-21.448, 24.074, -11.886
323	HIS	A	9000	6Q5	A	2.79	2.74	109.20	82.73	||	3841	O.co2	515	O2	3919	-21.851, 22.512, -14.100	-23.957, 24.722, -10.845	-21.448, 24.074, -11.886

Salt Bridges

RESNR	RESTYPE	RESCHAIN	RESNR_LIG	RESTYPE_LIG	RESCHAIN_LIG	DIST	PROTISPOS	LIG_GROUP	LIG_IDX_LIST	LIGCOO	PROTCOO
323	HIS	A	9000	6Q5	A	3.76 ||	Carboxylate	3839,3841	-21.295, 21.829, -14.748	-23.391, 19.443, -12.739	

6Q5:B:9000 (6Q5) - SMALLMOLECULE

Interacting chain(s): B

Hydrophobic Interactions

RESNR	RESTYPE	RESCHAIN	RESNR_LIG	RESTYPE_LIG	RESCHAIN_LIG	DIST	LIGCARBONIDX	PROTCARBONIDX	LIGCOO	PROTCOO
287	LEU	B	9000	6Q5	B	3.94	3882	2109	-19.512, 23.871, 15.615	-18.760, 20.132, 16.614
323	HIS	B	9000	6Q5	B	3.62	3881	2425	-16.253, 28.815, 15.240	-16.424, 28.628, 11.633
364	ARG	B	9000	6Q5	B	3.89	3885	2746	-23.128, 24.515, 17.133	-26.081, 26.967, 17.752
365	MET	B	9000	6Q5	B	3.86	3879	2757	-18.991, 28.503, 18.176	-22.074, 30.196, 19.769
368	ALA	B	9000	6Q5	B	3.88	3876	2782	-18.152, 25.419, 17.155	-19.122, 25.171, 20.904
388	PHE	B	9000	6Q5	B	3.79	3903	2948	-15.610, 30.999, 17.375	-12.080, 31.372, 18.709
388	PHE	B	9000	6Q5	B	3.77	3900	2945	-14.790, 33.953, 16.434	-11.219, 33.180, 17.374
391	LEU	B	9000	6Q5	B	3.99	3900	2971	-14.790, 33.953, 16.434	-12.130, 36.698, 15.281

Hydrogen Bonds

RESNR	RESTYPE	RESCHAIN	RESNR_LIG	RESTYPE_LIG	RESCHAIN_LIG	SIDECHAIN	DIST_H-A	DIST_D-A	DON_ANGLE	PROTISDON	DONORIDX	DONORTYPE	ACCEPTORIDX	ACCEPTORTYPE	LIGCOO	PROTCOO
479	HIS	B	9000	6Q5	B	||	1.92	2.69	134.37	||	3898	O3	3684	N2	-16.878, 35.920, 17.378	-18.215, 37.816, 16.016

Water Bridges

RESNR	RESTYPE	RESCHAIN	RESNR_LIG	RESTYPE_LIG	RESCHAIN_LIG	DIST_A-W	DIST_D-W	DON_ANGLE	WATER_ANGLE	PROTISDON	DONOR_IDX	DONORTYPE	ACCEPTOR_IDX	ACCEPTORTYPE	WATER_IDX	LIGCOO	PROTCOO	WATERCOO
286	GLN	B	9000	6Q5	B	3.78	2.79	111.72	79.32	||	3874	O.co2	2101	O2	4074	-17.702, 25.905, 13.706	-22.735, 24.355, 12.810	-19.450, 25.734, 11.544
323	HIS	B	9000	6Q5	B	2.82	2.79	111.72	86.96	||	3874	O.co2	2424	O2	4074	-17.702, 25.905, 13.706	-19.425, 28.344, 10.481	-19.450, 25.734, 11.544

Salt Bridges

RESNR	RESTYPE	RESCHAIN	RESNR_LIG	RESTYPE_LIG	RESCHAIN_LIG	DIST	PROTISPOS	LIG_GROUP	LIG_IDX_LIST	LIGCOO	PROTCOO
323	HIS	B	9000	6Q5	B	3.83 ||	Carboxylate	3872,3874	-17.172, 25.221, 14.372	-14.312, 26.677, 12.288	

Table 3c. Remdesivir binding site(s) in 5X8S protein targets.

domains which should be further addressed in future studies that target the S1 subunit. In regard to the S2 subunit, the FP was found to bear a high potential of druggability exclusively in hSARSr-CoVs (its conservation degree decreases when considering other beta -CoV species). On the other hand, the Colchicine, Remdesivir, Colchicine and Ursolic acid combination of drugs demonstrates a higher conservation-druggability potential among hSARSr-CoVs and in SARSr- and MERSr-CoVs and is the most conserved druggable domain within the S2 subunit. Other S2 domains, such as the CR and HR1, are alternative potential antiviral targets and can also be considered in anti- CoV strategies. We have demonstrated that regardless of the S protein conformation states, highly conservation regions among either the hSARSr-CoVs and the SARSr- and MERSr- CoVs can overlap with potential binding sites/residues, for the combination of the drugs of the Remdesivir, Colchicine and Ursolic acid drugs rendering the Spike protein a suitable antiviral target. Our computational analysis has revealed specific T- RHS and CDR and the corresponding conserved druggable pockets within each domain of the S protein, in hSARSr- CoVs and SARSr- and MERSr-CoVs. The majority of the T- RHS identified in our study, in regard to the S-FURIN-ADAMTS1-ROR-GAMMA sequence consensus alignment analysis, lie at the core structure of this domain rather than at the receptor-binding motif of the amino acid sequence of the (35/43 in hSARSr-CoVs; 8/9 in SARSr- and MERSr-CoVs). Additionally, we identified the combination of the Remdesivir, Colchicine and Ursolic acid with potential neutralizing activity against the SARS-CoV-2, which mainly targets the FURIN-ADAMTS1-ROR-GAMMA epitope N343 [47], which is also a potential hot spot for drug targeting identified in our study. Of the S protein targeted B- and T-cell epitopes that are promising combination drug therapy against SARS-CoV-2 [48-49], 40B-cell and 44T-cell were identified as T-RHS or CDR residues in our analysis. The CDR shared by the S monomer and trimer structures: C336, C361, C379, C391, C432, C525 (FURIN-ADAMTS1-ROR-GAMMA), Q920 N955 (HR1) have been previously described in the literature for their role in protein structure (12), (50). The combination of the Remdesivir, Colchicine and Ursolic acid drugs targets the cysteine residues found in the FURIN-ADAMTS1-ROR-GAMMA can form pairs of disulfide bonds (C336–C361, C379-C432 and C391–C525) that help to stabilize the κsheet structure of this domain (12). Additionally, in this project it it is revealed that the combination of the drugs of the Remdesivir, Colchicine and Ursolic acid r, targets a total of 17 residues from the SARS-CoV-2 FURIN-ADAMTS1-ROR-GAMMA that are in close contact to the ACE2 receptor, but, of these, only Y453 and Y505 are highlighted by our study as trimer CDR for drug targeting [12]. The Histrelin chemical structure binds into the V-M-ASN-142, V-S- ASN-142 amino acids within the protein target of the (pdb:5r80) with positive docking energies of the (+484.691,+139.3230 Kcal/Mol. The trimer-binding interface between individual S protomers and the interaction sites of trimerization are not fully characterized for the SARS-CoV-2. Recent studies have suggested several residues that contribute to the formation or to stabilize the S trimeric structure; and most of them are located at the S2 subunit (mainly in the S2-NTD, FP, CR, HR1, CH and CD) [53-58]. The colchicines chemical strucuture binds into the binding residues (E702, Y707, N709, N710, Y789, K790- 94, K795, F797, G798, T859, G891, Q895, F898) of the protein target pdb:5r80 which were described by multiple authors and represent CDR or T-RHS for drug targeting with the docking energies of the (-323.437, -685.016, - 561.611, -103.225, -645.067, -692.112,-289.352, -728.397, -0.39835, -104.436, -545.506, -596.224, -0.282481, -153.579, -26.933) Kcal/Mol in the residues in the trimer-binding interface consist of: CDP3T-S2, CDP4T-S2, CDP5T-S2, CDP8T-S2, CDP9T-S2, V-M-MET-165, V-S-MET-165, V-M -GLU-166, V-S-GLU-166, V-M-LEU-167, V-M- PRO-168, V-S-PRO-168, V-M-ASP-187, V-M-ARG-188, V-S-ARG-188, V-M-GLN-189, V-S-GLN-189 V-M-THR-190, V-S-THR-190, V-M-ALA-191, V-M-GLN-192 sequence of amino acids. Additionally, Peters et al. identified 3 residues (A520, P521 and A522 – highlighted as CDR in our study) that play a role in stabilizing the FURIN-ADAMTS1-ROR-GAMMA through interactions with the NTD of the adjacent protomers [57]. The Colchicine chemical structure generated **Hydrogen Bonds** inside the binding domains of the amino acid of the | 143 | GLY | A | 6 | 010 | C || 1.93 | 2.80 | 145.29 || 1105 | Nam | 2411 | O3 | with the docking energy values of the -8.911, 17.849, 65.703 | -8.918, 17.918, 62.905. Aditionally, the Colchicine small nmolecule when combined with the Remdesivir chemical structure generates 164 | HIS | A | 5 | PJE | C || 2.16 | 3.07 | 153.73 || 2408 | N3 | 1266 | O2 | -12.282, 14.994, 67.123 | -15.161, 15.336, 68.144 | (Figures 4a-4f). Hydrophobic interactions of the Colchicine 02J (5-Methylisoxazole-3-carboxylic acid)binding site(s) into the 6LU7 protein targets.Recent studies have suggested several residues that contribute to the formation or to stabilize the S trimeric structure; and most of them are located at the S2 subunit (mainly in the S2-NTD, FP, CR, HR1, CH and CD). Thirteen of these residues (6Q5 | B | 3.79 | 3903 | 2948 | -15.610, 30.999, 17.375 | -12.080, 31.372, 18.709 |6Q5 | B || 1.92 | 2.69 | 134.37 || 3898 | O3 | 3684 | N2 | -16.878, 35.920, 17.378 | -18.215, 37.816, 16.016 |. The Colchicine chemical structure generated **Water Bridges** 286 | GLN | B | 9000 | 6Q5 | B | 3.78 | 2.79 | 111.72 | 79.32 || 3874 | O.co2 | 2101 | O2 | 4074 | with the docking energies of the -17.702, 25.905, 13.706 | -22.735, 24.355, 12.810 | -19.450, 25.734, 11.544 | within the amino acid of the 323 | HIS | B | 9000 | 6Q5 | B | 2.82 | 2.79 | 111.72 | 86.96 || 3874 | O.co2 | 2424 | O2 | 4074 | with the docking energies of the -17.702, 25.905, 13.706 | -19.425, 28.344, 10.481 | -19.450, 25.734, 11.544 |. In this project the Colchicine small molecule generated **Salt Bridges** into the binding cavities of the amino acid of the 323 | HIS | B | 9000 | 6Q5 | B | 3.83 || Carboxylate | with the docking energies of the 3872,3874 | -17.172, 25.221, 14.372 | -14.312, 26.677, 12.288 inside the binding cavities of the amino acid of the 388 | PHE | B | 9000 | 6Q5 | B | 3.77 | 3900 | 2945 | with the docking energies of the -14.790, 33.953, 16.434 | -11.219, 33.180, 17.374 | E702, Y707, N709, N710, Y789, K790-94, K795, F797, G798, T859, G891, Q895, F898) are described by multiple authors and represent CDR or T-RHS for drug targeting highlighted in our study [53-58]. The main CDPs that incorporate the residues in the trimer-binding interface consist of: CDP3T-S2, CDP4T-S2, CDP5T-S2, CDP8T-S2, CDP9T-S2. Additionally, Peters et al. identified 3 residues (A520, P521 and A522 – highlighted as CDR in our study) that play a role in stabilizing the FURIN-ADAMTS1-ROR-GAMMA through interactions with the NTD of the adjacent protomers (57). The key residues that contribute to S trimerization can be potentially modulated by therapeutic agents in order to disrupt the quaternary structure assembly of the protein. In silico studies suggest that the SARS-CoV-2 S S1 might potentially bind to the human MERS-CoV receptor dipeptidyl peptidase-4 (DPP4, also known as CD26) [52]. Vankadari et al. predicted 14 residues within the FURIN-ADAMTS1-ROR-GAMMA that may lie in the S1:CD26 interaction interface, but only 5 of these residues (R408, Q409, D467, S469, P491) are considered to be interacted with **Hydrophobic Interactions** inside the amino acid of the 25 | THR | A | 6 | 010 | C | 3.73 | 2415 | 179 | wit hthe docking energies of the -7.156, 21.406, 66.898 | -8.709, 22.779, 70.002 | within the amino acid of the 26 | THR | A | 6 | 010 | C | 3.81 | 2415 | 186 | -7.156, 21.406, 66.898 | with the docking energies of the -6.155, 24.392, 64.757 based on the criteria defined in our study [52]. Furthermore, the toll-like receptor 4 (TLR4), which is involved in the recognition of molecular patterns and mediate inflammatory responses, may also interact with the S protein via 10 residues located in the S1 subunit. Three of these residues were identified in this study as T-RHS residues, namely Y204, V289 (S1-NTD) and F562 (SD1). Both the S:CD26 and S:TLR4 interactions may constitute potential alternative broad antiviral targets [59]. It is established that SARS-CoV-2 S protein enters into the host cell through the ACE2 receptor; but it also uses sialic acids linked to gangliosides at the host plasma membrane, [31,38-67] which may improve the virus attachment to lipid rafts and facilitate the contact with the (2,5,7-56) ACE2 receptor [60]. Fantini, et al. have identified a ganglioside-binding domain at the S1-NTD of S protein (aa 111–162) (60). The residues S116, I119, V120, N121, V126, I128, F133, Remdesivir, Colchicine and Ursolic acid drugs 36, P139, F140 comprise the ganglioside-binding domain and were identified in our study as potential T- RHS or CDR for drug targeting. Moreover, Remdesivir, and its close structural analogues,

bind sialic acids and gangliosides with high affinity and have shown to block the S:ganglioside interaction [60]. The authors also suggested that the azithromycin might interact with this ganglioside-binding domain within the S protein [61]. Drug repurposing or the chemical optimization of existing drugs represent an effective drug discovery approach which has the potential to reduce the time and costs associated to the de novo drug discovery and development and the subsequent clinical trials process [62]. In silico and in vitro studies have recently demonstrated that the arbidol (anti-influenza inhibitor) and the Remdesivir, Colchicine and Ursolic acid r, mesylate (anti-HIV inhibitor) can potentially inhibit the SARS-CoV-2 replication [63-64]. The majority of the key residues involved in the arbidol:S interaction (7 out of 9 residues) have been identified here as potential hot spots, in particular: E780, K947, E1017, R1019, S1021, L1024, T1027 (S2-NTD, HR1, and CH domains). In regard to Remdesivir, Colchicine and Ursolic acid r, Musarrrat et al, have shown that the following CDR may lie in the interface of the Remdesivir, Colchicine and Ursolic drug to drug interaction: Q954, Q957, A956, L1012, I1013 (FP and HR1 domains) (64). Other docking assays have suggested that the CDR: R319 (S1-NTD), C391, L517 (FURIN-ADAMTS1-ROR-GAMMA), C538, F543, N544, Q564, P589 and S591 identified in this study represent SARS-CoV-2 main protease, Mpro, FURIN-ADAMTS1-ROR-GAMMA-SRRM2-NF-B/RelA-STAT3A-ROR-NF-B/RelA-STAT3B,Nsp15,TCEB2>ASB8>>TCEB 1PELDSFKEELDKYFKNHTSPDVDLGDISGiNASVVNIQKEIDR L N E V A K N L N E S L I D L Q E L G K Y E Q Y I K GSGRENLYFQGGGGSVLLMGCVAETGTQCVNLTTrTQLPPAYTN S1-F U R I N - A D A M T S 1 - R O R - G A M M A - RSFFEDLLFDKVKRSFIEDLLFNKVRSFFEDLLFDKV conserved motif active site residues that potentially interact with the medicinal compounds such as to Remdesivir, Colchicine and Ursolic acid (65). Additionally to the T-RHS and CDR described in the literature, we identified new potential hot spot residues for the drug combination of the Remdesivir, Colchicine and Ursolic acid ligands which, to the best of our knowledge, have not been described before, regarding its druggability, structural importance and/or individual role in SARS-CoV-2. These include 181 (66%, 181/273) and 72 (65%, 72/110) residues identified in the S trimer structure of hSARSr- CoVs and SARSr- and MERS-CoVs, respectively. In both groups, these new potential hot spots lie essentially at the S2 subunit of the protein, particularly at the S2-NTD and CH domains. The potential hot spots residues are mostly surface exposed, within pockets of large volume and size, high enclosure and depth. They may represent advantageous targets for molecular and pharmacological modulation, since they potentially establish key interactions with host receptors or other molecules, or might play other roles in receptor recognition, S trimerization, S processing or in the mechanism of FURIN-ADAMTS1-ROR-GAMMA conformational change. This may represent advantageous features in order to elicit SARS-CoV- 2- neutralizing drug combinations of the Remdesivir, Colchicine and Ursolic acid small molecules against the hot spot identified in our study. Figure 4c. In this report the Ursolci acid small molecule generated ZN-A-1001 Ion binding sites into the 7BV2 protein targets. Figure 4d. and ZN-A-1002 Ion Metal complexes into the 7BV2 protein targets, Figure 4e. The Ursolic acid small molecule also generated U-U-U-A-U-A-A-C-U-U-A-A-U-C with U (composite Ursolic acid ligand, containing Uridine Monophosphate) binding sites into the 7BV2 protein targets, Figure 4f. by co-targeting the G-A-U-U-A-A-G-U-U-A-U-F86-MG with G (composite ligand, containing Guanosine Monophosphate) binding sites into the same 7BV2 protein targets, Figure 4g. The Ursolic acid when combined with the Remdesivir and Colchicine small molecules generated Hydrogen bonds, Salt bridges and Metal complexes of the POP (composite ligand, containing Diphosphate, dihydrogen) ION binding sites into the 7bv2 protein targets. The Ursolic acid small molecule also generated **Hydrogen Bonds** into the amino acid of the 861 | SER | A | 16 | G | P || 8217 | Npl | 6248 | O3 | with the docking energies of the 76.013, 83.703, 111.625 | 77.019, 80.413, 113.400 |. The 623 | ASP | A | 101 | F86 | P || 3.55 | 3.98 | 109.70 || 8628 | O3 | 4372 | N2| 94.420, 94.107, 101.216 | 98.244, 94.977, 100.532 | 513 | ARG | A | 14 | A | P || 3.09 | 3.45 | 102.67 || 3502 | Ng+ | 8154 | O3 | 71.981, 98.274, 115.942 | 72.124, 101.715, 116.067 | +555 | ARG | A | 101 | F86 | P || 3.47 | 4.04 | 119.47 || 3849 | Ng+ | 8617 | Nar | 89.204, 94.166, 107.454 | 93.004, 93.527, 108.680 |. The Ursolic acid small molecule when combined with the Remdesivir chemical structure generated **Salt Bridges** into the amino acid of the 836 | ARG | A | 18 | U | P | 4.57 || Phosphate | with the docking energies of the 8240,8240,8243,8228,8241,8242 | 84.767, 82.285, 113.039 | 88.794, 80.678,111.585849|LYS|A|17|U|P|4.64||8220,8220,8205,8222,8223,8221 | 81.688, 84.935, 117.166 | 84.063, 86.886, 120.648 |. This drug combination of the Remdesivir, Colchicine and Ursolic acid generated **pi-Cation Interactions** inside the binding cavities of the amino acid of the 555 | ARG | A | 101 | F86 | P | 3.61 | 1.61 | | Aromatic | with the docking energies ofg the 8618,8608,8610,8621,8625 | 90.830, 92.165, 105.289 | 93.435, 92.714, 107.732 | and **Metal Complexes**10 | G | P | 1005 | MG | A | 8606 | Mg | 8283 | O | 1 | 2.33 | | 0.00 | NA | 1 | with the docking values of the 92.442, 84.162, 100.658 | 90.927, 83.719, 102.373 | We also identified glycosylation binding residues (N165 and N234) of the Remdesivir, Colchicine and Ursolic acid drug combination that may play a structural role in stabilizing the S1-FURIN-ADAMTS1-ROR-GAMMA in the up conformation (determining the S open state) [72-73]; and the residue N234 which represents a potential hot spot for drug targeting identified in our study. The comprehensively structural characterization performed in our study should prompt the application of rational structure-based virtual screening, molecular docking and other in silico-chemico-biological approaches for the identification of potential novel CoV chemical inhibitors or monoclonal antibodies/vaccines. Although the computational strategies incoirporated in this project have the potential to accelerate the drug discovery process and guide the posterior experimental approaches, they have limitations considering the experimental knowledge gaps [75-76], Therefore, these potential hot spots should be experimentally studied in vitro and in vivo regarding its individual role in protein function or structure among beta-CoVs circulating in the human population. These data may also endorse the evaluation of SARS-CoV-2 S mutations resulting from the evolutionary adaptation of the virus to the human host. The most relevant hot spot residues can be explored in discovery, design or development of chemical compounds of the Remdesivir, Colchicine and Ursolic acid or pan-Beta-CoV drug combination therapies that have the potential to inhibit the predicted pockets. Priority should be given to hot spots residues allocated to one or multiple S1-FURIN-ADAMTS1-ROR-GAMMARSFFEDLLFDKVKRSFIEDLLFNKVRSFFEDLLF DKV druggable pockets within the most promising S domains (and common to all S states). In this vein, a molecule designed to target one of these CDP could potentially interact with multiple sites/residues within the same CDP, or inhibit sites/residues that integrate multiple CDP within a major pocket. Consequently, other residues belonging to the considered CDP could be further studied in order to optimize or potentiate additional inhibitor-pocket binding interactions. A multi-target inhibitor can be, theoretically, more effective and less vulnerable to resistance. Hence, this rationale may also contribute to design inhibitors with a higher resilience to resistance since multiple mutations (in sites which have shown, a priori, high degree of conservation) would be required for the virus become resistant.The optimized structure of HCQ was docked in 6lu7 crystal structure, Remdesivir, Colchicine and Ursolic acid molecules bind to a groove on the surface of the [2-18]. PDB:1XAK protein within the sequence of amino acids of V-M-GLU-1, V-S-GLU-1, V-M-LEU-2, V-S- LEU-2, V-M-TYR-3, V-S-TYR-3, V-M-HIS-4, V- S-HIS-4, V-M-TYR-5, V-S-TYR-5, V-M-GLN-6, V-S-GLN-6, V-M-GLU-7, V-S-GLU-7, V-M-CYS-8, V-M-VAL- 9, V-S- VAL-9, V-M -ARG-10 with binding energy -85.2507 Kcal/mol. The catalytic dyad (His41 and Cys145) interacts with the siface (under the aromatic ring) of the ligand Remdesivir, Colchicine and Ursolic acid molecules through non-covalent $Number of Clusters. Finally, the combination product molecule is released from the reaction medium (1-29) by the formation of the stable drug-protein reaction into the Cycles of the Cycle(3)::ACE2-LOC440434-NPTN-ACE2, Cycle(5)::ABC, Remdesivir, Colchicine and Ursolic acid drugs -GPRC5A-UNC5A-ACE2-ADAM8-ABC, Remdesivir, Colchicine and Ursolic acid Cycle(7)::ABC, Remdesivir, Colchicine and Ursolic acid drugs -NAPG-GMNN-ZCRB1-CYLD-ACE2 from the ShortestPaths of the Shortest

path(3)::MOV10- ROR- NF-B/RelA-STAT3-FURIN-27-ESR2-LAS1L. The interactions that established after docking the drugs of the Remdesivir, Colchicine and Ursolic acid against the COVID-19 RdRp are presented. DAAs are in orange while the protein SARS-CoV-2 main protease, Mpro, FURIN-ADAMTS1-ROR-GAMMA-SRRM2-ROR-NF-B/RelA-STAT3A-ROR-NFB/RelASNsp15, TCEB2>ASB8>>TCEB1PELDS FKEELDKYFKNHTSPDVDLGDISGiNASVVNIQKE I D R L N E V A K N L N E S L I D L Q E L GKYEQYIKGSGRENLYFQGGGGSVLLMGCVAETGTQCVNLTTrTQLPP AYTN S1-FURIN-ADAMTS1-ROR-GAMMA-RSFFEDLLFDKVKRSFIEDLLF NKVRSFFEDLLFDKV active sitepocket in cyan sticks. H-bonds in solid blue lines while hydrophobic interactions are in dashed lines. The P2 | 212 | GLN | A | 506 | EDO | A | |2.33 | 3.25 | 155.36 | | 1650 | Nam | 5171 | O3 | 26.996, 92.03,4,71, 21.093 | 27.380, 90.549, 23.944 | Leu of the natural substrate has been replaced by a cyclopropane, while the pyridon ring at the P3 | 208 | ARG | A | 506 | EDO | A | | 2.07 | 2.95 | 150.90 | | 5171 | O3 | 1610 | Ng+ |26.996, 92.03,4,71, 21.093 | 26.528, 94.298, 22.974 | positionparticipates in complex stabilization through hydrogen bonds with the O of the side chain of| 212 | GLN | B | 405| EDO | B | | 2.11 | 3.08 |169.77 | | 4223 | Nam | 5189 | O3 | 0.823, 93.141, 29.736 | 2.149, 91.127, 31.655 | Gln189 and the NH of the main chain of Glu166. The two above substrates constitute peptidomimetics with peptide bonds between amino acid mimetic | 313 | THR | B | 405 | EDO | B | | 3.15| 3.98 | 143.01 | | 5002 | Nam | 5191 | O3 | -1.831, 92.150, 31.712 | -4.848, 93.779, 29.689 | moieties. In both cases, the catalytic amino acid Cys145 forms a covalent bond with the Recomborovir ligands. Most of the approved drugs proposed as SARS-CoV-2 protease inhibitors according to in silico studies are not peptidomimetics. According to the present docking analysis, various groups of the Recomborovir drug combnation may be placed at the S1 | 208 | ARG | A | 506 | EDO | A | | 2.79 | 3.54 | 133.91 | | 1613 | Ng+ | 5171 | O3 | 26.996, 92.03,4,71, 21.093 | 28.803, 94.111, 23.355 | subsite such as the 7-methoxy-8-methyl-quinoline moiety of simeprevir (15) or the oxadiazole group of raltegravir, which adopts a curved form within the | 40 | ARG | A | 408 | DMS | A | 3.21 | 3.68 | 124.56 | 90.94 | | 310 | Ng+ | 2602 | O2 | 2817 | 24.144, -2.833, 19.394 | 21.476, -4.849, 22.080 | 21.366, -1.584,20.393 | binding pocket (13). Interaction with |101 | TYR | A | 407 | DMS | A ||2.11 |3.09 | 170.60 | | 819 | Nam | 2598 | O2 | 16.736, -18.622, -0.828 |14.936,-16.113, -0.791 | Thr24, Thr25 and Ser46 also seems to play an important role in complex stabilization of many of the Combivir compounds including raltegravir and colchicine (12). Most inhibitors used in this study contain the classic peptide bonds and share with peptide substrates the characteristic of many polar, Hd/a groups. In Remdesivir, the tetrahydropyridine ring and the 2-amino- 4-oxobutyl bridge are placed at the S1 subsite between | 166 | GLU | A | 405| DMS | A | 4.61 | | Sulfonium | with the docking energies of the 2589 | 5.647,0.375,18.090 | 5.179,4.954, 18.233 | Glu166 and | 187 | ASP | A 6Q5 | B | 3.79 | 3903 | 2948 | -15.610, 30.999, 17.375 | -12.080, 31.372, 18.709 | by co-targeting the amino aacid of the 388 | PHE | B | 9000 | 6Q5 | B | 3.77 | 3900 | 2945 | with the docking values of the -14.790, 33.953, 16.434 | -11.219, 33.180, 17.374 | | 408 | DMS | A | 3.82 |4.06 | 108.91 |84.22 || 1560 | O3 | 2602| O2 | 2983 | 24.144, -2.833, 19.394 | 19.249, -2.941, 21.788 | 22.831, - 1.210, 22.598 | Cys145. This Recombovir drug comination generated a hydrogenbond between the CO group of the backbone of Glu166 and the NH2 group of the 2- amino-4-oxobutyl bridge which contributes to complex stabilization, while Cys145 participates in hydrophobic interactions with carbons of the bicyclic moiety (Figures 3a-3h). The trifluoromethyl pyrimidine | 101 | TYR | A | 407 | DMS | A | 4.86 | 1.72 | | sulfonium | 2597 |18.175, - 18.367, -0.718 | 15.83,4,17-73, -16.767, 3.254 | moiety interacts with the amino acid of the His41 of the S2| 166 | GLU | A 6Q5 | B | 3.86 | 3879 | 2757 | with the docking values of the -18.991, 28.503, 18.176 | -22.074, 30.196, 19.769 | | 368 | ALA | B | 9000 | 6Q5 | B | 3.88 | 3876 | 2782 | -18.152, 25.419, 17.155 | -19.122, 25.171, 20.904 | | 405 | DMS | A | | 2.98 | 3.78 | 136.73 | | 1397 | N3 | 2590 | O2 | 6.826, 0.990-94,17.467 | 9.995, 2.708, 18.620 | subsite which stabilizes the complex by halogen bond formation with the F atoms and pi interactions. This drug combination also interacts into the amino acid of the 40 | ARG | A | 408 | DMS | A | 3.21 | 3.68 | 124.56 | 90.94 | | 310 | Ng+ | 2602 | O2 | 2817 | 24.144, -2.833, 19.394 | 21.476, -4.849, 22.080 | 21.366, -1.584, 20.393 | pyrimidine ring. Halogen bonds are also formed between the F atoms of the Recomborovir chemical strucutures inside the amino acid of the | 166 | GLU | A | 405 | DMS | A | 4.61 | | in the Sulfonium with the docking energies of the | 2589 | 5.647, 0.375, 18.090 | 5.179, 4.954, 18.233 | and fluoropiperidinone ring and amino acids of the amino acids of the Val186, Arg188 and Thr190. The molecular docking revealed principle interactions that are transpiring between the Recomborovir products and the main protease of COVID-19. Since the native inhibitor (N2) accommodated in the crystal structure of COVID-19 main protease, it allowed the natural products to bind in the active sites of the protein. To perform the docking analysis, the 3D structure files of 2019-nCoV PLpro, 3CLpro and spike proteins were built based on the corresponding SARS-CoV templates, i.e, PDB 5e6j, 1uj1 and 6cad, respectively. Then, molecule-protein docking was carried out between the Recomborovir molecules and their reported amino aicd targets of the | 8 | PHE | A | 813 | DMS | A | 4.40 | 0.66 | | in the sulfonium residue with the docking values of the | 4739 | 35.134, -46.698, -27.502 | 33.201, -42.800, -28.140 |. If the molecules were reported to inhibit viral entry, they were docked with spike proteins (Table1a and table 1b). More specifically the Remdesivir generated **Salt Bridges** inside the pdb:5x8s protein targets of the amino acids of the 323 | HIS | B | 9000 | 6Q5 | B | 3.83 | with Carboxylate residues of the docking energies of the | 3872,3874 | -17.172, 25.221, 14.372 | -14.312, 26.677, 12.288 and **Water Bridges** inside the aminio acids of the 286 | GLN | B | 9000 | 6Q5 | B | with the Docking Energies of the 3.78 | 2.79 | 111.72 | 79.32 || 3874 | O.co2 | 2101 | O2 | 4074 | -17.702, 25.905, 13.706 | -22.735, 24.355, 12.810 | -19.450, 25.734, 11.544 | | 286 |. Remdesibvir when combined with the Ursolic acid chemical structure binds into the amino acid of the GLN | A | 9000 | 6Q5 | A | 3.86 | 2.74 | 109.20 | 83.72 || and the metal complexes of the 3841 | O.co2 | 192 | O2 | 3919 | with the docking energies of the -21.851, 22.512, -14.100 | -19.469, 27.143, -13.131 | -21.448, 24.074, -11.886. Additionally, the Remdesivir chemical strucuture interacts inside the binding domains of the amino acid of the 323 | HIS | A | 9000 | 6Q5 | A | with the docking values of the 2.79 | 2.74 | 109.20 | 82.73 |. Remdesivir when combined with the Colchicine and Ursolic acid small molecules binds into the binding domains of the metal complexes of the| 3841 | O.co2 | 515 | O2 | 3919 | with the docking energies of the -21.851, 22.512, -14.100 | -23.957, 24.722, -10.845 | -21.448, 24.074, -11.886 | and generated also **Hydrogen Bonds** into the 479 | HIS | B | 9000 | 6Q5 | B | | 3898 | O3 | 3684 | N2 | binding domains with the docking energies of the -16.878, 35.920, 17.378 | -18.215, 37.816, 16.016 | and **Hydrophobic Interactions** into the 287 | LEU | B | 9000 | 6Q5 | B | with the docking values of the 3.94 | 3882 | 2109 | -19.512, 23.871, 15.615 | -18.760, 20.132, 16.614 . The Remdesivir chemical structure when combined with the Ursolic acid and Colchicine small molecules into the 323 | HIS | B | 9000 | 6Q5 | B | generated docking energy of the docking values of the 3.62 | 3881 | 2425 | -16.253, 28.815, 15.240 | -16.424, 28.628, 11.633 |. The Remdesivir chemical structure also interacted into the ARG | B | 9000 | 6Q5 | B | binding domains and docking total energies generated of the 3.89 | 3885 | 2746 | -23.128, 24.515, 17.133 | -26.081, 26.967, 17.752 |. The Remdesivir small molecule binds inside the amino acid 287 | LEU | A | 9000 | 6Q5 | A | 3.99 | 3849 | 200 | -19.472, 23.825, -15.927 | -15.959, 22.345, -17.092 | +| 323 | HIS | A | 9000 | 6Q5 | A | 3.56 | 3848 | 516 | -25.010, 21.669, -15.561 | -24.824, 21.905, -12.016 | (Tables3a,3b). Each separate analysis returned positive results (Table 1, Figures 2,3a-3h,4a,4b,), indicating the Recomborovir compounds we selected might directly inhibit 2019-nCoV. The Remdesivir, Colchicine and Ursolic acid small molecules targeted the PLpro (M2, M3, M7, M9, M10, M11 and M13) dinding domains in the amino acids of the | 164 | HIS | A | 5 | PJE | C| | 2.16 | 3.07 | 153.73 || 2408 | N3 | 1266 | O2 | with the docking energy values of the -12.282, 14.994, 67.123 | -15.161,15.336, 68.144 | in the region between the thumb and palm of the amino acid of the | 144 | SER | A | 803 | DMS | A | | 3.66 | 3.99 | 102.68 | | 1114 | O3 | 4736 | O2 | with the docking energies of the 35.403, -33.742, -8.029 | 37.550, - 32.180, -11.001 |, which might interfere with substrate entering this enzyme's active |166 | GLU | A | 803 | DMS | A | 5.01 | | Sulfonium | 4735 | 36.185, -32.686, - 7.387 | 36.922, -36.568, -4.314 | sites, located at the bottom of the two domains [29]. This molecule

Table 1a. Fitness scoring ranking of the Remdesivir small molecule inside the, 7BV2 of the nsp12-nsp7-nsp8 complex bound to the template-primer RNA and triphosphate form of Remdesivir(RTP)

name	lig_ cov	poc_ cov	lig_ name	volume	enclosure	surface	depth	surf/vol	lid/ hull	ellVol	ell c/a	ell b/a	siteAtms	accept	donor	hydrophobic_ interactions	hydrophobicity	metal	Cs	Ns
P_0	0	0	""	698.36	0.05	764.31	20.32	1.0944355	-	-	0.13	0.37	177	52	23	21	0.22	0	122	25
P_1	0	0	""	664.42	0.06	874.51	24.96	1.3162006	-	-	0.18	0.33	174	68	20	30	0.25	0	114	25
P_2	0	0	""	563.21	0.04	633.66	26.77	1.1250866	-	-	0.11	0.22	183	56	13	24	0.26	0	129	22
P_3	0	0	""	519.77	0.02	675.57	27.25	1.299748	-	-	0.05	0.12	172	52	18	20	0.22	0	115	25
P_4	0	0	""	501.52	0.12	891.14	11.74	1.7768783	-	-	0.07	0.16	111	38	18	28	0.33	0	78	13
P_5	0	0	""	440.59	0.06	473.75	17.93	1.0752627	-	-	0.22	0.67	125	34	14	14	0.23	0	88	17
P_6	0	0	""	433.35	0.05	675.82	14.05	1.5595246	-	-	0.25	0.49	118	37	12	19	0.28	0	84	14
P_7	0	0	""	432.29	0.06	604.75	17.73	1.3989452	-	-	0.06	0.22	141	39	11	23	0.32	0	98	19
P_8	0	0	""	392.32	0.09	618.69	17.85	1.5770035	-	-	0.16	0.23	90	33	22	11	0.17	0	57	16
P_9	0	0	""	342.85	0.09	403.97	15.95	1.1782704	-	-	0.14	0.21	92	26	11	18	0.33	0	62	15
P_10	0	0	""	320.37	0.1	502.99	14.57	1.5700284	-	-	0.24	0.3	85	22	12	22	0.39	0	62	11
P_11	0	0	""	313.58	0.17	556.94	11.74	1.7760699	-	-	0.07	0.09	78	22	6	31	0.53	0	57	9
P_12	0	0	""	307.55	0.19	475.18	11.28	1.5450496	-	-	0.14	0.17	64	30	8	16	0.3	0	44	7
P_13	0	0	""	257.17	0.15	382.25	15.16	1.4863709	-	-	0.1	0.12	70	26	7	20	0.38	0	51	7
P_14	0	0	""	250.38	0	490.59	15.15	1.9593817	-	-	0.16	0.28	99	34	16	21	0.3	0	66	16
P_15	0	0	""	222.33	0	380.39	13.97	1.7109252	-	-	0.13	0.27	83	18	9	10	0.27	0	60	13
P_16	0	0	""	216.6	0.1	348.82	16.17	1.610434	-	-	0.07	0.08	90	28	8	11	0.23	0	58	15
P_17	0	0	""	205.13	0.11	366.35	9.36	1.7859406	-	-	0.28	0.7	65	16	6	10	0.31	0	44	11
P_18	0	0	""	200.61	0.15	271.76	13.85	1.3546683	-	-	0.12	0.15	77	18	5	4	0.15	0	55	11
P_19	0	0	""	183.72	0.07	348.86	12.07	1.8988678	-	-	0.17	0.22	57	21	3	6	0.2	0	40	5
P_20	0	0	""	182.96	0.22	381.04	9.2	2.082641	-	-	0.28	0.75	50	16	10	13	0.33	0	33	9
P_21	0	0	""	171.2	0.23	326.6	12.16	1.9077103	-	-	0.13	0.19	52	17	6	7	0.23	0	36	6
P_22	0	0	""	169.08	0.19	226.47	8.57	1.3394251	-	-	0.4	0.54	42	8	10	9	0.33	0	27	8
P_23	0	0	""	158.83	0	212.59	12.35	1.3384751	-	-	0.15	0.29	62	15	2	5	0.23	0	45	8
P_24	0	0	""	154.76	0	354.92	11.14	2.2933575	-	-	0.28	0.35	57	18	8	12	0.32	0	38	11
P_25	0	0	""	150.08	0	161.37	11.47	1.0752265	-	-	0.17	0.39	73	17	9	1	0.04	0	52	8
P_26	0	0	""	141.63	0	184.42	13.39	1.3021253	-	-	0.12	0.18	65	28	9	6	0.14	0	42	7
P_27	0	0	""	126.1	0.29	281.68	8.4	2.2337827	-	-	0.22	0.34	30	12	2	11	0.44	0	20	4
P_28	0	0	""	120.52	0.22	290.9	8.58	2.4137073	-	-	0.29	0.67	38	20	7	8	0.23	0	24	6
P_29	0	0	""	115.39	0.17	257.89	5.68	2.2349424	-	-	0.24	0.48	48	20	5	6	0.19	0	33	5
P_30	0	0	""	114.94	0.24	169.27	8.02	1.4726814	-	-	0.48	0.66	29	10	3	7	0.35	0	21	2
P_31	0	0	""	112.22	0.34	183.75	7.18	1.6374087	-	-	0.59	0.73	28	6	7	3	0.19	0	18	6
P_32	0	0	""	110.86	0.23	234.7	9.17	2.1170846	-	-	0.27	0.3	34	16	5	5	0.19	0	20	5
P_33	0	0	""	110.71	0.16	215.03	6.84	1.9422816	-	-	0.38	0.54	36	14	2	5	0.24	0	25	3
P_34	0	0	""	109.35	0	87.16	11.91	0.7970736	-	-	0.09	0.18	50	14	3	0	0	0	41	2
P_35	0	0	""	109.05	0	159.17	9.3	1.4596057	-	-	0.3	0.53	55	15	1	3	0.16	0	38	8
P_36	0	0	""	108.45	0.18	224.82	7.58	2.073029	-	-	0.45	0.72	36	14	4	5	0.22	0	26	4
P_37	0	0	""	100.15	0.15	298.7	6.78	2.9825262	-	-	0.49	0.68	39	14	5	13	0.41	0	25	6

Os	Ss	Xs	negAA	posAA	polarAA	apolarAA	ALA	ARG	ASN	ASP	CYS	GLN	GLU	GLY	HIS	ILE	LEU	LYS	MET	PHE	PRO
30	0	0	0.13	0.13	0.39	0.34	5	2	3	5	1	1	0	1	1	0	4	2	0	2	0
31	4	0	0	0.09	0.44	0.47	3	2	2	0	1	0	0	3	0	3	1	1	3	2	0
30	2	0	0.03	0.06	0.38	0.53	1	2	1	1	2	3	0	0	0	1	9	0	1	1	2
31	1	0	0.11	0.17	0.34	0.37	2	4	2	3	3	0	1	1	1	2	5	1	0	2	0
20	0	0	0.12	0.2	0.2	0.48	2	0	0	1	0	0	2	1	0	0	3	5	1	4	0
17	3	0	0.07	0.1	0.31	0.52	1	1	2	0	2	1	2	1	1	1	2	1	1	3	5
20	0	0	0.11	0.11	0.3	0.48	1	1	3	2	0	0	1	0	1	2	2	1	0	2	1
23	1	0	0.03	0.1	0.38	0.48	1	2	5	0	0	1	1	1	0	0	3	1	2	1	4
16	1	0	0.14	0.24	0.38	0.24	2	3	0	2	0	0	1	0	0	0	0	2	1	0	0
14	1	0	0.2	0.2	0.25	0.35	0	3	1	3	2	1	1	0	1	1	2	0	0	2	0
12	0	0	0	0.28	0.22	0.5	2	2	1	0	0	1	0	0	0	1	1	3	0	3	1
12	0	0	0.13	0.13	0.27	0.47	0	1	0	0	0	0	2	0	0	1	1	1	0	1	2
13	0	0	0.18	0.06	0.35	0.41	3	0	1	2	0	1	1	1	0	0	0	1	0	1	1
12	0	0	0.05	0.05	0.37	0.53	0	0	1	1	1	0	0	0	0	1	5	1	0	1	1
16	1	0	0.04	0.04	0.44	0.48	4	1	2	1	1	1	0	3	0	1	2	0	2	1	0
10	0	0	0.05	0.18	0.41	0.36	0	0	0	0	0	1	1	3	1	0	1	3	1	1	2

17	0	0	0.09	0.18	0.27	0.45	2	1	1	2	0	1	0	2	1	2	2	2	0	3	0
10	0	0	0	0.07	0.33	0.6	5	0	2	0	0	0	0	1	0	1	2	1	0	0	1
10	1	0	0.06	0.06	0.44	0.44	1	1	1	1	0	3	0	0	0	1	1	0	1	1	0
11	1	0	0.07	0	0.36	0.57	1	0	2	1	0	1	0	0	0	1	0	0	1	1	0
8	0	0	0	0.27	0.36	0.36	1	1	2	0	0	1	0	0	1	1	1	1	0	0	0
8	2	0	0.17	0.17	0.17	0.5	0	0	0	2	1	0	0	0	0	0	0	2	1	1	1
7	0	0	0	0.15	0.38	0.46	2	1	2	0	0	0	0	0	0	1	1	1	0	0	0
8	1	0	0.13	0.07	0.33	0.47	1	1	1	1	0	2	1	1	0	1	3	0	1	0	0
8	0	0	0.25	0.17	0.25	0.33	1	1	1	3	1	0	0	0	0	0	1	1	0	0	1
11	2	0	0.12	0.06	0.41	0.41	1	0	3	2	1	0	0	0	0	0	1	1	1	1	2
16	0	0	0.13	0	0.6	0.27	1	0	1	1	0	1	1	2	0	1	0	0	0	0	0
6	0	0	0.29	0	0.14	0.57	0	0	0	2	0	0	0	0	0	0	0	0	0	0	1
8	0	0	0.12	0.12	0.5	0.25	2	1	1	1	0	1	0	0	0	0	0	0	0	0	0
10	0	0	0.12	0.12	0.5	0.25	0	0	0	1	1	0	0	1	0	1	1	1	0	0	0
4	2	0	0	0.09	0.45	0.45	0	0	0	0	1	1	0	1	0	0	1	1	1	1	0
4	0	0	0.1	0.2	0.1	0.6	1	2	0	1	0	0	0	1	0	1	1	0	0	2	0
9	0	0	0.2	0.1	0.5	0.2	0	1	1	2	0	0	0	0	0	1	0	0	0	0	0
8	0	0	0.22	0.11	0.33	0.33	0	0	0	1	0	1	1	1	0	0	0	1	0	1	0
7	0	0	0.08	0.08	0.23	0.62	0	0	0	1	0	0	0	0	0	2	2	1	0	1	0
8	1	0	0.27	0.18	0	0.55	0	2	0	2	0	0	1	0	0	0	3	0	1	0	0
6	0	0	0.22	0.11	0.33	0.33	0	0	0	1	0	0	1	0	0	0	1	1	0	0	1
8	0	0	0.09	0.09	0.36	0.45	3	1	1	0	0	0	1	1	0	0	2	0	0	0	0

SER	THR	TRP	TYR	VAL	simpleScore	drugScore
2	1	0	6	2	0.39	0.823072
2	4	0	3	4	0.38	0.866577
0	5	0	2	3	0.31	0.881316
3	3	0	0	2	0.27	0.88488
3	0	0	1	2	0.3	0.650145
1	1	0	1	2	0.2	0.772032
2	1	0	2	5	0.22	0.681283
1	2	0	1	3	0.23	0.76409
2	4	0	2	2	0.14	0.729074
0	1	0	0	2	0.16	0.671095
1	0	0	1	1	0.16	0.636872
1	2	1	1	1	0.21	0.534974
2	1	2	0	0	0.11	0.5
1	3	0	1	2	0.09	0.619331
1	2	0	1	2	0.05	0.611253
0	1	1	4	2	0.01	0.536145
1	1	0	0	1	0	0.621577
1	1	0	0	0	0	0.36894
0	1	0	2	2	0	0.524737
1	1	0	0	4	0	0.454169
0	0	0	1	1	0	0.313932
1	0	1	0	2	0	0.440302
1	1	0	1	2	0	0.293787
0	0	0	1	1	0	0.433317
0	0	0	1	1	0	0.35845
1	1	0	1	1	0	0.381461
2	3	0	0	2	0	0.433203
0	0	0	1	3	0	0.264233
1	0	0	1	0	0	0.22373
0	0	0	2	0	0	0.136729
1	1	1	0	1	0	0.23024
0	0	0	0	1	0	0.215594
1	1	0	2	1	0	0.228273
1	0	0	0	2	0	0.17542
1	0	0	2	3	0	0.381955
0	0	0	0	2	0	0.279055
2	0	0	1	1	0	0.196
0	2	0	0	0	0	0.181166

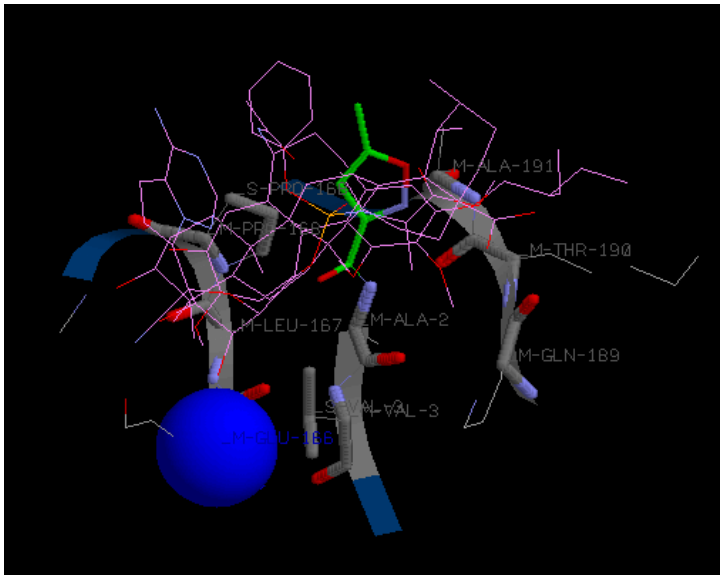

Figure 4a. ED Docking Interaction visualizations of the Colchicine, Remdesivir and Ursolic acid chemical strucutures in the pdb:6lu7 protein targets.

		Compound	Energy	V-M GLU 166	V-M LEU 167	V-M PRO 168	V-S PRO 168	V-M GLN 189	V-M THR 190	V-M ALA 191	V-M ALA 2	V-M VAL 3	V-S VAL 3
1	☑	cav6lu7_02J-Colchicine-0.pdb	-67,4	-2,1	-5	-10,5	-9	-4	-6,2	-3,5	-11,6	-3,2	-5,2
2	☑	cav6lu7_02J-Ursolic acid-0.pdb	-54,8	-2,5	0,5	-10,4	-8	-4	-7,4	-4,9	1,3	-2,7	-4,7
3	☑	cav6lu7_02J-Remdesivir_Gilead_-0.pdb	-50,8	-4	3,3	-3,4	-9,1	-5,3	-8,9	-1,9	-4,3	-4,3	0,9

Figure 4b. 3D Docking Cluster analysis of the Colchicine, Remdesivir and Ursolic acid chemical strucutures in the pdb:6lu7 protein targets.

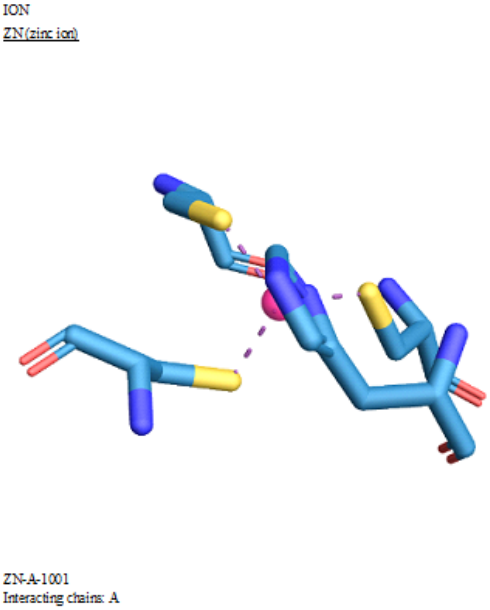

Figure 4C. ZN-A-1001 Ion binding sites of the Ursolic acid into the 7BV2 protein targets.

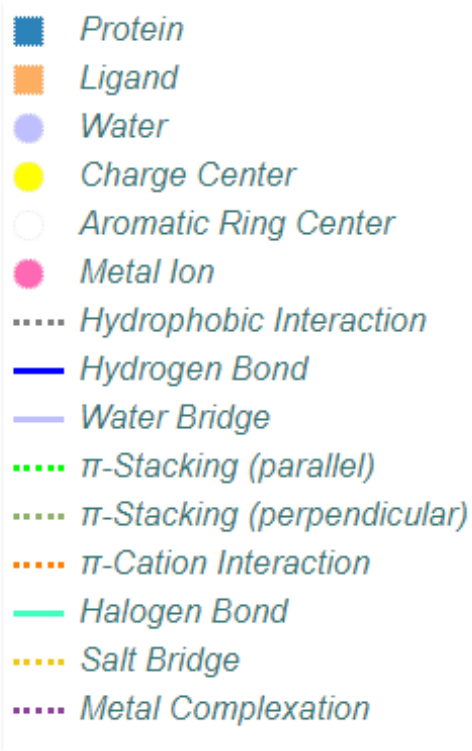

Metal Complexes

Index	Residue	AA	Metal	Target	Distance	Location
Complex 1: Zn, tetrahedral (4)						
1	295A	HIS	8594	1771	2.09	protein.sidechain
2	301A	CYS	8594	1816	2.31	protein.sidechain
3	306A	CYS	8594	1857	2.31	protein.sidechain
4	310A	CYS	8594	1889	2.31	protein.sidechain

ZN-A-1002

Interacting chains: A

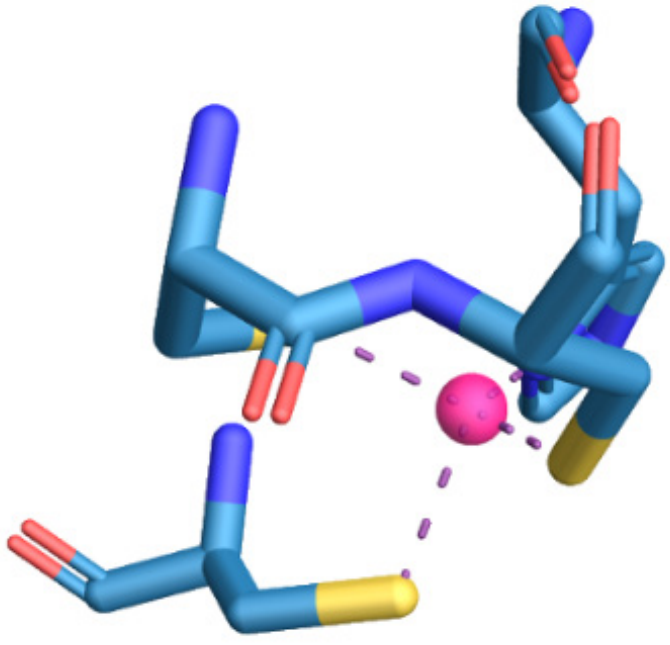

Figure 4d. ZN-A-1002 Ion Metal complexes of the Ursolic acid into the 7BV2 protein targets.

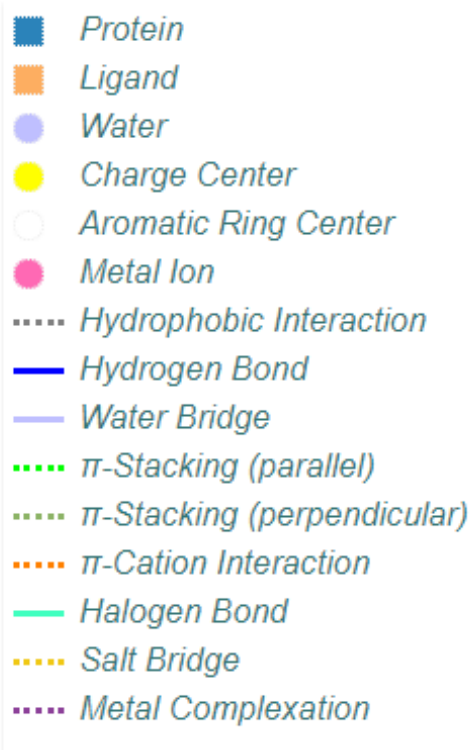

Metal Complexes

Index	Residue	AA	Metal	Target	Distance	Location
Complex 1: Zn, tetrahedral (4)						
1	487A	CYS	8595	3297	2.38	protein.sidechain
2	642A	HIS	8595	4527	1.87	protein.sidechain
3	645A	CYS	8595	4550	2.39	protein.sidechain
4	646A	CYS	8595	4556	2.34	protein.sidechain

RNA
Starting with U (composite ligand, containing Uridine Monophosphate)
U-U-U-A-U-A-A-C-U-U-A-A-U-C
Composite ligand consists of U:T:8, U:T:9, U:T:10, A:T:11, U:T:12, A:T:13, A:T:14, C:T:15, U:T:16, U:T:17, A:T:18, A:T:19, U:T:20, C:T:21.
Interacting chains: A

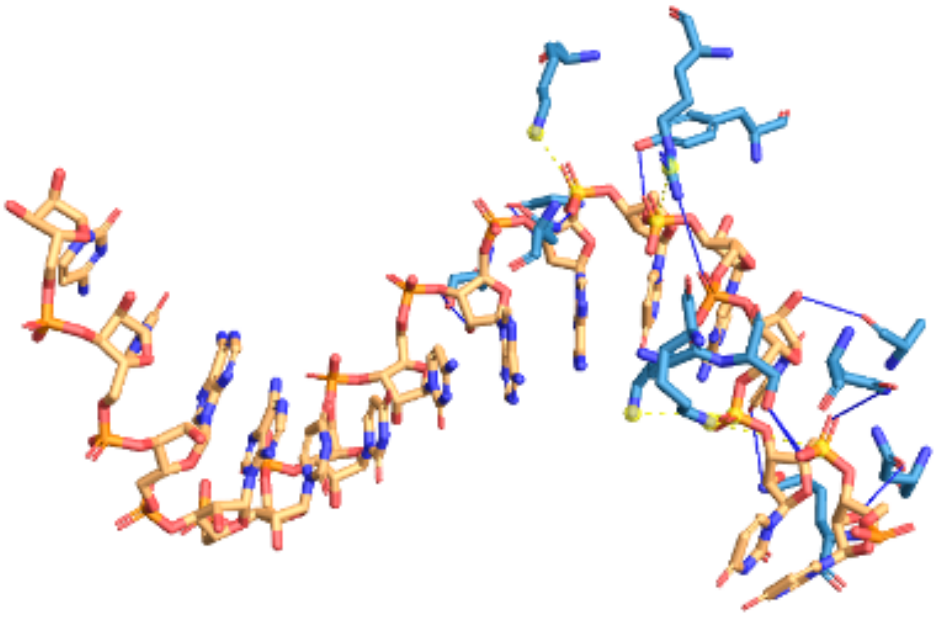

Figure 4e. Ursolic acid U-U-U-A-U-A-A-C-U-U-A-A-U-C with U (composite Ursolic acid ligand, containing Uridine Monophosphate) binding sites into the 7BV2 protein targets.

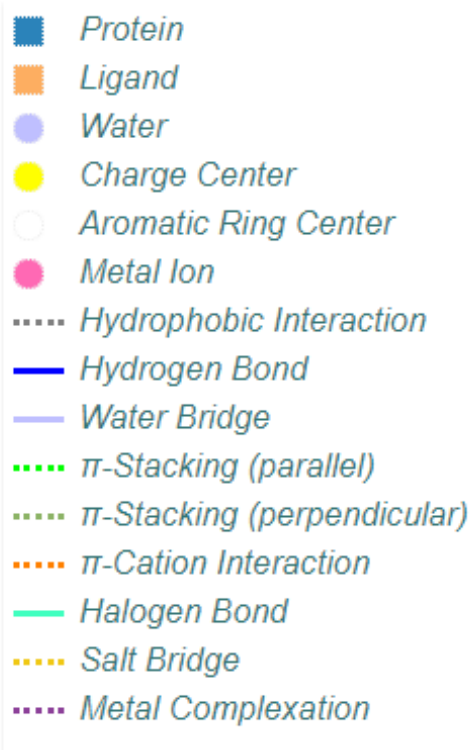

Hydrogen Bonds

Index	Residue	AA	Distance H-A	Distance D-A	Donor Angle	Protein donor?	Sidechain	Donor Atom	Acceptor Atom
1	496A	ASN	1.91	2.64	128.77	✓	✓	3365 (Nam)	8407 (O3)
2	501A	SER	2.48	3.21	132.45	✗	✓	8325 (O3)	3404 (O3)
3	501A	SER	2.12	2.99	148.42	✓	✓	3404 (O3)	8326 (O3)
4	507A	ASN	2.58	3.43	143.55	✓	✓	3450 (Nam)	8324 (O2)
5	543A	ASN	3.04	3.54	113.10	✗	✓	8313 (O3)	3752 (O2)
6	545A	LYS	2.96	3.86	146.92	✓	✓	3770 (N3)	8360 (O2)
7	558A	ALA	2.91	3.52	121.77	✗	✗	8353 (O3)	3868 (O2)
8	569A	ARG	3.38	3.85	111.72	✓	✓	3947 (Ng+)	8364 (O2)
9	590A	GLY	3.17	3.91	133.56	✗	✗	8415 (O3)	4104 (O2)
10	592A	SER	2.73	3.08	101.92	✓	✓	4117 (O3)	8435 (O3)
11	592A	SER	2.19	2.61	104.41	✗	✓	8437 (O3)	4117 (O3)
12	689A	TYR	2.77	3.27	112.65	✗	✓	8395 (O3)	4872 (O3)

Salt Bridges

Index	Residue	AA	Distance	Protein positive?	Ligand Group	Ligand Atoms
1	500A	LYS	4.74	✓	Phosphate	8343, 8343, 8331, 8344, 8345, 8346
2	511A	LYS	5.37	✓	Phosphate	8323, 8323, 8311, 8324, 8325, 8326
3	569A	ARG	5.03	✓	Phosphate	8385, 8385, 8371, 8388, 8386, 8387
4	577A	LYS	4.21	✓	Phosphate	8405, 8405, 8393, 8406, 8407, 8408

RNA+ION
Starting with G (composite ligand, containing Guanosine Monophosphate)
G-A-U-U-A-A-G-U-U-A-U-F86-MG
Composite ligand consists of G:P:10, A:P:11, U:P:12, U:P:13, A:P:14, A:P:15, G:P:16, U:P:17, U:P:18, A:P:19, U:P:20, F86:P:101, MG:A:1005.
Interacting chains: A, P

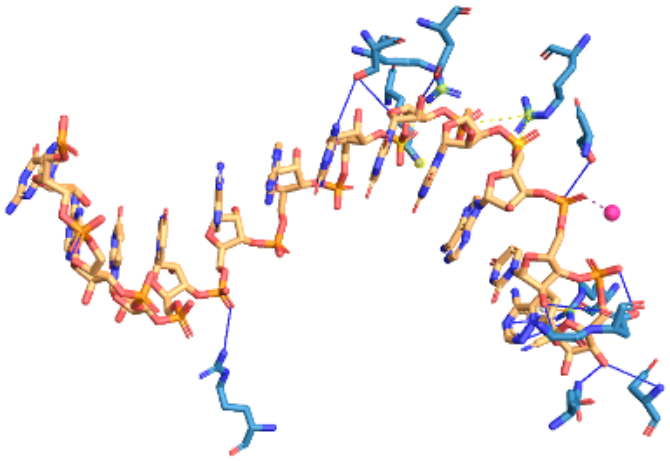

Figure 4f. Ursolic aid G-A-U-U-A-A-G-U-U-A-U-F86-MG with G (composite ligand, containing Guanosine Monophosphate) binding sites of the Ursolic avid intothe into the 7BV2 protein targets.

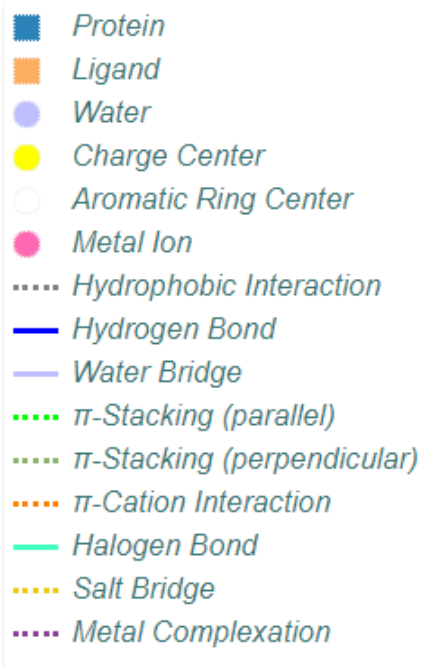

Hydrogen Bonds

Index	Residue	AA	Distance H-A	Distance D-A	Donor Angle	Protein donor?	Sidechain	Donor Atom	Acceptor Atom
1	513A	ARG	3.09	3.45	102.67	✓	✓	3502 (Ng+)	8154 (O3)
2	555A	ARG	3.47	4.04	119.47	✓	✓	3849 (Ng+)	8617 (Nar)
3	555A	ARG	3.16	3.92	134.87	✓	✓	3850 (Ng+)	8615 (Nar)
4	623A	ASP	3.55	3.98	109.70	✗	✗	8628 (O3)	4372 (N2)
5	691A	ASN	2.89	3.60	129.54	✓	✓	4885 (Nam)	8628 (O3)
6	759A	SER	2.21	3.00	137.32	✓	✓	5447 (O3)	8292 (O3)
7	760A	ASP	3.12	3.82	130.09	✗	✓	8292 (O3)	5454 (O2)
8	760A	ASP	2.51	3.45	163.02	✗	✓	8629 (O3)	5455 (O3)
9	814A	SER	2.91	3.53	122.40	✓	✓	5880 (O3)	8284 (O2)
10	861A	SER	2.90	3.87	169.93	✗	✓	8217 (Npl)	6248 (O3)
11	861A	SER	2.89	3.64	135.36	✓	✓	6248 (O3)	8226 (O3)
12	865A	ASP	3.03	3.36	102.95	✓	✓	6277 (O3)	8230 (O3)
13	865A	ASP	2.75	3.36	121.52	✗	✓	8230 (O3)	6277 (O3)

π-Cation Interactions

Index	Residue	AA	Distance	Offset	Protein charged?	Ligand Group	Ligand Atoms
1	555A	ARG	3.61	1.61	✔	Aromatic	8618, 8608, 8610, 8621, 8625

Salt Bridges

Index	Residue	AA	Distance	Protein positive?	Ligand Group	Ligand Atoms
1	836A	ARG	4.57	✔	Phosphate	8240, 8240, 8243, 8228, 8241, 8242
2	836A	ARG	4.24	✔	Phosphate	8260, 8260, 8248, 8261, 8262, 8263
3	849A	LYS	4.64	✔	Phosphate	8220, 8220, 8205, 8222, 8223, 8221
4	858A	ARG	4.87	✔	Phosphate	8220, 8220, 8205, 8222, 8223, 8221

Metal Complexes

Index	Residue	AA	Metal	Target	Distance	Location
Complex 1: Mg, NA (1)						
1	10P	G	8606	8283	2.33	ligand

SMALLMOLECULE+ION
POP (composite ligand, containing Diphosphate, dihydrogen)
POP-A-1003
Composite ligand consists of POP:A:1003, MG:A:1004.
Interacting chains: A

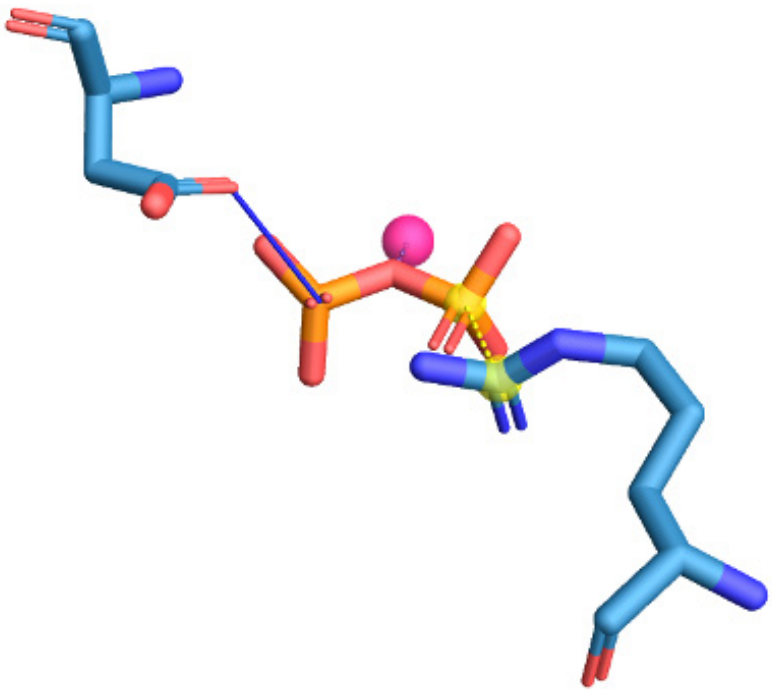

Figure 4g. Hydrogen bonds, Salt bridges and Metal complexes of the Ursolic acid POP (composite ligand, containing Diphosphate, dihydrogen) ION binding sites into the 7bv2 protein targets.

Small Molecule
02J (5-Methylisoxazole-3-carboxylic acid)
02J-C-1
Interacting chains: A

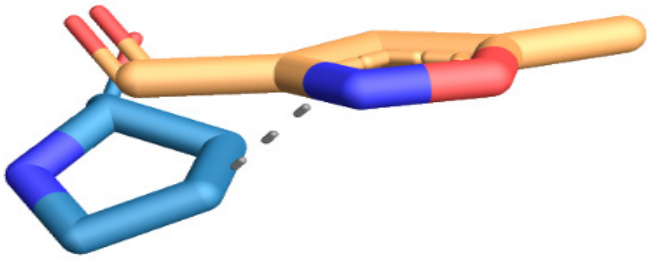

Figure 5a. Hydrophobic interactions of the Colchicine 02J (5-Methylisoxazole-3-carboxylic acid)binding site(s) into the 6LU7 protein targets.

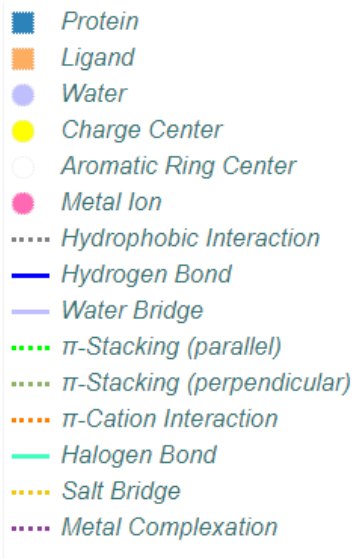

Hydrophobic Interactions

Index	Residue	AA	Distance	Ligand Atom	Protein Atom
1	168A	PRO	3.53	2369	1303

PJE (composite ligand)
PJE-C-5
Composite ligand consists of PJE:C:5, 010:C:6.
Interacting chains: A

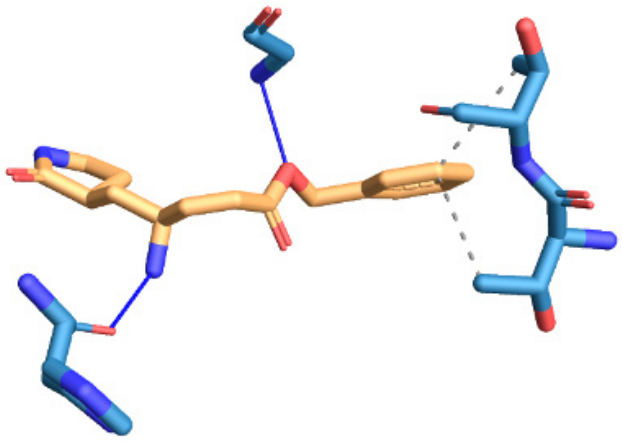

Figure 5b. Hydrogen bonds and hydrophobic interactions of the Colchicine PJE:C:5, 010:C:6. binding site(s) into the 6LU7 protein targets

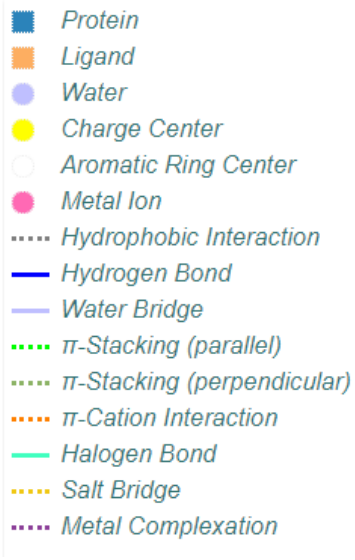

SMALLMOLECULE
6Q5
6Q5-A-9000
Interacting chains: A

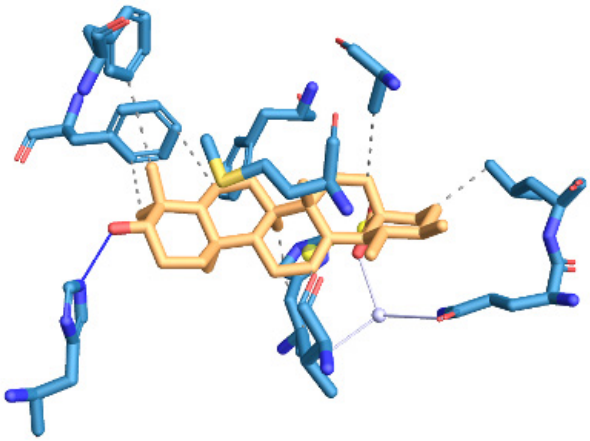

Figure 5c. Hydrophobic Interactions, Hydrogen Bonds, Water Bridges and Salt Bridges of the 6Q5-A-9000 Interacting chains: A Remdesivir binding site(s) in 5X8S protein targets.

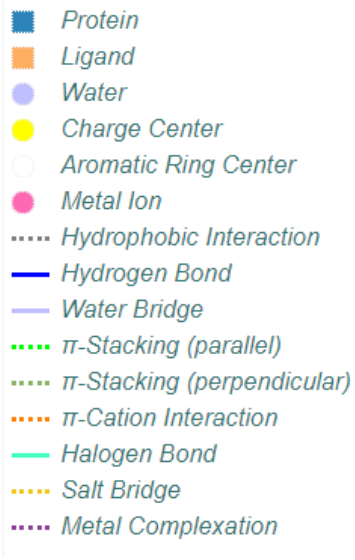

Hydrophobic Interactions

Index	Residue	AA	Distance	Ligand Atom	Protein Atom
1	287A	LEU	3.99	3849	200
2	323A	HIS	3.56	3848	516
3	361A	VAL	3.98	3857	816
4	365A	MET	3.80	3846	848
5	368A	ALA	3.88	3843	873
6	378A	PHE	3.86	3870	957
7	388A	PHE	3.84	3867	1036
8	388A	PHE	3.78	3870	1039
9	401A	PHE	3.92	3868	1133

Hydrogen Bonds

Index	Residue	AA	Distance H-A	Distance D-A	Donor Angle	Protein donor?	Sidechain	Donor Atom	Acceptor Atom
1	479A	HIS	1.99	2.81	141.07	✖	✔	3865 (O3)	1769 (N2)

Water Bridges

Index	Residue	AA	Dist. A-W	Dist. D-W	Donor Angle	Water Angle	Protein donor?	Donor Atom	Acceptor Atom	Water Atom
1	286A	GLN	3.86	2.74	109.20	83.72	✖	3841 (O.co2)	192 (O2)	3919
2	323A	HIS	2.79	2.74	109.20	82.73	✖	3841 (O.co2)	515 (O2)	3919

Salt Bridges

Index	Residue	AA	Distance	Protein positive?	Ligand Group	Ligand Atoms
1	323A	HIS	3.76	✔	Carboxylate	3839, 3841

6Q5-B-9000
Interacting chains: B

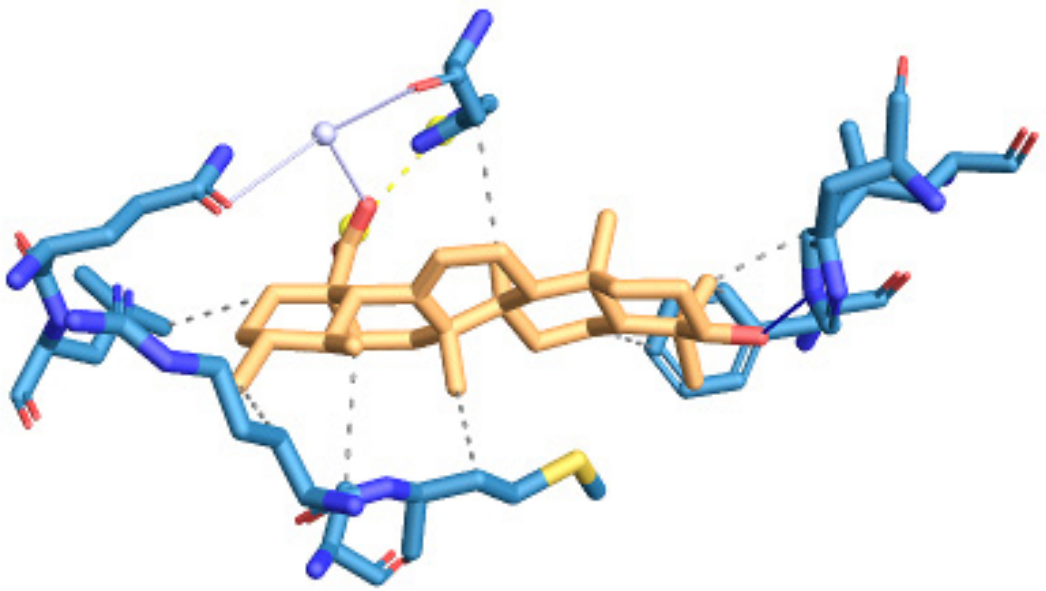

Figure 5d. Hydrophobic Interactions, Hydrogen Bonds, Water Bridges and Salt Bridges of the 6Q5-A-9000 Interacting chains: B Remdesivir binding site(s) into the 5X8S protein targets.

combination named Recombovir reported to inhibit the 3CLpro (M1, M2, M3, M4, M5, M7, M8, M10, M11, M12 and M13) mainly entered the region between domains 2 and 3, and this | 295 | ASP | A | 813 | DMS | A | 5.38 | | Sulfonium | 4739 | 35.134, -46.698, -27.502 | 30.989, -48.448, -24.558 | region is important for 3CLpro to form a dimmer (30). Recomborovir was reported to inhibit viral entry, accordingly it bound the fusion cone of spike protein; this cone structure is important for viral membrane fusion (Figures 2, 3a-3h and 4). The Recombovir drug combination targets the backbone of the Leu278 Gly279 Ile280 loop whichh is coordinating the P+2 (Asp) side chain, while P+1 (Ser) side chain is coordinated by the Ile280 carbonyl. This interaction is further strengthened by the backbone interaction between the amide hydrogen/carbonyl of the Recomborovir compounds at Gly284 and the P–3 (Ile) carbonyl/amide hydrogen. This combination of the Recombovir Chemical Structures generated a small molecule sulindac (red) binding to the CAV5R80_PDZ domain Dvl1 (PDB: 2KAW). Only few Recombovir interactions are present in the sulindac binding to the Dvl1 CAV5R80_PDZ domain; hydrogen bonds are present between the sulindac carboxylic acid and the Leu278 Gly279 Ile280 loop and the sulindac sulfoxide and Arg338. The fluorinated indole ring system of sulindac inserts into the hydrophobic pocket between B and B, acting as the P0 hydrophobic residues in canonical binders revealed the principle amino acid residues that are associated with ligand binding including PRO 168, ALA 191, THR 190-94, GLU 166, GLN 189, MET 49, ARG 188, HIS 41, ASP 187, HIS 164, CYS 145, GLY 143, THR 26, THR 24, THR 25, SER 144, MET 165, ASN 142, HIS 163, HIS 172, GLN 192,LEU 141 and PHE 140 pocket and the protein surface, which explains the highest probability to obtain this type of quantum thinking Recomborovir drug combination solutions [23-29].

Discussions

In this research report, we found the Cluster of the Recombovir-(Drug Combination) which were identified during screening of a compound diversity set performed by the BiogenetoligandorolTM cluster of algorithms on the intersection track (Lys711 and Arg355/SARS-CoV2 PLpro and Lys711 and Arg355. The chemical strucutures of the Remdesivir, Colchicine and Ursolic acid) targeted into the Lys711 and Arg355 residues and inside the residues of the Phe19, Trp23, and Leu26, which are located in an alpha-helical region of the SARS- CoV2 PLpro N terminus that binds to the N-terminal Lys711 and Arg355 hydrophobic pocket [17]. The scaffold of the drug combination of the Remdesivir, Colchicine and Ursolic acid small molecules target into the binding domaisn of these three critical SARS-CoV2 PLpro residues; the combination of the compounds therefore competes with endogenous SARS-CoV2 PLpro for binding to Lys711 and Arg355. In the absence of a structure between Lys711 and Arg355 and SARS-CoV2 PLpro and knowing that the combination of the Recombovir-(Drug Combination) small molecules disrupts this interaction, it would have been possible to exploit our strategy to infer some of the contact residues between Lys711 and Arg355 and SARS-CoV2 PLpro, Lys711 and Arg355 which are involved in three additional interactions for which a structure is available [6,7,9,12-93]. We created a new track to display the contacts of this drug combination with each of those: Lys711 and Arg355, and SARS-CoV2 PLpro. Interestingly, this drug combination consisted of the Remdesivir, Colchicine and Ursolic acid chemical structures targets the Lys711 and Arg355 homo-dimerization site and intersects within the Lys711 and Arg355-Recombovir-(Drug Combination) binding sites, suggesting that they may also interfere within the binding pockets of the Lys711 and Arg355 homodimerizations. The key residues that contribute to S trimerization can be potentially modulated by therapeutic agentsof the Remdesivir, Colchicine and Ursolic acid drugs in order to disrupt the quaternary structure assembly of the protein. In silico studies suggest that the SARS-CoV-2 S S1 might potentially bind to the human MERS-CoV receptor dipeptidyl peptidase -4 (DPP4, also known as CD26) [52]. Furthermore, the combination of the drugs of the Remdesivir, Colchicine and Ursolic acid targets the toll-like receptor 4 (TLR4), which is involved in the recognition of molecular patterns and mediate inflammatory responses, may also interact with the S protein via 10 residues located in the S1 subunit. Three of these residues were identified in this study as T-RHS residues, namely Y204, V289 (S1-NTD) and F562 (SD1) [22,25,28,34,56,77,78,90]. Both the S:CD26 and S:TLR4 interactions may constitute [34,36,39.45,56,67], potential alternative broad antiviral targets [59]. It is established that SARS-CoV- 2 S protein enters into the host cell through the ACE2 receptor; but it also uses sialic acids linked to gangliosides at the host plasma membrane, which may improve the virus attachment to lipid rafts and facilitate the contact with the ACE2 receptor. Fantini et al. have identified a ganglioside-binding domain at the S1-NTD of S protein (aa 111–162) [60]. The residues S116, I119, V120, N121, V126, I128, F133 are targeted also by the combination of the drugs of the Remdesivir, Colchicine and Ursolic acid drugs into the ganglioside-binding domain which were identified in our study as potential T-RHS or CDR for drug targeting. Moreover, Remdesivir, and its close structural analogues, bind sialic acids and gangliosides with high affinity and have shown to block the S:ganglioside interaction. The authors also suggested that the Recomborovir-(Drug Combination) might interact with this ganglioside- binding domain within the S protein [61]. Drug repurposing or the chemical optimization of existing drugs represent an effective drug discovery approach and Drug Combination based therapeutic approach which has the potential to reduce the time and costs associated to the de novo drug discovery and development and the subsequent clinical trials process [62-72,80-94]. This Insilico revelas that the combination of the drugs of the Remdesivir, Colchicine and Ursolic acid can potentially inhibit the SARS-CoV-2 replication. The majority of the key residues involved in this drug combination interaction (7 out of 9 residues) have been identified here as potential hot spots, in particular into the Shortest path(3) of the MOV10-LMAN2-UBC-LAS1L, Shortest path(3)::MOV10-ROR- NF-B/RelA-STAT3-FURIN-5-UBC-LAS1L, Shortest path(3)::MOV10-ROR- NF-B/RelA-STAT3-FURIN-5-TP53>MCL1,Shortest path(3)::MOV10-ROR- NF-B/RelA-STAT3-FURIN-27-TP53>MCL1, Shortest path(3)::MOV10-LMAN2- NXF1-MCL1, Shortest path(3)::MOV10-ROR- NF-B/RelA-STAT3-FURIN-5-NXF1-MCL1, Shortest path(3)::MOV10-ROR- NF-B/RelA-STAT3-FURIN-27-NXF1-MCL1, Shortest path(3)::MOV10-LMAN2-UBC-MCL1, Shortest path(3)::MOV10-ROR- NF-B/RelA-STAT3-FURIN-5-UBC-MCL1, Shortest path(3)::MOV10-ROR- NF-B/RelA-STAT3-FURIN-27-UBC-MCL1,Shortest path(3)::MOV10-LMAN2-CCDC8-MDN1, Shortest path(3)::MOV10-LMAN2-UBC-MDN1, Shortest path(3)::MOV10-ROR- NF-B/RelA-STAT3-FURIN-5-UBC-MDN1, Shortest path(3)::MOV10- ROR- NF-B/RelA-STAT3-FURIN-27-UBC-MDN1, Shortest path(3)::MOV10-ROR- NF-B/RelA-STAT3-FURIN-5-SUMO2-MDN1, Shortestpath(5)::MOV10-LMAN2-UBC-LOX-FN1-ROR-NF-B/RelA-STAT3AE780, K947, E1017, R1019, S1021,L1024, T1027 (S2-NTD, HR1, and CH domains). Other docking assays have suggested that the CDR: R319 (S1-NTD), C391, L517 (FURIN-ADAMTS1-ROR-GAMMA), C538, F543, N544, Q564, P589 and S591 identified in this study represent SARS-CoV-2 main protease, Mpro, FURIN-ADAMTS1-ROR-GAMMA-SRRM2-ROR- NF-B/RelA-STAT3A-ROR- NF-B/RelA-STAT3B sp15,TCEB2 >ASB8>>TCEB1PELDSFKEELDKYFKNHTSPDVDLGDISGiNASVVNIQKE IDRLNEVAKNLNESLIDLQELGKYEQYIKGSGRENLYFQGGGGSVLLMGC VAETGTQCVNLTTrTQLPPAYTNS1FURIN-ADAMTS1-ROR-GAMMARSFFEDLLFDKVKRSFIEDLLFNKVRSFFEDLLFDKV conserved active siteresidues [65]. The HR1 has also been identified in our study as a promising conserved druggable region for this drug combination named RecomborovirTM based on the finding that HR1 and HR2 regions are able to interact with each other to form a 6-helical bundle – essential for viral and cell membrane fusion – several authors have reported HR1- and HR2-derived peptides that can inhibit this fusion [66-89]. Specifically, this unique drug combination exhibited a broad insilico inhibitory activity against the SARS-CoV-2 and other SARSr- and MERSr-CoVs (66), (67), (68), (69), (70), (71). Additionally, in this research paper we identified new potential hot spot residues for the combination of the drugs of the Remdesivir, Colchicine and Ursolic acid drugs which, to the best of our knowledge, have not been described before, regarding its druggability, structural importance and/or individual role in SARS-CoV-2. These include 181 (66%, 181/273) and 72 (65%, 72/110) residues identified in the S trimer structure of hSARSr-CoVs and SARSr-and MERS-CoVs, respectively. In both groups, these new

potential hot spots lie essentially at the S2 subunit of the protein, particularly at the S2-NTD and CH domains (residues listed in Tables1a,1b,2,3a,3b). Hence, this rationale computer-aided approach may also contribute to design the more potent inhibitors named RoccuffirnaTM with a higher resilience to resistance since multiple mutations (in sites which have shown, a priori, high degree of conservation) would be required for the virus become resistant.The optimized structure of HCQ was docked in (6lu7 crystal structure, whereas Remdesivir, Colchicine and Ursolic acid Azithromycin, EIDD-2801, Recombovir molecules bind to a groove on the surface of the (2-8) PDB:1XAK protein within the sequence of amino acids of V-M -GLU-1, V- S-GLU-1, V-M-LEU-2, V- S- LEU-2, V-M-TYR-3, V-S-TYR-3, V-M-HIS-4, V-S-HIS-4, V-M-TYR-5, V-S-TYR-5, V-M-GLN-6, V-S-GLN-6, V-M-GLU-7, V-S-GLU-7, V-M-CYS-8, V-M-VAL-9, V-S-VAL-9, V-M-ARG-10 with the binding energy of -85.2507 Kcal/mol. The catalytic dyad (His41 and Cys145) interacts with the si- face (under the aromatic ring) of the ligand Remdesivir, Colchicine and Ursolic acid Remdesivir, Umifenovir, Azithromycin, EIDD-2801, Recombovir molecules through non-covalent interaction. To the best of our knowledge, there are no published studies to date addressing and comparing the conservation and druggability of the CoV S protein, for such a wide range of sequences (n = 1086 S1; n = 1096 S2) from four Beta-CoVs (SARS-CoV-2, SARS-CoVs, MERS-CoVs and Bat-SL-CoVs) and the crystallographic structures of all available SARS-CoV-2 S proteins (S-FURIN-ADAMTS1-ROR-GAMMA, monomer and trimer structures in either closed, semi-open and open state conformations, when applied) [2,4,5-12]. In the majority of recent studies, a comparative docking analysis analysis of the S protein has been performed with one reference strain for each CoV type and thereby taking into account only the most prevalent residue harbored at a given position; It does not represent diversity [8-11], and it overestimates the protein conservation score. To overcome this, we performed the conservation analysis [1,3,4-93] using the total number of protein sequences treated for each CoV type, [12,14] so that the conservation estimation takes into [15,16] account the variations in the aa composition [17,18] within each CoV. The present study has revealed the most propitious S domains to target the combination of the drugs of the Remdesivir, Colchicine and Ursolic acid bind into a motif protein target in regard to the conservation and druggability analysis of both S monomer and trimer conformations. The S1-FURIN-ADAMTS1-ROR-GAMMA represents a promising anti -COV target and is the most conserved druggable domain in the monomer analysis for hSARSr -CoVs and for SARSr- and MERSr-CoVs; and in the trimer analysis for hSARSr-CoVs. For the SARSr- and MERSr-CoV trimer, the FURIN-ADAMTS1-ROR-GAMMA ranks second after the SD1 domain; which is concordant with different CoVs using distinct host receptors for entry (20,21- 45). The SD1 stands as the most conserved druggable domain among all four Beta-CoVs analyzed. In this context, both FURIN-ADAMTS1-ROR-GAMMA and SD1 domains should be further addressed in future studies that are targeted by the Recombovir-(Drug Combination)chemical structures into the S1 subunit. In regard to the S2 subunit, the FP was found to be targeted also by the combination of the Recombovir-(Drug Combination)chemical structures as a high potential of druggability exclusively in hSARSr-CoVs (its conservation degree decreases when considering other beta-CoV species). On the other hand, the drugs of the Recombovir-(Drug Combination)bind with the CH regions which demonstrates a higher conservation- druggability potential among hSARSr-CoVs and in SARSr- and MERSr-CoVs [28,29,30-94] and is the most conserved druggable domain within the S2 subunit. Other S2 domains, such as the CR and HR1, are also alternatively be targeted vy the same cluster of chemical structures as potential antiviral targets and can also be considered in anti-CoV strategies. Conversely, the contacts that Lys711 and Arg355 makes with the cluster of the Recombovir-(Drug Combination)drugs and SARS-CoV2 PLpro are distinct from the ones with the Colchicine small molecule. The Lys711 and Arg355/ Recombovir-(Drug Combination) and Lys711 and Arg355/SARS-CoV2 PLpro interactions may not be affected by the combination of the EIDD2801, Remdesivir, Betrixaban, Ritonavir, Minocycline, Darunavir, GC76, Umifenovir, Azithromycin, Histrelin and Bleomycin chemical strucutres, suggesting an agonistic effect of the second cluster of the EIDD2801, Remdesivir, Betrixaban, Ritonavir, Minocycline, Darunavir, GC76, Umifenovir, Azithromycin, Histrelin and Bleomycin compounds. Our prediction that the combination of the EIDD2801, Remdesivir, Betrixaban, Ritonavir, Minocycline, Darunavir, GC76, Umifenovir, Azithromycin, Histrelin and Bleomycin does not interfere with the Lys711 and Arg355/SARS-CoV2 PLpro interaction is supported by data showing that Lys711 and Arg355 and SARS-CoV2 PLpro co-immunoprecipitate with the following Recombovir-(Drug Combination) treatment, which is consistent with Darunavir, Azithromycin and Recombovir-stimulated by the Lys711 and Arg355-dependant degradation of SARS-CoV2 PLpro (28, 30). As discussed above, ACE2 and TMPRSS2 are very likely correct targets, but again they are not necessarily the only targets even for cell entry of current SARS-CoV-2, and the mechanisms used by each new coronavirus strain can differ, as the result of even a single amino acid residue change. In such circumstances, the conservation of the RSFFEDLLFDKVKRSFIEDLLFNKVRSFFEDLLFDKVKRSFIEDLLFNKV motif might be considered suspicious. The activation cleavage is at the arginine (R) and workers tend to conclude that this site is more essential for action than S1/S2, and mutation of the arginine 331 specifically inhibits trypsin-dependent fusion in both cell– cell fusion and laboratory assays. But also, with the arginine retained, the drug combination of the Recombovir-(Drug Combination) can reduce the expression levels of the spike protein as above, and others can do so in laboratory conditions. Because of the conservation, one might therefore hold the seemingly reasonable quantum thinking hypothesis that this repeated site is not also susceptible to cleavage and virus activation by other extracellular proteolytic enzymes, but also doing something else. Whether or not this is so, all this drug to protein neural network complexity makes detailed interaction models of spike protein binding and activation difficult, and while the “best bet” for free energy ranking the choices of the targeted Recombovir-(Drug Combination) chemical structures makes a reasonable, currently conventional, choice which is actually an correct assumption that can accelerate productive research into therapeutic agents. In the case of the hunt for prevention and cure of virus diseases, and particularly COVID-19, there seems to be increased justification for a “fuzzier” set-theoretic picture of this combined cluster of targeted pharmacophores as a quantum ensemble of different binding sites, or of repurposed ligands in a protein to ligand-oriented perspective, as follows. Many of these, and perhaps all, suggest that even if one of the selected hit candidates is using an incorrect picture of the antiviral mechanisms of entry, activation and replication, even using the “wrong” or less important protein to drug target interaction, this cluster of the Recombovir-(Drug Combination) chemical structures might achieve some important success. In brief summary, the justifications for the ensemble repurposed pharmacophore in the coronavirus case, i.e. the contributions to “fuzziness”, include parsimony, that proteins and parts of Shortest path(5)::MOV10-ROR- NF-B/RelA-STAT3-FURIN-5-UBC-LOX-FN1-ROR- NF-B/RelA-STAT3A, Shortest path(5)::MOV10-ROR- NF-B/RelA-STAT3-FURIN-27-UBC-LOX-FN1-ROR- NF-B/RelA-STAT3A, Shortest path(5)::MOV10-LMAN2-CCDC8- MDN1-FN1-ROR- NF-B/RelA-STAT3A, SARS- CoV-2 main protease, Mpro, DPP4, ADABP, ADCP2, CD26, DPPIV, TP103, FURIN, FUR, PACE, PCSK3,GS, FURIN-ADAMTS1-ROR-GAMMA-SRRM2-ROR- NF-B/RelA-STAT3A-ROR- NF-B/RelA-STAT3B, Nsp15,CTSB, APPS, CPSB, RECEUP, SLC6A19 B0AT1, HND, TMPRSS2 PRSS10 transmembrane serine protease 2 transmembrane prproteins sometimes have more than one function encouraged by limited numbers of accessible sites (due to e.g. glycosylation) and exemplified by parallel alternative mechanisms of cell entry, multiple methods of drug action, escape from scientific defense measures by virus mutation, polymorphism of human proteins involved, different expression levels of human proteins involved, and the potential problem of the “specter of vaccine development” (concerns about missing the appropriate region of the virus that allows common cold viruses to escape the appropriate immune response). To the above may be of course added the fact that even if an experimental researcher is convinced of the value a specific drug combination as appropriate drug cluster, the picture for the computational

chemist is a fuzzy one. The system itself, real and simulated, is to be seen as a statistical mechanical ensemble of multiple quantum states, sampled over the population of these Recombovir-(Drug Combination)molecules and across their conformational behavior in time. Not least, protein binding sites are often partially disordered before binding, and in any case there may be several binding modes. Picking the right one drug combination of the Recombovir-(Drug Combination)can be difficult because there is a fine balance between solvent and conformational entropy, and shannon entropy is notoriously hard to compute. The hit compounds of the Recombovir-(Drug Combination)drugs reported here have potential to inhibit the 6LU7 crystal structure of COVID-19 main protease variant but are not guaranteed to have any activity; however, this lays the groundwork for computational drug discovery for new compounds to reduce transmission and symptoms of SARS-CoV-2. Atomic-level resolution of complex virus- receptor interactions provides new opportunities for predictive biology. In this instance, we used prior knowledge gleamed from multiple SARS-CoV strains (isolated from different hosts in different years) and ACE2 receptors (from different animal species) to model predictions for novel 2019-nCoV. Our structural analyses confidently predict that 2019-nCoV uses ACE2 as its host receptor, consistent with two other new publications [30,31]. Compared to previously isolated SARS-CoV strains, 2019-nCoV likely uses human ACE2 less efficiently than human SARS-CoV (year 2002) but more efficiently than human SARS-CoV (year 2003). Because ACE2-binding affinity has been shown to be one of the most important determinants of SARS-CoV infectivity, 2019-nCoV has evolved the capability to infect humans and some capability to transmit among humans. Alarmingly, our data predict that a single N501T mutation (corresponding to the S487T mutation in SARS-CoV) may significantly enhance the binding affinity between 2019-nCoV FURIN-ADAMTS1-ROR-GAMMA and human ACE2. Thus, 2019-nCoV evolution in patients should be closely monitored for the emergence of novel mutations at the 501 position (to a lesser extent, also the 494 position). Similarly to SARS-CoV, 2019-nCoV most likely has originated from bats, given its close phylogenetic relationship with other κgenus lineage b bat SARS-CoV (Figure2a,2b,2c,2d,2e,2f,2g,). Moreover, 2019-nCoV likely recognizes ACE2 from a diversity of animal species, including palm civets, as its receptor. In the case of SARS-CoV, some of its critical RBM residues were adapted to human ACE2, while some others were adapted to civet ACE2 (26); this type of partial viral adaptation to two host species promoted virus replication and cross-species transmission between the two host species. In the case of 2019-nCoV, however, there is no strong evidence for adaptive mutations in its critical RBM residues that specifically promote viral binding to civet ACE2. Hence, either palm civets were not intermediate hosts for 2019-nCoV, or they passed 2019-nCoV to humans quickly before 2019- nCoV had any chance to adapt to civet ACE2. Like SARS-CoV, 2019-nCoV will likely replicate inefficiently in mice and rats, ruling them out as intermediate hosts for 2019-nCoV. Moreover, we predict that either 2019-nCoV or laboratory mice and rats would need to be genetically engineered before a robust mouse or rat model for 2019-nCoV would become available. Pigs, ferrets, cats, and nonhuman primates contain largely favorable 2019-nCoV-contacting residues in their ACE2 and hence may serve as animal models or intermediate hosts for 2019-nCoV. It is worth noting that SARS-CoV was isolated in wild palm civets near Wuhan in 2005 (9), and its FURIN-ADAMTS1-ROR-GAMMA had already been well adapted to civet ACE2 (except for residue 487). Thus, bats and other wild animals in and near Wuhan should be screened for both SARS-CoV and 2019-nCoV. These above analyses are based on the modeling of 2019-nCoV FURIN-ADAMTS1-ROR-GAMMA-ACE2 interactions, heavily grounded in a series of atomic -level structures of SARS-CoV isolated from different hosts in different years [18, 24,26]. There are certainly other factors that affect the infectivity and pathogenesis of 2019- nCoV and will need to be investigated. Nevertheless, our decade-long structural studies on SARS-CoV have firmly shown that receptor recognition by SARS-CoV is one of the most important determinants of its cross-species and human-to-human transmissions, a conclusion that has been confirmed by different lines of research (13, 14]. One of the long-term goals of our previous structural studies on SARS- CoV was to build an atomic -level iterative framework of virus-receptor interactions that facilitates epidemic surveillance, predicts species-specific receptor usage, and identifies potential animal hosts and likely animal models of human diseases. This study provides a robust test of this reiterative framework, providing the basic, translational, and public health research communities with predictive insights that may help study and battle this novel 2019-nCoV.We have used structural homology modeling through the use of computer, quantum mathematical, Euclidean geometrics and statistical methods to determine a dock-able target for the SARS-CoV- 2 spike protein and have utilized the newly characterized SARS-CoV-2 Spike SARS-COV-2 Main protease PDB:6LU7 with Unliganded SARS-CoV-2 main protease, Mpro, FURIN-ADAMTS1-ROR-GAMMA-SRRM2- ROR- NF-B/RelA-STAT3A-ROR- NF-B/RelA-STAT3B, Nsp15, TCEB2->ASB8>>TCEB1 PELDSFKEELDKYFKNHTSPDVDLGDISGiNASVVNIQKEIDRL NEVAKNLNESLIDLQELGKYEQYIKGSGRENLYFQGGGG SVLLMGCVAETGTQCVNLTTrTQLPPAYTN ConsensusRSFFEDLLFDKVKRSFIEDLLFNKVRSFFEDLLFDKV active site(2019-NCOV, Coronavirus Disease 2019, variant in our docking models. It is also exciting to uncover that this combination of the drugs of the Remdesivir, Colchicine and Ursolic acid may also be potentially used for the treatment of SARS-CoV-2 infections. At this point it is important to be mentioned that the Biogenea Pharmaceuticals Ltd for Pharmaceutical Biotechnology Drug Design laboratory celebrates with people, procedures, and vision that bring new drugs into the market through Mol. Biochemistry & Mol. Pharmacology. We target the development and manufacture of new drugs like a small molecule, a nano-ligand targeted COVID-19-D614G mutation using Topology Euclidean Geometrics for Toxicity Predictive Neural Networks: A Quantum Gravitational for Persistent Homology Pharmacophoric Kinematic Algorithm (Q-Hypatia) in Practice. Such medicines draw on talent passion and experience of a wide range of professionals. The goal of Grigoriadis Ioannis and partners is to bring this group into the limelight and, in doing so, to integrate the entire process, from the registration of an Investigational New Drug (IND) or Pharmaco - biochemistry License Application (BLA) through to the market launch of new therapies and beyond. Our new computerized quantum algorithms have led us to more than one groundbreaking Pharmaco- biochemical results that are to be published in the very near future time.

COVID-19 is the first modern, severe global pandemic caused by a coronavirus, and there are no guarantees that it will be the last. Our society needs not only to develop an effective and efficient combination drug therapy scheme as well as combined treatments for the current disease but also has to have a set of drug retargeting depp learning protocols and quantum standards to promptly address all future, similar pandemics. In this manuscript, we presented our strategy to recognize potential drug-binding residues in human and viral proteins. We analyzed six currently approved drugs (Remdesivir, Colchicine and Ursolic acid). Our results indicate that small, drug-like compounds preferentially bind to kinetically active and adjoining residues, and thus seek stable residues characterized by fast normal modes with small amplitude fluctuations [43]. Some of the drugs we analyzed preferentially seek active patches that are hydrophobic (Remdesivir), while others prefer hydrophilic surfaces (remdesivir, eflornithine). We can postulate that in a water environment, drugs that bind to hydrophilic patches will be more stable, as their removal will lead to the reduction in structural entropy, but a full account of this proposition will require calculations of binding free energy differences using, for instance, still numerically expensive molecular dynamics simulations [3,4,17,73-76]. We can also propose that the combination of the Remdesivir, Colchicine and Ursolic acid drugs/small molecules that bind to deep pockets will be more stable, and thus more effective. Our algorithm accurately recognizes such pockets as binding spots for drugs (Figures 2,3a-3h and 4a,4b), and small peptides (see, in particular, Figures 2,3a-3h and 4a,4b, in (43)). Multidrug cocktails are frequently used to treat viral diseases [77]. Our analysis shows that in designing antiviral drug cocktails, the binding affinity between the drugs of the Remdesivir, Colchicine and Ursolic acid kinetically active (stable) sites should be combined with the information on their

hydrophobic and hydrophilic properties in an attempt to avoid binding competition, increase drug cocktail efficiency, and reduce toxicity and other unwanted side effects. Our results are concordant with full atom docking and simulations studies [13-19] that emphasized Remdesivir, Colchicine and Ursolic acid compounds that we also analyzed. This indicates that protein–ligand docking is a multistep process, guided both by coarse-grained properties of a bigger binding partner, and detailed, atomic-scale properties of the binding pocket and a small ligand.In our analysis, we used both viral–parasitic, as well as human proteins. The analysis shows that kinetically active residues exist in both human and non-human proteins/enzymes and that drugs bind indiscriminately to them regardless of their origin. The Remdesivir, Colchicine and Ursolic acid compounds that bind to human proteins potentially offer longer-lasting treatments as host cells and tissues have less chance of developing drug resistance through single point mutations. The procedure we described here is fast and effective and can analyze a protein structure much faster than computationally more demanding docking or molecular dynamics simulations, with complex multistep pipelines [78-81]. It is based on the assumption that proteins do not experience significant conformational changes upon ligand binding, which is oftenthe case when binding spots are hydrophobic [61]. Its advantage is not in its efficiency, but also in its ability to suggest general binding patterns between proteins and drugs or small peptides. It can be used to filter binding areas on protein surfaces and thus facilitate preclinical stages in drug design. Binding spots in various proteins can be very effectively predicted with our BiogenetoligandorolTM approach and accessed with other bioinformatics tools for charge and shape complementarity, exposed surface area, binding affinity, atomic mass, and other properties as well. However, the BiogenetoligandorolTM algorithm has its limitations. It predicts binding areas in relatively broad strokes. Additional tools able to filter out residues with relatively small surface accessible areas, and/or with incompatible charge and hydrophobic properties to the ligands of interest could improve the prediction. Additionally, the BiogenetoligandorolTM algorithm cannot determine binding free energies or binding orientations of small molecules. For that aim, other docking tools or molecular dynamics studies should be applied, as explained above. The BiogenetoligandorolTM procedure is often not effective with homodimers or with protein complexes formed of similarly sized protein FURIN-ADAMTS1-FURIN-ADAMTS1-ROR-GAMMA-CTSL1-SERPINB13-CSTB-FURIN-ADAMTS1-ROR-GAMMA- DEXD-CSTA chains [43]. When two or more molecules of different sizes form a complex of drug combination, the larger partner, i.e, the protein, does not have to significantly change its conformation during binding to accommodate smaller ligand [61]. This preserves its contact map (matrix) and the distribution of fast binding modes and hot residues. However, when two proteins of similar sizes interact, they may rearrange their conformations simply through their sheer size, and thus interrupt their contact maps (matrices). See Figures 1a-1g, Figures 3a-3h, and 4a, in [43] for the analysis and statistics of cases where the BiogenetoligandorolTM fails. Therefore, the BiogenetoligandorolTM approach is primarily aimed at binding residues recognition in cases where the binding partner is a small chemical compound or small peptide. Its druggability to predict fitness scoring effectiveness can be improved by combining its output with other chemistry informatics tools. Therefore, it can be used as a step in complex inverse docking and quantum simulation pipelines. We envision the BiogenetoligandorolTM quantum thinking procedure as the first step in a ligand parallel and inverse docking and free energy simulation pipeline. It can suggest an area on the surface of the target protein where potential drugs should bind. The next steps will limit their calculation to that area only. If the area suggested by the BiogenetoligandorolTM is a tenth of the protein's surface area, this means that all subsequent computational costs are reduced accordingly. The cost of BiogenetoligandorolTM and surface area calculations is negligible in comparison. Therefore, the approach based on the BiogenetoligandorolTM algorithm offers an effective and efficient method to speed up preclinical in silico stages in structural drug design. Recent advances in machine learning helped advance our ability to predict and design protein structures [82], but the full theoretical foundations for protein folding and binding is still lacking. The quality of the machine learning protocol directly depends on the quality and size of training datasets and, thus, in many ways follows classical methods based on statistical potentials and homology modeling [83,84]. Our results can also help in that respect as they offer interpretation on how residue packing inside protein segments guides their assemblage. The results depicted here show that in proteins that interact with small, drug-like molecules contacting scaffolds are defined by kinetically hot and residues surrounding them, regardless of the nature of the small ligand, assuming that the protein structure does not change significantly after binding. A similar conclusion related to protein–protein interactions was given in [43]. As we showed above, the full binding behavior cannot be accessed through the analysis of kinetically active residues and their neighbors only. The full atom analysis is still required for the detailed assessment of protein–drug binding. The coarse-grained analysis (BiogenetoligandorolTM algorithm) thus perceives only the outline of the binding funnel, while a full atom analysis (docking and binding free energy studies) grasps finer patterns inside that outline. This approach should in principle be similar to the current improvements in deep neural network (DNN) architectures aimed at image recognition and classification (Brendel and Bethge [85]). The improvement is based on splitting images into small local image features (e.g, outlines) without taking into account their spatial ordering, a strategy closely related to the pre deep-learning bag-of-features (BoF) models [86]. The image classification improvement stems from the observation that standard DNN architectures perceive images primarily through textures, as opposed to human perception, which is primarily based on the outlines and shapes of objects [87]. If we translat this to the problem of protein–ligand binding, we can say that the outline is determined primarily by the protein and the packing of its residues, and fine binding features ("binding textures") stem from the joint properties of the smaller binding partner and the binding pocket of the protein. In this sense, the BiogenetoligandorolTM approach is similar to human vision, and molecular docking and dynamics studies to the machine, DNN-based vision. This observation opens a space for further work, where the molecular binding will be treated as a two-step process where the coarse-grained shape of a binding funnel will be determined by the larger partner in the first step, and the final binding position and orientation by the multiple and detailed features of the binding funnel and a smaller partner inside that funnel.

Conclusions

The newly emerged coronavirus in Wuhan city in China has a health concern since the last outbreak of these types of viruses (SARS) in the year 2002–2003 in the same country leaving>700 deaths and 8000 cases in hospitals. Besides, another outbreak in the Middle East region has an entirely different infection pattern (MERS) leaving >800 deaths and 2500 hospitalizations. Colchicine binds into the pdb:6lu7 SARS-COV-2 proein targets with the docking energies of the (-2.06654, -4.97965, -10.4743, -8.98984, -4.03283, -6.24897, -3.46474, -11.5726, -3.22075, -5.20269) and generates docking energies of the -67,4Kcal/Mol. Ursolic acid and Remdesivir are generating negative docking energies also of the -54,8 Kcal/Mol and -50,8Kcal/Mol respectively when co-targeted with the Colchicine small molecule at the same protein targets within the pdb:6lu7 binding cavities. More sprecifically the two chemical structures of the Remdesivir and Ursolic acid small molecules generates an in-silico inhibitory effect against the sequence of the amino acids of the V-M-GLU-166, V-M-LEU-167, V-M-PRO-168, V-S-PRO-168, V-M-GLN-189, V-M-THR-190, V-M-ALA-191, V-M-ALA-2, V-M-VAL-3, V-S-VAL-3, V-M-GLU-166, V-M-LEU-167, V-M-PRO-168, V-S-PRO-168, V-M-GLN-189, V-M-THR-190, V-M-ALA-191, V-M-ALA-2, V-M-VAL-3, V-S-VAL-3 with the the below docking energy values (-400.794, 329.678, -337.184, -907.342, -52.667, -894.194, -194.094, -427.299, -425.681, 0.931221) for the Remdesivir and (-236.408, 0.254828, -101.104, -832.191, -405.854, -74.901, -498.389, 177.232, -269.511, -40.622) for the Ursolic acid chemical strucuture. The present study aimed to test and suggest possible inhibitors, DAA drugs, currently in the market stop the infection immediately Remdesivir, Colchicine and Ursolic acid can be used against the new strain

of coronavirus that emerged with promising results. GTP derivatives may be used as specific inhibitors against COVID-19. At the end of block-buster era for drug discovery, drug repurposing is a promising approach to address the productivity gap„ that the global pharmaceutical giants are currently facing, which will improve the drug-discovery productivity. In this original article we applied Inverse docking protocols with the integration of various COVID-19 disease databases, to perform data mining for the de novo drug repurposing, in the potential binding cavities of a set of clinically relevant macromolecular FURIN-ADAMTS1 targets. The critical issues related to inverse docking part are the prediction of correct binding pose and the estimation of some measure of the binding affinity. We have evaluated of several docking methods for inverse docking applications since the effectiveness of these methods in multiple target identification is unclear. A S1-FURIN-ADAMTS1-ROR-GAMMA- RSFFEDLLFDKVKRSFIEDLLFNKVRSFFEDLLFDKV FURIN-ADAMTS1-ROR-GAMMA-ORF1a-FURIN-ADAMTS1 Recombovir-(Drug Combination) driven inverse docking protocol (Table 3a and Table 3b) was developed, which has a ~10% binding affinity enhancement in docking success rate compared with the best inverse single docking algorithm. Finally, an comprehensive web platform by applying AI deep learning models was designed based on our BiogenetoligandorolTM protocol [2,4,5,7,11-24,28] for drug repurposing to significantly reduce user time for data gathering and multi-step analysis without human intervention, which consists of the following three tools:

(i) An automated S1-FURIN-ADAMTS1-ROR-GAMMA-consensus motif-containing [3,5,6,8,16-42,78] 2086 approved drugs with original therapeutic information.

(ii)A known target database containing 831 protein structures from [23,26,28,31-45,67] PDB covering 30 therapeutic areas. Differentiated with other tools.

BiogenetoligandorolTM outperforms other standalone algorithm in a better accuracy and more efficient way in summary. We anticipate that the Remdesivir drug could interact with the active chemical compounds of the Ursolic acid and Colchicine to kill SARS-COV2 viruses (Figures14-25, (Tables 2,3a,3b). Nevertheless, we would like to mention that, although that electrostatics, pH and other conditions can play a determinant role, it is well known quantum geometrics that are not considered in this work can also dramatically affect protein-ligand (un)binding. We also anticipate that the Colchicine drug generates a synergistic binding effect with the small molecules of the Remdesivir and Ursolic acid drugs (Figures 3e-3h, 4a-4f and Tables 3a and 3b) within the binding pockets of the protein targets (pdb:6yb7 and pdb:1xak). Therefore, solutions provided by BiogenetoligandorolTM have indicated to us that the Colchicine, Remdesivir and Ursolic acid drugs are considered to be <<co-administered>> Bleomycin (Figures 3e-3h,4a-4f,and Tables 2 and 5) which is something more than important and have to be considered as a first approximation that may require subsequent parallel refinement and docking analysis using more accurate free energy ranking models. In conclusion, BiogenetoligandorolTM -LigandorolTM is not proposed as an alternative drug repurposing method, but rather as a complementary deep learning quantum mechanics tool to be used in tandem with other drug retargeting computational and small molecule repositioning experimental methods.

Acknowledgments

I would like to express my special thanks of gratitude to my teacher (George Grigoriadis Pharmacist) as well as our principal (Nikolaos Grigoriadis Phd Pharmacist) who gave me the golden opportunity to do this wonderful project on the Quantum Chemistry topic, which also helped me in doing a lot of Research and i came to know about so many new things I am really thankful to them.

Significance Statement

Drug repurposing/repositioning/rescue proposed a computational method to identify potential drug indications by integrating various applications of an existing drug to a new disease indication. In this paper we filtered out residues with relatively small surface accessible areas, and/or with incompatible charge and hydrophobic properties to the ligands of the Remdesivir, Colchicine and Ursolic acid small molecules which could improve the prediction binding free energies or binding orientations of different drug combinations of the Remdesivir, Colchicine and Ursolic acid to treat COVID19. Finally, an comprehensive web platform by applying AI deep learning models was designed based on our BiogenetoligandorolTM protocol for drug repurposing to significantly reduce user time for data gathering and multi-step analysis without human intervention.In conclusion, BiogenetoligandorolTM -LigandorolTM is not proposed as an alternative drug repurposing method, but rather as a complementary deep learning quantum mechanics tool to be used in tandem with other drug retargeting computational and small molecule repositioning experimental methods.

References

1. Sun, Xiaoxuan, Yicheng Ni and Miaojia Zhang. “Rheumotologitsts’ View on the Use of Hydroxychloroquine to Treat COVID-19.” *Emerging Microbes & Infections* 9(2020): 830-832.
2. Huang, Yu-Feng, Chen Bai, Fan He and Ying Xie, et al. “Review on the Potential Action Mechanisms of Chinese Medicines in Treating Coronavirus Disease 2019 (COVID-19)” *Pharmacol Res* 158(2020): 104939.
3. F, Shen, Fu Z, Wu Y and Kuang GY et al. “The Potential Targets and Mechanisms of Shufeng Jiedu Capsule for Novel Coronavirus Pneumonia (COVID-19) Based on Network Pharmacology and Molecular Docking.” *Guiding J Tradit Chin Med Pharm* 26(2020): 8-15.
4. Saha, Rudra P, Ashish Ranjan Sharma, Manoj K Singh and Saikat Samanta, et al. “Repurposing Drugs, Ongoing Vaccine, and New Therapeutic Development Initiatives Against COVID-19.” *Front Pharmacol* 11(2020): 1258.
5. Du, Lanying, Yuxian He, Yusen Zhou and Shuwen Liu et al. “The Spike Protein of SARS-CoV-a Target for Vaccine and Therapeutic Development.” *Nature Reviews Microbiology* 7(2009): 226-236.
6. Gordon, Calvin J, Egor P Tchesnokov, Joy Y Feng and Danielle P Porter, et al. “The Antiviral Compound Remdesivir Potently Inhibits RNA-Dependent RNA Polymerase from Middle East Respiratory Syndrome Coronavirus.” *J Biol Chem* 295(2020): 4773-4779.
7. Kraft, Colleen S, Angela L Hewlett, Scott Koepsell and Anne M Winkler, et al. “The Use of TKM-100802 and Convalescent Plasma in 2 Patients with Ebola Virus Disease in the United States.” *Clin Infect Dis* 61 (2015): 496-502.
8. Rifaioglu, Ahmet Sureyya, Heval Atas, Maria Jesus Martin and Rengul Cetin-Atalay et al. “Recent Applications of Deep Learning and Machine Intelligence on In Silico Drug Discovery: Methods, Tools and Databases.” *Brief Bioinform* 20(2019): 1878-1912.
9. Wang, Jiang, Guo-Li Li, Sheng-Li Ming and Chun-Feng Wang et al. “BRD4 Inhibition Exerts Anti-Viral Activity Through DNA Damage-Dependent Innate Immune Responses.” *PLoS Pathog* 16(2020): e1008429.
10. Shen F, Fu ZY, Wu YR and Li L et al. “Based on Network Pharmacology and High-Throughput Molecular Docking to Study the Potential Molecular Mechanism of Active Compounds in Jinhua Qinggan Granules that Bind to the Specific Target Protein of SARS-CoV-2 to Interfere with COVID-19.” *Modernization of Traditional Chinese Medicine and Materia Materia-World Science and Technology* 3(2020): 622-631.
11. Cova, Tânia, and Alberto Pais. “Deep Learning for Deep Chemistry: Optimizing the Prediction of Chemical Patterns.” *Front Chem* 7(2019): 809.
12. Tian, Bing, Jun Yang, Yingxin Zhao, and Teodora Ivanciuc et al. “BRD4 Couples NF-B/RelA with Airway Inflammation and the IRF-RIG-I Amplification Loop in Respiratory Syncytial Virus Infection.” *J Virol* 91(2017): e00007-17.
13. Yang, Zijiang, Stefanos Papanikolaou, Andrew Reid and Wei-keng Liao, et al. “Learning to Predict Crystal Plasticity at the Nanoscale: Deep Residual Networks and Size Effects in Uniaxial Compression Discrete Dislocation Simulations.” *Scientific Reports* 10(2020): 8262.

14. Karimi, Mostafa, Di Wu, Zhangyang Wang and Yang Shen. "DeepAffinity: Interpretable Deep Learning of Compound-Protein Affinity Through Unified Recurrent and Convolutional Neural Networks." *Bioinformatics* 35(2019): 3329-3338.

15. Sun, Xiaoxuan, Yicheng Ni and Miaojia Zhang. "Rheumotologitsts' View on the Use of Hydroxychloroquine to Treat COVID-19." *Emerging Microbes & Infections* 9(2020): 830-832.

16. Mishra, Shashank Shekhar, Shashi Ranjan, Chandra Shekhar Sharma and Hemendra Pratap Singh et al. "Computational Investigation of Potential Inhibitors of Novel Coronavirus 2019 Through Structure-Based Virtual Screening, Molecular Dynamics and Density Functional Theory Studies." *J Biomol Struct Dyn* (2020): 1-13.

17. Bochevarov, Art D, Edward Harder, Thomas F Hughes, Jeremy R Greenwood et al. "Jaguar: A HighPerformance Quantum Chemistry Software Program with Strengths in life and Materials Sciences." I*nternational Journal of Quantum Chemistry* 113(2013): 2110-2142.

18. Aanouz, I, A Belhassan, K El-Khatabi and T Lakhlifi et al. "Moroccan Medicinal Plants as Inhibitors Against SARS-CoV-2 Main Protease: Computational Investigations." *J Biomol Struct Dyn* 6(2020): 1-9.

19. Sullivan, David J, Yi Liu, Bryan T Mott and Nikola Kaludov et al. "Discovery of Novel Liver-Stage Antimalarials through Quantum Similarity." *PLoS One* 10(2015): e0125593.

20. Sushko, Iurii, Sergii Novotarskyi, Robert Körner and Anil Kumar Pandey et al. "Online Chemical Modeling Environment (OCHEM): Web Platform for Data Storage, Model Development and Publishing of Chemical Information." *J Comput Aided Mol Des* 25 (2011): 533-554.

21. Walker, Theo, Christopher M Grulke, Diane Pozefsky and Alexander Tropsha. "Chembench: a Cheminformatics Workbench." *Bioinformatics* 26(2010): 3000-3001.

22. Saha, Rudra P, Ashish Ranjan Sharma, Manoj K Singh and Saikat Samanta, et al. "Repurposing Drugs, Ongoing Vaccine, and New Therapeutic Development Initiatives Against COVID-19." *Front Pharmacol* 11(2020): 1258.

23. Du, Lanying, Yuxian He, Yusen Zhou and Shuwen Liu et al. "The Spike Protein of SARS-CoV — A Target for Vaccine and Therapeutic Development" *Nat Rev Microbiol* 7(2009): 226-236.

24. Gordon, Calvin J, Egor P Tchesnokov, Joy Y Feng and Danielle P Porter, et al. "The Antiviral Compound Remdesivir Potently Inhibits RNA-Dependent RNA Polymerase from Middle East Respiratory Syndrome Coronavirus." *J Biol Chem* 295(2020): 4773-4779.

25. Rifaioglu, Ahmet Sureyya, Heval Atas, Maria Jesus Martin and Rengul Cetin-Atalay et al. "Recent Applications of Deep Learning and Machine Intelligence on In Silico Drug Discovery: Methods, Tools and Databases." *Brief Bioinform* 20 (2019): 1878-1912.

26. Jing, Yankang, Yuemin Bian, Ziheng Hu and Lirong Wang et al. "Deep Learning for Drug Design: an Artificial Intelligence Paradigm for Drug Discovery in the Big Data Era." *AAPS J* 20(2018): 58.

27. Ma, Chao, Lirong Wang and Xiang-Qun Xie. "GPU Accelerated Chemical Similarity Calculation for Compound Library Comparison." *J Chem Inf Mode*l 51(2011): 1521-1527.

28. Karimi, Mostafa, Di Wu, Zhangyang Wang and Yang Shen. "DeepAffinity: Interpretable Deep Learning of Compound-Protein Affinity Through Unified Recurrent and Convolutional Neural Networks." *Bioinformatics* 35(2019): 3329-3338.

29. Balasubramanian, Krishnan. "Mathematical and Computational Techniques for Drug Discovery: Promises and Developments." *Curr Top Med Chem* 18(2018): 2774-2799.

30. Shang, Jian, Gang Ye, Ke Shi and Yushun Wan et al. "Structural Basis of Receptor Recognition by SARS-CoV-2." *Nature* 581(2020): 221-224.

31. Wan, Yushun, Jian Shang, Rachel Graham and Ralph S et al. "Receptor Recognition by the Novel Coronavirus from Wuhan: an Analysis Based on Decade-Long Structural Studies of SARS Coronavirus." *J Virol* 94(2020): e00127-e00220.

32. Elfiky, Abdo A. "Anti-HCV, Nucleotide Inhibitors, Repurposing against COVID-19." *Life Sci* 248(2020): 117477.

33. Behloul, Nouredine, Sarra Baha, Ruihua Shi and Jihong Meng. "Role of the GTNGTKR Motif in the N-Terminal Receptor-Binding Domain of the SARS-CoV-2 Spike Protein." *Virus Res* 286(2020): 198058.

34. Heuzé, David. "MedinCell Has Launched a COVID-19 Research Initiative Based on Its Experience to Formulate Long-Acting Injectable Ivermectin." (2020).

35. Cavasotto, Claudio N, Natalia S Adler and Maria G Aucar. "Quantum Chemical Approaches in Structure-Based Virtual Screening and Lead Optimization." *Front Chem* 6(2018): 188.

36. Vidler, Lewis R, Panagis Filippakopoulos, Oleg Fedorov, Sarah Picaud et al. "Discovery of Novel Small-Molecule Inhibitors of BRD4 Using Structure-Based Virtual Screening." *J Med Chem* 56(2013): 8073-8088.

37. Sadeghi, Anahita. "Sofosbuvir and Daclatasvir as a Potential Candidate for Moderate or Severe COVID-19 Treatment, Results from a Randomised Controlled Trial." (2020).

38. Perišić, Ognjen. "Heterodimer Binding Scaffolds Recognition via the Analysis of Kinetically Hot Residues." *Pharmaceuticals* (Basel) 11(2018): 29.

39. Haliloglu, Turkan, Ivet Bahar and Burak Erman. "Gaussian Dynamics of Folded Proteins." *Phys Rev Lett* 79(1997): 3090-3093.

40. Bahar, I, A R Atilgan and B Erman. "Direct Evaluation of Thermal Fluctuations in Proteins Using a Single-Parameter Harmonic Potential." *Fold Des* 2(1997): 173-181.

41. Náray-Szabó, Gábor, Julianna Oláh and Balázs Krámos. "Quantum Mechanical Modeling: A Tool for the Understanding of Enzyme Reactions." Biomolecules 3(2013): 662-702.

42. Demirel, Melik C, Ali Rana Atilgan, Ivet Bahar, and Robert L Jernigan, et al. "Identification of Kinetically Hot Residues in Proteins." *Protein Sci* 7(1998): 2522-2532.

43. Bahar, Ivet, Burak Erman, Robert L Jernigan and Ali Rana Atilgan et al. "Collective Motions in HIV-1 Reverse Transcriptase: Examination of Flexibility and Enzyme Function." *J. Mol Biol* 285(1999): 1023-1037.

44. Yang, Lee-Wei, Eran Eyal, Chakra Chennubhotla and JunGoo Jee et al. "Insights into Equilibrium Dynamics of Proteins from Comparison of NMR and X-Ray Data with Computational Predictions." *Structure* 15(2007): 741-749.

45. Haliloglu, Turkan, Ozlem Keskin, Buyong Ma and Ruth Nussinov. "How Similar Are Protein Folding and Protein Binding Nuclei? Examination of Vibrational Motions of Energy Hot Spots and Conserved Residues." *Biophys J* 88(2005): 1552-1559.

46. Bogan, Andrew A and Kurt S Thorn. "Anatomy of Hot Spots in Protein Interfaces." *J Mol Biol* 280(1998): 1-9.

47. Moreira, Irina S, Pedro A Fernandes, and Maria J Ramos. "Hot Spots-A Review of the Protein-Protein Interface Determinant Aminon Acid Residues." Proteins Struct Funct Bioinform 68(2007): 803-812.

48. Tuncbag, Nurcan, Attila Gursoy and Ozlem Keskin. "Identification of Computational Hot Spots in Protein Interfaces: Combining Solvent Accessibility and Inter-Residue Potentials Improves the Accuracy." *Bioinformatics* 25(2009): 1513-1520.

49. Barbault, Florent and François Maurel. "Simulation with Quantum Mechanics/Molecular Mechanics for Drug Discovery." *Expert Opin Drug Discov* 10(2015): 1047-1057.

50. Lise, Stefano, Daniel Buchan, Massimiliano Pontil and David T Jones. "Predictions of Hot Spot Residues at Protein-Protein Interfaces Using Support Vector Machines." *PLoS One* 6(2011): e16774.

51. Kozakov, Dima, David R Hall, Gwo-Yu Chuang and Regina Cencic et al. "Structural Conservation of Druggable Hot Spots in Protein-Protein Interfaces." *PNAS* 108(2011): 13528-13533.

52. Tuncbag, Nurcan, Attila Gursoy, Ruth Nussinov, and Ozlem Keskin. "Predicting Protein-Protein Interactions on a Proteome Scale by Matching Evolutionary and Structural Similarities at Interfaces Using PRISM." *Nat Protoc* 6(2011): 1341-1354.

53. Pettersen, Eric F, Thomas D Goddard, Conrad C Huang, and Gregory S Couch, et al. "UCSF Chimera-A Visualization System for Exploratory Research and Analysis." *J Comput Chem* 25(2004): 1605-1612.

54. Humphrey, William, Andrew Dalke, and Klaus Schulten. “VMD: Visual Molecular Dynamics.” *J Mol Graph* 14(1996): 33-38.

55. Vetterling, William T, William H Press, Saul A Teukolsky, and Brian P Flannery. “Numerical Recipes Example Book (C++): The Art of Scientific Computing.” *Cambridge University Press* (2002).

56. Gunasekaran , Kannan, and Ruth Nussinov. “How Different are Structurally Flexible and Rigid Binding Sites? Sequence and Structural Features Discriminating Proteins that Do and Do Not Undergo Conformational Change upon Ligand Binding.” *J Mol Biol* 365(2007): 257-273.

57. Weisstein, EW. “Singular Value Decomposition.” *Wolfram Mathworld* (2020).

58. Read, JA, K W Wilkinson, R Tranter, and R B Sessions, et al. “Chloroquine Binds in the Cofactor Binding Site of Plasmodium Falciparum Lactate Dehydrogenase.” *J Biol Chem* 274(1999): 10213– 10218.

59. Huta, Brian P, Matthew R Mehlenbacher, Yan Nie, and Xuelei Lai, et al. “The Lysosomal Protein Saposin-B Binds Chloroquine.” *ChemMedChem* 11(2016): 277–282.

60. Henry, Brandon Michael, Gaurav Aggarwal, Johnny Wong, and Stefanie Benoit, et al. “Lactate Dehydrogenase Levels Predict Coronavirus Disease 2019 (COVID-19) Severity and Mortality: A Pooled Analysis.” *Am J Emerg Med* 38(2020): 1722-1726.

61. Huang, Xin, Hao Chen, and Paul L Shaffer. “Crystal Structures of Human GlyR_alpha3 Bound to Ivermectin.” *Structure* 25(2017): 945-950.

62. Appleby, Todd C, Jason K Perry, Eisuke Murakami, and Ona Barauskas, et al. “Structural Basis for RNA Replication by the Hepatitis C Virus Polymerase.” *Science* 347(2015): 771-775.

63. Gao, Yan, Liming Yan, Yucen Huang, and Fengjiang Liu, et al. “Structure of the RNA-Dependent RNA Polymerase from COVID-19 Virus.” *Science* 368(2020): 779-782.

64. Jackson, Laurie K, Elizabeth J Goldsmith, and Margaret A Phillips. “X-Ray Structure Determination of Trypanosoma Brucei Ornithine Decarboxylase Bound to D-Ornithine and to G418. Insights into Substrate Binding and ODC Conformational Flexibility.” *J Biol Chem* 278(2003): 22037-22043.

65. Kirchdoerfer, Robert N, Nianshuang Wang, Jesper Pallesen, and Daniel Wrapp, et al. “Stabilized Coronavirus Spikes are Resistant to Conformational Changes Induced by Receptor Recognition or Proteolysis.” *Sci Rep* 8(2018): 15701

66. Walls, Alexandra C, Xiaoli Xiong, Young-Jun Park, and M Alejandra Tortorici, et al. “Unexpected Receptor Functional Mimicry Elucidates Activation of Coronavirus Fusion.” *Cell* 176(2019): 1026-1039.

67. Xiong, Xiaoli, M Alejandra Tortorici, Joost Snijder, and Craig Yoshioka, et al. “Glycan Shield and Fusion Activation of a Deltacoronavirus Spike Glycoprotein Fine-Tuned for Enteric Infections.” *J Virol* 92(2018): e01628-e01717.

68. Peters, Martin B, Kaushik Raha, and Kenneth M Merz Jr. “Quantum Mechanics in Structure-Based Drug Design.” *Curr Opin Drug Discov Devel* 9(2006): 370-379.

69. Bryce, Richard A. “What Next for Quantum Mechanics in Structure-Based Drug Discovery?.” *Methods Mol Biol* 2114(2020): 339-353.

70. Perišić, Ognjen, and Hui Lu. “On the Improvement of Free-Energy Calculation from Steered Molecular Dynamics Simulations Using Adaptive Stochastic Perturbation Protocols.” *PLoS One* 9(2014): e101810.

71. Noh, Sang Young, and Rebecca Notman. “Comparison of Umbrella Sampling and Steered Molecular Dynamics Methods for Computing Free Energy Profiles of Aromatic Substrates through Phospholipid Bilayers.” *J Chem Phys* 153(2020): 034115.

72. Moscona, Anne. “Global Transmission of Oseltamivir-Resistant Influenza.” *N Engl J Med* 360(2009): 953- 956.

73. Kitchen, Douglas B, Hélène Decornez, John R Furr, and Jürgen Bajorath. “Docking and scoring in virtual screening for drug discovery: Methods and applications.” *Nat Rev Drug Discov* 3(2004): 935-949.

74. Davis, Ian W, and David Baker. “RosettaLigand Docking with Full Ligand and Receptor Flexibility.” *J Mol Biol* 385(2009): 381-392.

75. Raveh, Barak, Nir London, Lior Zimmerman, and Ora Schueler-Furman. “Rosetta FlexPepDock ab-initio: Simultaneous Folding, Docking and Refinement of Peptides onto Their Receptors.” *PLoS One* 6(2011): e18934.

76. Ballante, Flavio. “Protein-Ligand Docking in Drug Design: Performance Assessment and Binding-Pose Selection.” *Methods Mol Biol* 1824(2018): 67-88.

77. Senior, Andrew W, Richard Evans, John Jumper, and James Kirkpatrick, et al. “Improved Protein Structure Prediction Using Potentials from Deep Learning.” *Nature* 577(2020): 706-710.

78. Lu, Hui, Long Lu, and Jeffrey Skolnick. “Development of Unified Statistical Potentials Describing Protein-Protein Interactions.” *Biophys J* 84(2003): 895-1901.

79. Eswar, Narayanan, Ben Webb, Marc A Marti-Renom, and MS Madhusudhan, et al. “Comparative Protein Structure Modeling Using Modeller.” *Curr Protoc Bioinformatics* 15(2006): 1-30.

80. Brendel, Wieland, and Matthias Bethge. “Approximating CNNs with Bag-of-Local-Features Models Works Ssurprisingly Well on ImageNet.” *arXiv* 1(2019):190400760.

81. Geirhos, Robert, Carlos RM Temme, Jonas Rauber, and Heiko H Schütt, et al. “Generalisation in humans and deep neural networks.” *Adv Neural Inf Process Syst* (2018): 7538-7550.

82. Jarada, Tamer N, Jon G Rokne, and Reda Alhajj. “A Review of Computational Drug Repositioning: Strategies, Approaches, Opportunities, Challenges, and Directions.” *J Cheminform* 12(2020): 46

83. Khailany, Rozhgar A, Muhamad Safdar, and Mehmet Ozaslan. “Genomic Characterization of a Novel SARS-CoV-2.” *Gene Rep* 19(2020): 100682.

84. Kim, Dongwan, Joo-Yeon Lee, Jeong-Sun Yang, and Jun Won Kim, et al. “The Architecture of SARS-CoV-2 Transcriptome.” *Cell* 181(2020): 914-921. e10.

85. Kaushal, Neha, Yogita Gupta, Mehendi Goyal, and Svetlana F Khaiboullina, et al. “Mutational Frequencies of SARS-CoV-2 Genome During the Beginning Months of the Outbreak in USA.” *Pathogens* 9(2020): 565.

86. Eleftheriou, Phaedra, Dionysia Amanatidou, Anthi Petrou, and Athina Geronikaki. “In Silico Evaluation of the Effectivity of Approved Protease Inhibitors against the Main Protease of the Novel SARS-CoV-2 Virus.” *Molecules* 25(2020): 2529.

87. Wang, Yunxia, Song Zhang, Fengcheng Li, and Ying Zhou, et al. “Therapeutic Target Database 2020: Enriched Resource for Facilitating Research and Early Development of Targeted Therapeutics.” *Nucleic Acids Res* 48(2020): D1031-D1041.

88. Onufriev, Alexey V, and Emil Alexov. “Protonation and pK Changes in Protein-Ligand Binding.” *Q Rev Biophys* 46 (2013): 181-209.

89. Forli, Stefano, Ruth Huey, Michael E Pique, and Michel F Sanne, et.al. “Computational Protein-Ligand Docking and Virtual Drug Screening with the AutoDock Suite.” *Nat Protoc* 11(2016): 905-919.

90. Trott, Oleg, and Arthur J Olson. “AutoDock Vina: Improving the Speed and Accuracy of Docking with a New Scoring Function, Efficient Optimization, and Multithreading.” *J Comput Chem* 31(2010): 455-461.

91. Huey, Ruth, Garrett M Morris, Arthur J Olson, and David S Goodsell. “A Semiempirical Free Energy Force Field with Charge-Based Desolvation.” *J Comput Chem* 28(2007): 1145-1152.

92. Forli, Stefano, and Arthur J Olson. “A Force Field with Discrete Displaceable Waters and Desolvation Entropy for Hydrated Ligand Docking.” *J Med Chem* 55(2012): 623-638.

93. Benvenga, Salvatore, and Fabrizio Guarneri. “Automated Docking of Flexible Ligands: Applications of AutoDock.” *J Mol Recognit* 9(1996): 1-5.

94. Maia, Eduardo Habib Bechelane, Letícia Cristina Assis, Tiago Alves de Oliveira, Alisson Marques da Silva, et al. “Structure-Based Virtual Screening: From Classical to Artificial Intelligence.” *Front Chem* 8(2020): 343.

95. Xu, Xianjin, Marshal Huang, and Xiaoqin Zou. "Docking-Based Inverse Virtual Screening: Methods, Applications, and Challenges." *Biophys Rep* 4(2018): 1-16.

How to cite this article: Grigoriadis. “RORγ- NF-κB/RelA-STAT3-FURIN-SARS-COV-2 Quantum Deep Learning Functional Similarities on Remdesivir, Ursolic Acid and Colchicine Drug Synergies to treat COVID19 in Practice" *Clin Schizophr Relat Psychoses* Spl 1(2020)